# Photodissociation Spectroscopy of Anionic Transition Metal Complexes

by

**Sydney Hamilton Kaufman**

B.Sc., McGill University, 2005

A thesis submitted to the

Faculty of the Graduate School of the

University of Colorado in partial fulfillment

of the requirements for the degree of

Doctor of Philosophy

Department of Chemistry and Biochemistry

2013

This thesis entitled:
Photodissociation Spectroscopy of Anionic Transition Metal Complexes
written by Sydney Hamilton Kaufman
has been approved for the Department of Chemistry and Biochemistry

_____

Professor J. Mathias Weber

_____

Professor G. Barney Ellison

Date _____

The final copy of this thesis has been examined by the signatories, and we find that both the
content and the form meet acceptable presentation standards of scholarly work in the above
mentioned discipline.

Kaufman, Sydney Hamilton (Ph.D., Chemical Physics)

Photodissociation Spectroscopy of Anionic Transition Metal Complexes

Thesis directed by  Professor J. Mathias Weber

Transition metal complexes play an important role in many aspects of chemistry; whether in supporting biological functions, as catalysts for organic reactions, in the environment, or in industry. This thesis is comprised of gas-phase spectroscopic studies of four transition metal species with implications for many different chemical applications.

Most knowledge of the target molecules in this thesis are derived from studies in the condensed phase, where the chemical environment can change molecular properties. As a result, it is difficult to gain an understanding of the intrinsic properties in solution as well as a molecular-level picture of chemical reactions that take place where many oxidation states, molecular species, and solvent interactions occur. By isolating one particular species in the gas phase, we are able to observe how each species interacts with light independent of perturbing effects of solvent and counter ions.

In this thesis, we perform spectroscopic experiments on mass-selected ions in the gas phase, where we are able to gain information on intrinsic molecular properties without the influence of a condensed phase chemical environment.

We employ photodissociation spectroscopy, where we mass-select a particular ionic species from solution and irradiate that molecular ion with the output of a tunable laser in the ultraviolet and visible regions. By monitoring the fragments produced, we can obtain an electronic absorption spectrum of the isolated species as well as gain insight into the photochemistry of the ions under study from the fragmentation pathways observed. We combine this method with solution absorption spectra as well as electronic structure calculations.

## Dedication

To my mom.

# Acknowledgements

I have been extremely lucky to have been surrounded by many wonderful people throughout my graduate school career who have provided me with much needed support, guidance, and encouragement. First, my advisor Mathias Weber who invited me to join his group even knowing that prior to starting graduate school, I had almost no laboratory experience. I am sure he had moments of regret, but I hope they were far between. I had a steep learning curve, but he taught me a great deal about research, management, and Star Wars. I cannot thank him enough for the great kindness he has shown me through some very difficult patches.

The bulk of my experimental training fell to my predecessor, Jesse Marcum who was endlessly patient in teaching me the details of each and every aspect of the research we perform. He is a tremendously talented teacher and his students are very lucky to have him. I would also like to thank the other members of the Weber group: Chris Adams, Ben Knurr, Casey Christopher, Xavier Xu whose humor and friendship I have greatly enjoyed during our time together. I wish each of them great success in their future endeavors.

CU has a vibrant gas-phase research community and I have been honored to get to know some of them through our Negative Ion Super Group. Professors Veronica Bierbaum, Barney Ellison, Carl Lineberger and their groups have provided me with invaluable scientific insight and have acted as great sounding boards for my research over the last five years.

JILA is a fantastic place to get your PhD; not only are you surrounded by brilliant scientists and researchers, but you have access to a fantastic support staff. I also owe a great debt of gratitude to the JILA Machine and Electronic Shops who were always available to help, never complained

vi

about my bothering them, and who are immensely talented. The members of JILA Computing, especially J.R. Raith never tired of my constant questions and requests for help.

I was extremely lucky to receive a National Science Foundation Graduate Research Fellowship and I am very grateful for my funding as well as their confidence in my future success. The research in the Weber group is further supported by the NSF through the JILA AMO Physics Frontier Center and the CAREER Program. I was also supported by the University of Colorado Boulder through Teaching Assistantships.

I would be remiss if I did not thank my patient and good-hearted boyfriend, David, who has put up with a lot of craziness from me, especially in the last few months as I have been writing this thesis. I could not have retained my sanity without him. I have also had the support of a wonderful and loving family. There are no words to express how much support, generosity, and love I have received from my Dad and Marlene; I am so lucky to have them as parents. Finally my mom, who I miss so much and I wish could have be here to have witnessed my receiving my PhD and everything I will do from now on. I am who I am because of her and I hope one day to be as great as she always told me I was.

# Contents

**Chapter**

# Tables

**Table**

# Figures

**Figure**

# Chapter 1

# Introduction

## 1.1    Motivation

The aim of the experiments described in this thesis has been to provide insight into the chemistry of a series of scientifically interesting and important transition metal complexes. These species have all been studied previously, mostly in the condensed phase, where the interaction with their chemical environment changes their properties. By combining gas-phase techniques, allowing us to isolate these molecules in the absence of counter-ions or solvent we are able to obtain a more complete picture of their spectra and photochemistry.

## 1.2    Spectroscopy in the Gas-Phase

Gas-phase, mass-separated spectroscopic techniques offer the advantage of untangling the complex electronic structures seen in condensed phase spectroscopy. In mass-selected, ion beam experiments, we cannot use traditional absorption techniques used in solution which rely upon reduced light penetration resulting from absorption by molecules as described by the Beer-Lambert Law. Because the density of absorbing species in our experiment is much lower than that found in solution (in our experiment, there are about $10^4$ absorbing species per laser shot, while in solution there are closer to $10^{20}$), any measurements of light attenuation would be almost impossible to detect. We instead choose to detect a product resulting from a molecule absorbing light, in this case photofragments. This technique, known as action spectroscopy, allows one to gain analogous information to that seen in a solution UV/Vis absorption spectrum.

In order to understand the intrinsic electronic properties of a molecule, that is without the influence of surrounding solvent, counter-ions, or neighboring species in a crystal, performing this type of gas-phase spectroscopic studies is essential. By comparison of gas-phase data with those obtained in the condensed phase, we may also learn about how the solvent or crystal environment affects the target molecule. Our understanding of chemical reactions can also be enhanced by studying principal species in the gas-phase. As reactions occur in solution, the abundance of species present can make obtaining a clear picture of the mechanistic steps difficult. One may hypothesize and perform confirmatory studies on kinetics and look for electronic signatures of expected intermediates, but an exact picture of each molecular contribution and the role of the solvent in facilitating chemical reactions can be difficult to determine. By studying a single species, without solvent or other molecules present, we can excite the molecule over a reaction barrier using photons and observe resulting bond cleavage on a species by species basis.

Gas-phase studies of transition metal ion complexes in particular have vastly improved our understanding of their condensed phase chemistry [1–4]. Mass-selected studies may act as model systems for understanding the complex multibody interactions which exist in solution [5,6]. Coupling mass spectrometric preparation of target ions with laser spectroscopy thereby circumvents many of the complications [7,8] of speciation of transition metal salts in solutions.

Additionally, gas-phase studies also offer important benchmarks for computational chemists. Because most calculations of chemical and electronic properties are performed upon isolated species, the accuracy of these calculations can be difficult to determine if only solution data are available for comparison. Solvatochromic shifts, counter-ions, and the presence of other absorbing species can alter the positions and intensities of electronic transitions. By providing a measure of the isolated species's absorption cross section, we can provide a more appropriate value for ascertaining the accuracy of computational simulations.

In this thesis, we also interpret our gas-phase findings in the context of observing reaction dynamics, particularly in the studies of chromate esters and permanganate. Both are well-studied and used in the oxidation of organic species. Despite this, there remain uncertainties in the manner

by which these processes take place. In these contexts, photodissociation spectroscopy may be a tool in understanding the molecular level picture of reaction processes. By initiating reactions using laser excitation we can observe molecular dissociation without solvent, use computational techniques to hypothesize changes in geometry, and extrapolate to wider reaction mechanisms.

In the technique employed in this thesis, photodissociation spectroscopy (PD Spectroscopy) described in greater detail in the Experimentation Chapter, we mass select a target molecule of interest, irradiate it with the tunable output of our laser system, and monitor the fragments produced as a function of input energy. Through PD spectroscopy, one may determine a measure of the absorption cross section and fragmentation quantum yield as a function of energy, and gain insight into the potential energy landscape and photochemical processes. Our results are complementary to other gas-phase experimental techniques such as photoelectron spectroscopy (PES), collision induced dissociation (CID), and infrared multiphoton dissociation (IRMPD). In PES, an electron is ejected by light absorption, giving information about the states of the neutral (or monoainion, in the case of photoemission from a dianion parent). In contrast, PD gives information about the excited state of the parent species, from which dissociation takes place.

In CID, excitation occurs via collision with electrostatically-accelerated background species. As the target molecule collides with the background gas, energy is transferred one collision at a time to the target, imparting the target molecule with enough internal energy to eventually undergo fragmentation. In some cases, the energy is imparted into the molecule by low energy collisions (slow heating). This is also the case with IRMPD, where absorption of many IR photons is necessary to result in bond cleavage. In photodissociation using visible or UV light, on the other hand, energy is quickly transferred into the molecule by absorption of a photon (fast heating), as shown in Figure 1.1.

The method of energy input has important consequences. First, energy imparted to the target by low energy collisions or absorption of many low energy photons affects the dissociation pathway available. As soon as the target has internal energy greater than its weakest bond energy (lowest threshold energy for dissociation), it will fragment. Any higher energy fragmentation pathways may
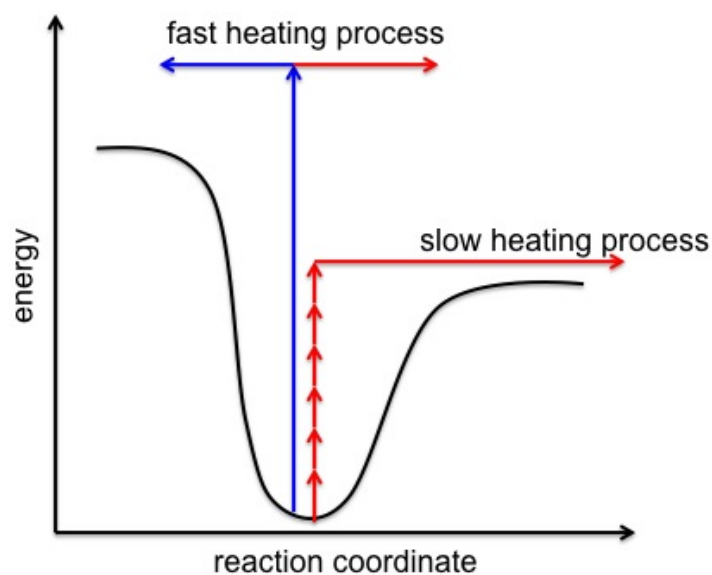
Figure 1.1: Cartoon showing dissociation pathways available in slow and fast heating processes. In a slow heating processes, most often only the lowest energy fragmentation pathway is accessible. In a fast heating process, like UV photodissociation, all fragmentation pathways with threshold energies below the photon energy are accessible. Adapted from [9].

not be sampled. In addition, collisions will occur with random impact parameters and the molecule will likely have time to explore all of the accessible phase space. By contrast, in UV and visible photodissociation spectroscopy, excitation occurs instantaneously and results in a specific electronic transition. Excitation and dissociation may happen before the energy is parsed out throughout the molecule, especially if dissociation occurs on a repulsive curve, where fragmentation can occur on the time scale of a molecular vibration [10].

Photodissociation spectroscopy is an extremely powerful tool. It has two main principal goals. The first is to obtain a gas-phase electronic absorption spectrum of the species under study. Since photodissociation cannot occur without the molecule first absorbing a photon, the intensity of the fragment signal will be in proportion to the absorption cross section. Second, we may obtain a picture of dynamics in the excited electronic state as the molecule undergoes dissociation. By examining which bonds break, the threshold energies for dissociation, and the energy-dependence of the fragment branching ratios, we may obtain an understanding of those mechanistic pathways and may be able to draw conclusions as to which will be important in solution reactions as well [10].

Photodissociation spectroscopy may also shed light upon the molecule's potential energy surface in various excited states. In some cases [11], we may observe fragment channels coupled to specific electronic transitions, as shown schematically in Figure 1.2.

We may also obtain information about the relaxation pathway the molecule takes to dissipate the energy imparted, which can shed further light upon the potential energy surface.

### 1.2.1    Relaxation Pathways

Fragmentation may occur by one of two classes of mechanisms, either direct or indirect. In direct dissociation, the molecule is excited to a repulsive curve from which dissociation occurs with no barrier, as shown in Figure 1.3. If the excited electronic state is dissociative, the molecule will quickly fragment [12] and any remaining energy will be partitioned between translational and internal energy of the resulting fragments [10].

Alternatively, indirect dissociation occurs when a barrier exists to fragmentation from the
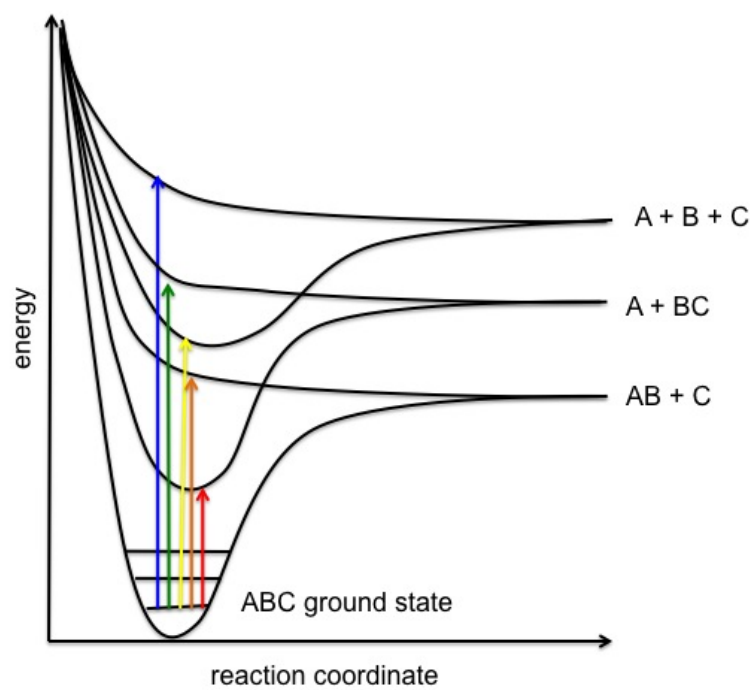
Figure 1.2: Schematic of the coupling of electronic transitions to specific dissociative pathways.
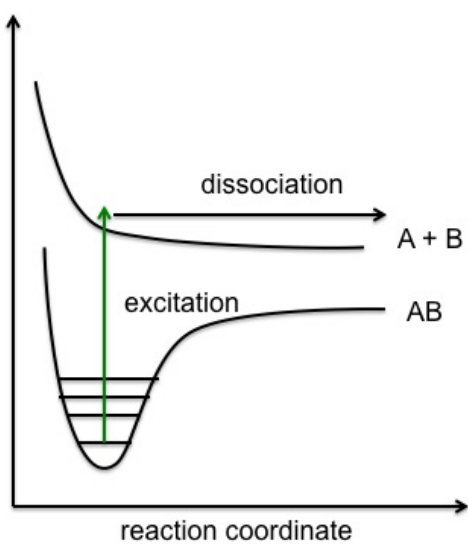


Figure 1.3: Schematic diagram of a direct photodissociation process.

excited state, as shown in Figure 1.4. This can occur if the molecule is excited to a bound state.
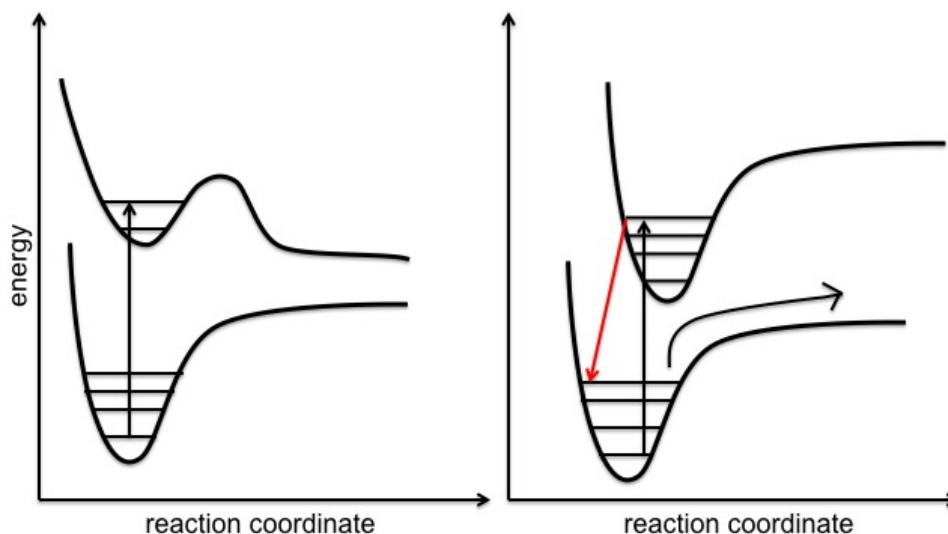


Figure 1.4: Schematic diagram of indirect photodissociation processes. The left panel shows excitation to a bound excited state. The right panel shows excitation to a bound state, followed by internal conversion resulting in a vibrationally hot state, after which the molecule may undergo fragmentation via vibrational predissociation.

Excitation is followed by internal conversion to a vibrationally hot, lower electronic state. The resulting internal vibrational energy of the molecule allows the molecule to undergo unimolecular dissociation. In the studies presented in this thesis, the latter is believed to be the primary fragmentation mechanism. We observe electronic excitations, most often attributed to ligand-to-metal charge transfers as characterized by computational techniques described within each chapter. This transfer of electron density onto the central metal is followed by bond cleavage on the time scale of the experiment, approximately 20 $\mu$s, from a vibrationally excited state.

### 1.2.2 The Role of the Solvent

One important application of gas-phase spectroscopy comes from comparisons with condensed phase data. Specifically, by comparing photodissociation-generated spectra with those obtained in solution, we can gain insight into the effect solvent perturbations have on electronic transitions. Depending on the geometry of the molecule, the nature of the electronic energy levels involved in

a transition, and the nature of the solvent and resulting shell, we may see solvatochromic shifts either to higher or lower energy, or see very little difference at all, as shown in Figure 1.5.
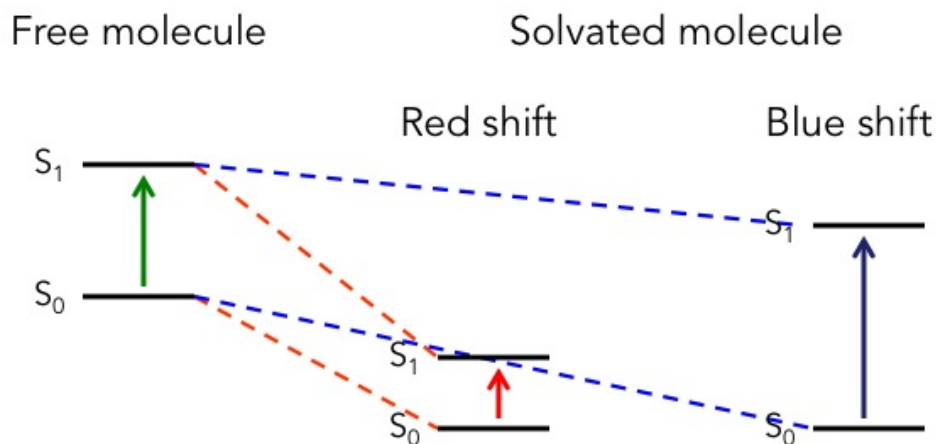


Figure 1.5: Illustration of the perturbing effects of solvent resulting in observation of a solvatochromic shift between gas-phase and condensed phase spectra.

Solvent molecules also play an important role in either enhancing reactivity, for example by stabilizing the transition state or weakening bonds, or reducing reactivity, for example if the solvent shell limits reactants' proximity [13]. In solution, the specific role of the solvent may be difficult to determine, but by removing it, we can obtain a notion of its role using the contrast between gas-phase and solution data.

## 1.3    Target Molecules

The species studied in this thesis, though all transition metal complexes, are diverse. Each has a unique set of properties, applications, and find wide use in scientific and industrial pursuits, yet questions remain about their chemistry. In each study, we observe at least one fragmentation channel which results in reduction of the central metal. Photoreduction or photo-induced reduction has a variety of potentially important uses. As exemplified in the Chromate Chapter, photoreduction can play an important role in environmental remediation of a dangerous chemical species. It may also be possible to use photoreduction in the formation of metal nanoparticles from transi-

tion metal salt precursors (as in the Copper Nitrate and Hexachloroplatinate Chapters) [14, 15]. Photoinduced redox chemistry is also an important mechanistic tool in many chemical reactions, for example, the photoinduced oxidation of organic species (as in the Permanganate and Chromate Chapters). In each case, we combine gas-phase spectra with computational and solution absorption data to elucidate the target molecules' intrinsic properties and explore how those properties affect its wider chemistry and chemical applications.

## 1.4    References

[1] T. Cooper, D. Carl, and P. Armentrout, "Hydration energies of zinc (II): Threshold collision-induced dissociation experiments and theoretical studies," The Journal of Physical Chemistry A, vol. 113, no. 49, pp. 13727–13741, 2009.

[2] P. Armentrout, "The thermochemistry of adsorbates on transition metal cluster ions: Relationship to bulk-phase properties," European Journal of Mass Spectrometry, vol. 9, no. 6, pp. 531–538, 2003.

[3] P. Armentrout and T. Baer, "Gas-phase ion dynamics and chemistry," The Journal of Physical Chemistry, vol. 100, no. 31, pp. 12866–12877, 1996.

[4] P. Armentrout, "Reactions and thermochemistry of small transition metal cluster ions," Annual Review of Physical Chemistry, vol. 52, no. 1, pp. 423–461, 2001.

[5] W. Robertson and M. Johnson, "Molecular aspects of halide ion hydration: The cluster approach," Annual Review of Physical Chemistry, vol. 54, no. 1, pp. 173–213, 2003.

[6] O. Cabarcos, C. Weinheimer, J. Lisy, and S. Xantheas, "Microscopic hydration of the fluoride anion," The Journal of Chemical Physics, vol. 110, p. 5, 1999.

[7] J. Marcum, S. Kaufman, and J. Weber, "Gas-Phase Experiments on Au(III) Photochemistry," The Journal of Physical Chemistry A, vol. 115, no. 14, pp. 3006–3015, 2011.

[8] A. Usher, D. McPhail, and J. Brugger, "A spectrophotometric study of aqueous Au(III) halide–hydroxide complexes at 25–80 ° C," Geochimica et Cosmochimica Acta, vol. 73, no. 11, pp. 3359–3380, 2009.

[9] J. Marcum, Electronic Photodissociation Spectroscopy of Electrosprayed Anions. PhD thesis, University of Colorado Boulder, 2011.

[10] R. Schinke, Photodissociation Dynamics: Spectroscopy and Fragmentation of Small Polyatomic Molecules, vol. 1. Cambridge University Press, 1995.

[11] J. C. Marcum and J. M. Weber, "Electronic photodissociation spectra and decay pathways of gas-phase $IrBr_6{}^{2-}$," The Journal of Chemical Physics, vol. 131, p. 194309, 2009.

[12] J. A. Beswick and J. Jortner, "Time scales for molecular photodissociation," Chemical Physics Letters, vol. 168, no. 3, pp. 246–248, 1990.

[13] J. M. Garver, Y.-r. Fang, N. Eyet, S. M. Villano, V. M. Bierbaum, and K. C. Westaway, "A direct comparison of reactivity and mechanism in the gas phase and in solution," Journal of the American Chemical Society, vol. 132, no. 11, pp. 3808–3814, 2010.

[14] C. Granqvist, L. Kish, and W. Marlow, Gas Phase Nanoparticle Synthesis. Springer, 2005.

[15] P. Khanna, S. Gaikwad, P. Adhyapak, N. Singh, and R. Marimuthu, "Synthesis and characterization of copper nanoparticles," Materials Letters, vol. 61, no. 25, pp. 4711–4714, 2007.

# Chapter 2

# Experimentation

## 2.1    Overview

The instrument described in this chapter was built and characterized by my predecessor, Jesse Marcum. In this chapter, an overview of the experimental set-up will be discussed. For a more in-depth description of the experimental set-up used, see [1].

To accomplish the goals of this work as outlined in the Introduction, it is necessary to combine a mass spectrometer, with an ion source allowing for gasification and mass separation of a species in solution, with a tunable laser system for photoexcitation. In electronic photodissociation spectroscopy, one UV or visible photon is used to excite an electronic transition of an ion in the gas-phase which may result in the breaking of one or more bonds.

A schematic representation of the process is shown in Figure 2.1, with the permanganate anion $(MnO_4^-)$ as an example. Photons of suitable energy can excite the target molecule to an excited
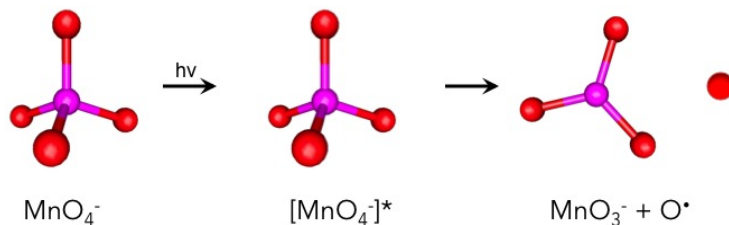


Figure 2.1: Schematic view of photodissociation process.

electronic state. If the photon energy is greater than the fragmentation energy of the molecule, dissociation may occur, resulting in the formation of charged and neutral fragments. We obtain a

photodissociation action spectrum by monitoring the fragment ion signal as a function of changing photon energy. An overview of the experimental steps required to obtain photodissociation and mass spectra is shown in schematic form in Figure 2.2, each of which will be described in greater detail in this chapter.
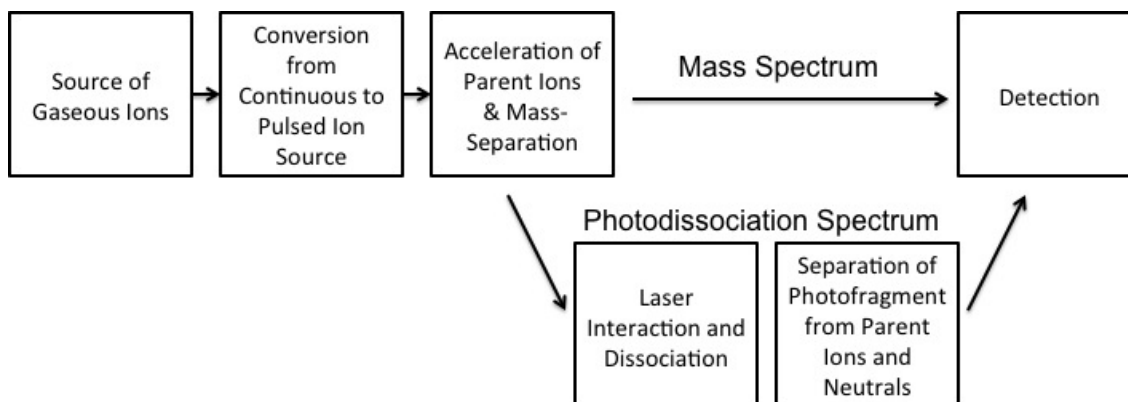


Figure 2.2: Block diagram outlining the essential steps of the experimental set-up for obtaining mass spectra and photodissociation spectra.

The experiment begins by transitioning ions of interest from solution into the gas-phase. Ions are accumulated in an ion trap and undergo mass separation in a mass spectrometer. By monitoring the mass-separated signal, we may obtain a mass spectrum of the ions generated from solution. Alternately, we may select a particular parent ion of interest and irradiate it obtain a photodissociation spectrum. A full schematic of the experimental instrument used is shown in Figure 2.3.

Ions in solution enter the gas-phase using an electrospray ionization source (ESI). These ions are then accumulated in a radio-frequency hexapole ion trap and guide. We use this ion trap to convert from a continuous source of ions, as generated from the electrospray, to a pulsed source to allow for time-of-flight mass spectrometry and to ensure better overlap with our pulsed laser system and increased signal-to-noise. The ions are then focused into the acceleration region of our Wiley-McLaren Time-of-Flight Mass Spectrometer (TOF-MS) using ion optics. The ions are accelerated perpendicular to the flight path generated by the source to separate the ions of interest
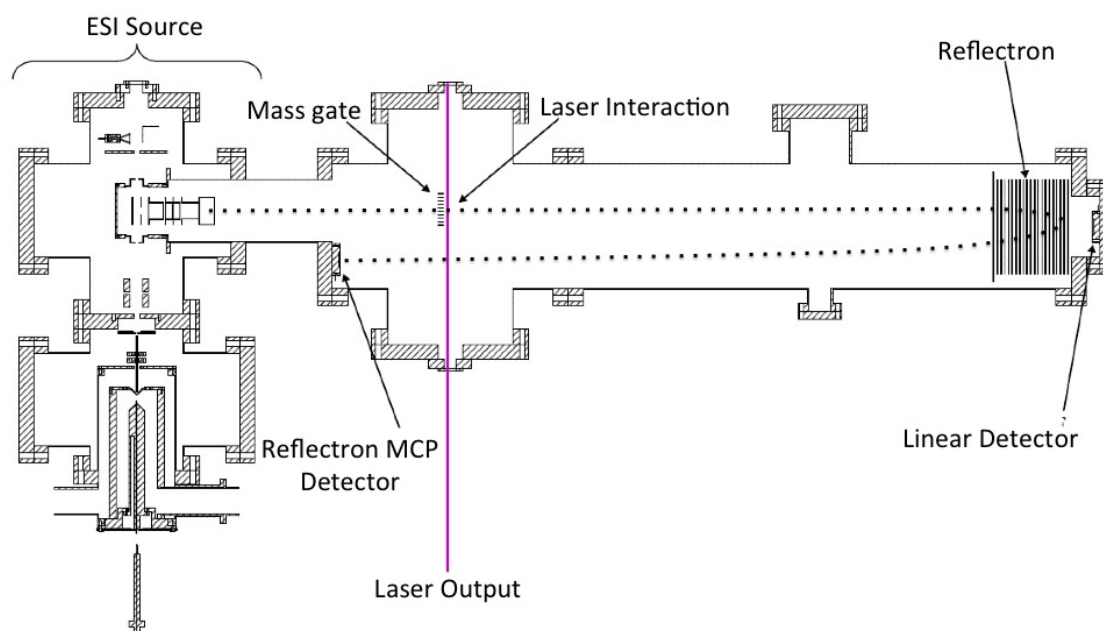
Figure 2.3: Schematic of the complete experimental set-up with regions outlined in the text shown. The ion trajectory through the field-free region is shown by the dashed line.

from neutral species and residual solvent. Other charged species produced by the ESI may be eliminated from the mass spectrum based on their mass-to-charge ratio (m/z) by adjusting the time between extraction from the hexapole trap and acceleration down the flight tube. To obtain a photodissociation spectrum, parent ions are irradiated with the output of our tunable laser system at the first space focus of the TOF-MS. After traveling through a field-free region, ions are then mass-separated using a dual-stage reflectron, reflected, and travel back down the field-free region where they are finally detected on the reflectron microchannel plate (MCP) detector.

The pressures in our vacuum chambers are controlled with a series of roughing and turbo-molecular pumps. The pressures in various regions of the chamber, along with pump type, and estimated mean free paths of ions in that chamber are listed in Table 2.1.

| Pumping Stage | Experimental Description | Pump Type | Pumping Speed | Pressure (mbar) | Mean Free Path (cm) |
|---|---|---|---|---|---|
| 0 | electrospray | none | N/A | 831 | $2 \times 10^{-5}$ |
| 1 | skimmer | roughing | 65 m$^3$/h | $\sim 10^{-1}$ | 0.16 |
| 2 | trap entrance | roughing | 65 m$^3$/h | $\sim 10^{-2}$ | 01.57 |
| 3 | trap exit | turbo | 350 L/s | $\sim 10^{-4}$ | 157 |
| 4 | acceleration | turbo | 350 L/s | $\sim 10^{-6}$ | 15,709 |
| 5 | flight tube | turbo | 520 L/s | $\sim 10^{-7}$ | 157,099 |

Table 2.1: Pressures used in regions of vacuum chamber along with pumping speeds and estimated mean free path for ions in those regions.

The mean free path is estimated from the kinetic theory of gases according to the following equation:

$$\lambda = \frac{k_B T}{\sqrt{2} p \sigma} \tag{2.1}$$

where $\lambda$ is the mean free path, $k_B$ is the Boltzmann constant, T is the temperature (taken to be 300 K), p is the pressure, and $\sigma$ is the collisional cross section of the colliding and stationary molecules. In this case, the background gas is the stationary molecule and the colliding molecule is the parent ion of interest. The collisional cross section was estimated according to:

$$\sigma = \pi \cdot d_{colliding} \cdot d_{stationary} \tag{2.2}$$

where $d_{colliding}$ is estimated using the calculated diameter of the permanganate ion, $\sim 4.0$ Å (see calculation details in Chapter 4) and $d_{stationary}$ is the diameter of nitrogen gas (taken to be $\sim 1.5$Å).

## 2.2    ESI Source

The entire source region of the instrument is shown in Figure 2.4 as adapted from [2].
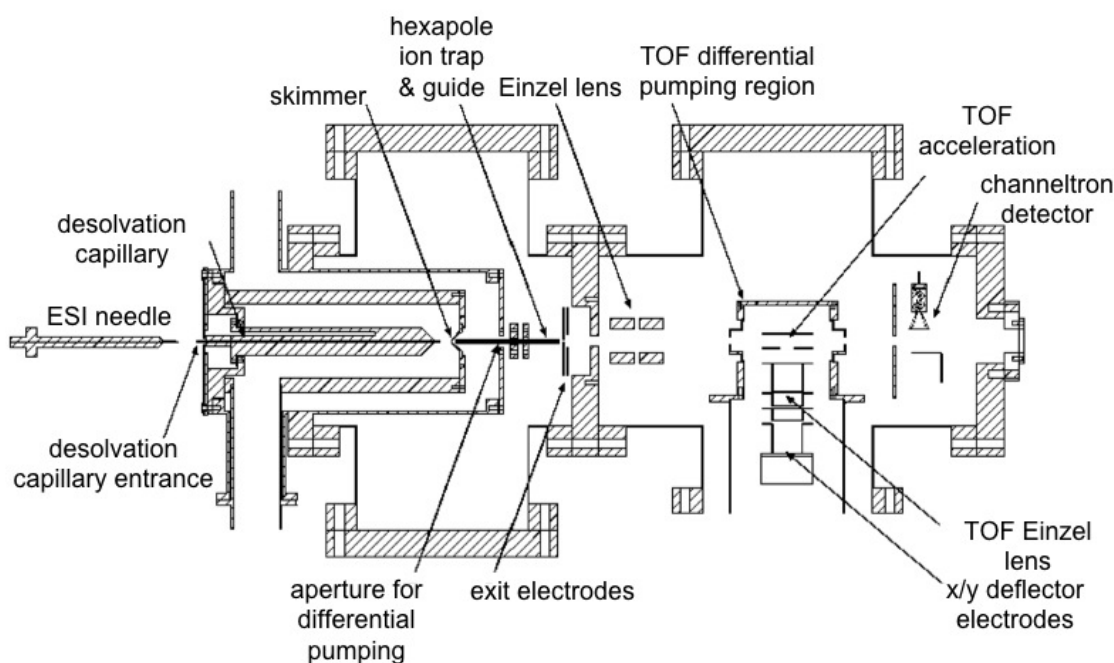


Figure 2.4: Zoom in of ESI source region of the instrument as adapted from [2].

The technique of electrospray ionization was developed as a method to promote large, fragile molecules into the gas-phase, especially biomolecules [3, 4]. A cartoon of the process is shown in Figure 2.5. To generate negative ions in the gas-phase by ESI, a solution containing the species of interest is injected through a capillary tube held within a stainless steel needle charged to about -2000 V. At the exit of the needle, edge effects from the needle create a strong electric field which generates a cone of liquids, called a Taylor cone [5, 6]. When sufficient Coulomb repulsion
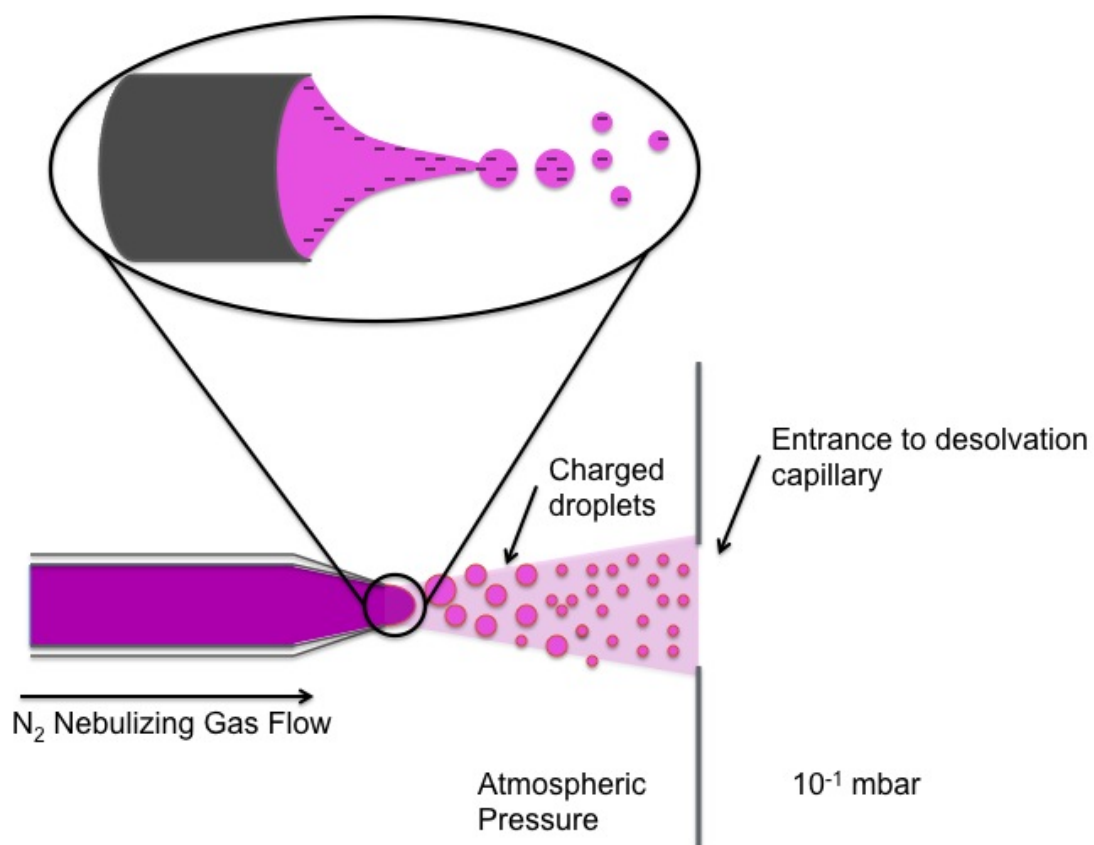
Figure 2.5: Cartoon representation of the electrospray ionization process.

builds up, charged droplets will be expelled away from the Taylor cone towards the desolvation capillary and the entrance to the vacuum chamber. The Coulomb repulsion within the droplets is in competition with cohesive surface tension holding the droplet together. As solvent evaporates, the charge density increases leading to an eventual Coulombic explosion and fission of the droplets into smaller droplets. The electrostatic explosion of a hypothetically spherical droplet should occur when the Rayleigh limit is reached according to [6],

$$q^2 = 8 \cdot \pi^2 \cdot \epsilon_0 \cdot \gamma \cdot D^3 \tag{2.3}$$

where q is the charge on the droplet, $\epsilon_0$ is the permittivity of the environment, $\gamma$ is the surface tension, and D is the diameter of the droplet. Destruction of the droplet is actually observed to occur before the Rayleigh limit is reached owing to mechanical deformation away from a spherical shape which reduces the internal charge necessary to overcome the cohesive forces [7].

Eventually, all solvent is either evaporated away or the negative ions are expelled from the droplets. Acceleration towards the entrance of the capillary occurs by two mechanism: the electric field from the needle to the capillary entrance held at approximately -100 V, and gas flow into the chamber.

This simplified picture of ESI overlooks an important point necessary for the successful operation of an electrospray ionization source: in order to generate a flow of negative ions into the chamber, an equal number of positive ions must be electrochemically reduced at the needle tip in order to complete the circuit of ion flow. This fact has a bearing on the solution which results in the best ion signal. For negative ion ESI, an acidic solution is often used because the mobility of the protons in solution facilitates charge neutralization [7].

The solvent of choice, concentration, pH, and spraying condition must be optimized for each chemical system. Depending on the solubility of species to be studied, water is often used to dissolve the solid salt, then the solution is spiked with methanol or acetonitrile to improve the facility towards electrospray. Because water has very high surface tension, the desolvation process

is hindered in a purely aqueous solution. Water may be used, but a much higher needle voltage is necessary for efficient droplet formation (-3000 V and higher in our setup).

It should also be noted that the species resulting from the ESI may not necessarily reflect what is present in solution [8]. A preponderance of charge within the droplet may result in a self-selection of those species which are able to accommodate excess charge. It may also lead to chemistry between analyte molecules or analyte-solvent interactions which would not be observed under normal solution conditions.

As the ions travel from the electospray needle through the desolvation capillary and through a skimmer (diameter of 1.5 mm), some species which are stable in solution may dissociate or be neutralized. As the ions are propelled from the capillary towards the skimmer, they undergo a large number of collisions with the background gas. The force of the collisions, and resulting transfer of energy to the ion will be determined by their kinetic, governed by the potential difference between the capillary and skimmer. For fragile species or those with high enough internal energy, unimolecular decay of the desired parent species may take place, reducing parent ion signal. For this reason, it is necessary to optimize the difference between the capillary and skimmer voltages to minimize collision-induced dissociation but still allow for ion transfer into the ion trap and guide.

The droplets enter the vacuum chamber through the desolvation capillary which may be heated to expedite evaporation of the solvent. In the experiments performed for this thesis however, no heating was used. The desolvation capillary is 21.5 cm long and has an inner diameter of 0.508 mm. The desolvation process is extremely effective, ensuring no solvent remains on the parent ions. This can be a detriment as it may be scientifically beneficial to maintain some solvent molecules surround the of the ion of interest. In planned future modification to the experimental setup, the desolvation capillary will be significantly shortened to allow for the study of solvated ions.

As the ions exit the skimmer which separates the first and second differential pumping regions, they enter into radio frequency hexapole ion trap and guide.

## 2.3    Ion Trap and Guide

The linear hexapole ion trap and guide is based on designs developed by Gerlich and co-workers [9–11].  Ions are trapped radially by rod-shaped electrodes which alternate in voltage polarity at a frequency between 2 and 10 MHz (depending on the m/z of the ions being trapped), as shown in Figure 2.6.
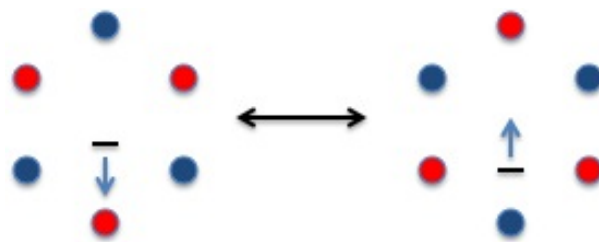


Figure 2.6: Cartoon Representation of the Hexapole Ion Trap and Guide.  Each of the six blue and red circles represents one rod within the hexapole trap. Each rod alternates polarity between positive, represented by red, and negative, represented by blue.  An anion in the center will be attracted to the electrodes of positive polarity, then, as the electrode reverses polarity, the anion will be repulsed, as shown by the arrow in the center of the trap.  The frequency of the polarity reversal is such that the ion is not able to escape from the trap.

An anion in the trap will be attracted to a pole of positive polarity, but will not be able to reach the electrode and escape the trap before the polarity of the electrode changes.  The ions feel a net trapping potential with an effective minimum centered within the hexapole. The voltage applied to the six electrodes of the trap may be adjusted to optimize the ion trapping and minimize RF heating with typical amplitudes ca.  +/- 700 V. The hexapole ion trap and guide is pivotal to the proper functioning of this experiment.  Its primary function is to accumulate ions from the continuous electrospray source into a more dense ion packet.  This strategy allows the ions to be injected into a pulsed TOF-MS and optimizes interaction with the pulsed laser output.  The hexapole also acts as an ion guide through the second differential pumping stage whose pressure is too high to rely upon electrostatic ion optics efficiently.  The ions are stored for a period of 25 ms.  During this time, the ions reach thermal equilibrium by collisions with neutral background gas.  As the ions enter the trap from the ESI and desolvation capillary, they may have a broad

internal energy distribution owing to adiabatic cooling and collisional heating during formation and transport within the vacuum region. Since the trap is at room temperature, the ions will leave the trap with a thermal energy distribution, around 300 K.

The ions are axially trapped by the skimmer, which acts as an entrance electrode, and two end-cap electrodes. The cycling of the voltage applied to the exit electrodes enables three actions: trapping of the ions, removing the barrier towards ions leaving the trap, and acceleration of the ions away from the trap towards the TOF acceleration region. By adjusting the ratio of applied voltages to the electrodes, it is possible to roughly focus the parent ions of interest in time as them reach the acceleration region. In order to improve the spatial resolution of the ion packet as it leaves the trap and enters the acceleration region, we employ a modified Einzel Lens [1, 12].

## 2.4      Reflectron Time-of-Flight Mass Spectrometer

Mass separation in preparation for irradiation is performed using a Wiley-McLaren reflectron time-of-flight mass spectrometer (TOF-MS) purchased from R.M. Jordan and used with minimal modifications.

### 2.4.1      Acceleration Region

Using a series of three electrodes (repeller, extractor, and grounded electrodes) as originally outlined by Wiley and McLaren [13], the ions are accelerated down a field-free flight tube perpendicular to their trajectory upon leaving the hexapole trap. The two acceleration fields focus ions with different initial positions and velocities as they enter the acceleration region. In addition, the location of the space focus of the mass spectrometer can be selected by adjusting the voltages applied to the repeller and extractor plates. The back, repeller plate of the accelerator is held at -4.0 kV, while the extractor is typically biased at -3.5 kV, imparting ions with an average kinetic energy of approximately 3.7 keV. As the ions of a particular mass travel through the field-free region, the faster ions catch up with the slower moving ions created toward the front of the acceleration region, meeting at the space focus at the same time.

As the ions are accelerated perpendicular to their initial trajectory, they retain momentum in their initial direction. To correct for this and ensure the ion trajectory results in their reaching the desired position for detection at the reflectron MCP shown in Figure 2.3, an ion lens and series of steering deflector plates are employed directly after acceleration.

### 2.4.2    Laser Interaction Region & Mass Gate

We select the space focus of the TOF-MS to be at the laser interaction region, where the ion packet is irradiated with the output of a tunable laser system. At the space focus, an MCP detector may be rotated down into the ion path, allowing adjustment of the extractor voltage and ion optics to ensure the narrowest possible temporal distribution of the ion packet and the greatest overlap with the laser beam and consequently optimized fragment ion signal. At this point in the ion path, we may also choose to employ a home built mass gate to suppress unwanted ions of similar masses as the ions under study, as previously described [14]. The mass gate briefly consists of a series of alternately charged parallel plates. A voltage is applied to the mass gate electrode, deflecting unwanted ions out of the ion beam. As the ions of interest approach the mass gate assembly, the voltage is pulsed to ground, allowing these ions to pass.

### 2.4.3    Dual-Stage Reflectron

The reflectron consists of a series of electrodes which generate a field acting as an ion mirror, allowing for improved mass resolution as well as secondary mass separation of the parent and fragment ions [15]. The reflectron corrects for disparities in initial kinetic energy of the parent ions. Ions with greater kinetic energy will be able to penetrate deeper into the retarding field of the reflectron, taking longer to turn around. Slower ions of the same mass-to-charge ratio will be turned around more quickly.

After photodissociation, all ions continue to travel down the field-free flight tube towards the reflectron with the same velocity, regardless of mass changes resulting from fragmentation. While parent and fragment ions travel through the field-free region together, the fragment ion kinetic

energy has changed. As they reach the reflectron, lighter fragment ions will be turned around more quickly, owing to their reduced kinetic energy as a result of reduced mass upon fragmentation [7]. Fragment ions are thereby temporally separated from remaing parent ions as they travel back down the flight tube towards the MCP detector. Neutral fragments, unaffected by the reflectron electric field, travel straight through where they may be detected on the linear MCP detector.

To describe the manner of fragment ion separation, we can first examine the penetration depth of the parent ion into the reflectron:

$$x_p(V_1) = \frac{E_p L}{z V_1} \tag{2.4}$$

where $x_p(V_1)$ is the depth of the parent ion penetration as a function of the reflectron voltage, L is the length of the reflectron, $V_1$ is the reflectron voltage, assuming a one-stage reflectron for simplicity, $E_p$ is the kinetic energy of the parent ion, and z is the charge of the ion. The kinetic energy of the parent upon entering the reflectron is:

$$E_p = \frac{m_p v^2}{2} \tag{2.5}$$

where v is the velocity of the parent ion along the axis of reflection and $m_p$ is the mass of the parent. Since the average velocity of the ion within the reflectron will be equal to one half their entering velocity, the time spent within the reflectron, $t_p$, will be equal to

$$t_p = \frac{4x_p}{v} = \frac{4E_p L}{vzV_1} \tag{2.6}$$

Likewise, the time of the fragment ion in the reflectron will be:

$$t_f = \frac{4x_f}{v} = \frac{4E_f L}{vzV_1} \tag{2.7}$$

We may determine a scaled reflectron voltage, $V_2$, such that the time in the reflectron for the fragment is the same as that of the parent with the original reflectron voltage, $V_1$, such that:

$$t_p = \frac{4E_p}{vzV_1} = t_f = \frac{4E_p}{vzV_2} \cdot \frac{m_f}{m_p} \tag{2.8}$$

Since all ions will retain their initial velocity upon leaving the reflectron, the flight time of the fragment ions to reach the MCP using a scaled reflectron voltage, $V_2$ will be the same as the parents under initial reflectron voltage, $V_1$, assuming $V_2$ is calculated according to,

$$\frac{V_2}{V_1} = \frac{m_f}{m_p} \tag{2.9}$$

We may therefore identify and select the expected fragment masses resulting from photodissociation.

The secondary reflectron voltage may be adjusted to optimize temporal focussing of the ions at the MCP. The reflectron voltage is typically -4.0 kV, the same as that applied to the accelerator. The focusing voltage is selected as a percentage of the reflectron voltage.

This description is based on parent and fragment species being singly charged, but the same argument applies for dianion parent species. The only difference in this case is that the fragments have a higher m/z than the parents, so the reflectron voltage must be scaled up rather than down to allow fragment ions to arrive at the detector at the appropriate time. For doubly charged species, for example $PtCl_6^{2-}$ in Chapter 6, the reflectron may be turned up as high as -4.5 kV. To accommodate all ion fragments, it is necessary to turn down the acceleration voltage to -2.25 kV (half of -4.5 kV) allowing for detection of fragment ions resulting from the loss of an electron with twice the m/z of the parent dianion.

## 2.5    Tunable Laser System

The versatility of this experimental set-up is due in part to the laser system used which consists of a pump laser, an optical parametric oscillator (OPO), and a set of non-linear optical crystals to perform second harmonic generation (SHG) or sum frequency mixing (SFM). This laser system allows us to generate wavelengths between 2200 and 220 nm.

We employ a Neodymium-doped yttrium aluminum garnet (Nd:YAG) solid-state pump laser (Innolas Spitlight 600). Q-switching is employed to maximize population inversion prior to lasing and obtain pulses with 5-7 ns duration. The repetition rate of the laser is 20 Hz. The output of the beam of the Nd:YAG ($\lambda$=1064 nm) is frequency doubled to 532 nm, then mixed with residual

1064 nm light to generate 355 nm. The 355 nm output is separated from any residual 1064 nm and 532 nm light, then is used to pump the OPO and SHG/SFM stages with a power of between 2-2.5 W (100-125 mJ/pulse).

The OPO (GWU preciScan ULD) consists of a resonator and nonlinear crystal, here a type II $\beta$-barium-borate (BBO), to perform parametric conversion. Within the crystal the pump laser beam, $\omega_p$, is converted into two lower energy beams, the signal, $\omega_s$, and idler, $\omega_i$, such that:

$$\omega_p = \omega_s + \omega_i \tag{2.10}$$

In order to see build up of any particular signal/idler frequencies, the phase-matching condition must be met:

$$\vec{\mathbf{k}_p} = \vec{\mathbf{k}_s} + \vec{\mathbf{k}_i} \tag{2.11}$$

where $\vec{\mathbf{k}}$ is the wave vector of each beam. The phase-matching condition, and thus selection of the signal and idler wavelengths is met for a single pair of wavelengths by the angle of the BBO crystal with $\vec{\mathbf{k}}_{\mathrm{p}}$ [16, 17]. Two crystals are employed for conversion within the OPO to reduce necessary size and thus cost of the crystal required to tune over the entire wavelength range. The wavelength ranges accessible by each of the crystal regions of the OPO are shown in Table 2.2.

| Crystal | Signal Frequency Range | Idler Frequency Range |
|---------|------------------------|------------------------|
| Blue    | 415 nm - 515 nm        | 1140 nm -2450 nm       |
| Red     | 505 nm - 710 nm        | 710 nm -1190 nm        |

Table 2.2: Range of signal and idler wavelengths generated by the two nonlinear crystals in the OPO.

The output beam from the OPO then enters the SHG/SFM stage. We may either double the frequency of the resulting beam (SHG) or we may mix residual 1064 nm output from the pump laser with the signal or idler (SFM). The wavelength ranges accessible are shown in Table 2.3.

The shortest wavelength we are able to generate, on the order of 220 nm produced by frequency doubling the highest energy output of the OPO's blue crystal, is limited by the non-linear

| Crystal | SHG Frequency Range | SFM Frequency Range |
|---------|---------------------|---------------------|
| **Blue** | 220 nm - 257 nm | 299 nm - 350 nm |
| **Red** | 257 nm - 354 nm | 350 nm - 404 nm |

Table 2.3: Range of wavelengths generated by SHG and SFM from the output of the OPO.

crystal employed, which becomes opaque to light at shorter wavelengths. The bandwidth of the resulting laser beam is $\sim$5 cm$^{-1}$.

## 2.6    Data Acquisition

We may obtain a number of different types of data on a particular system using the set-up described. The most basic information is a mass spectrum of the species resulting from ESI, an example mass spectrum of $PtCl_6{}^{2-}$ is shown in Figure 2.7. The typical mass resolution for this instrument, $m/\Delta m$, is on the order of 1,000.

A photodissociation action spectrum is generated by monitoring a particular ionic fragment as a function of changing photon energy. We may also obtain a depletion spectrum, wherein we monitor the parent species under irradiation and observe how the signal is reduced by the formation of photofragments. Since no depletion spectra were taken for this thesis, this section will focus on taking action spectra.

### 2.6.1    Timing

Precise timing is required to ensure the proper sequence of voltage pulses and laser pulse as the ions progress through the instrument. Each of the components is controlled by a digital delay pulse generator (Quantum Composer, 9518 Plus). A table including each of the components' timing, pulse length, and reference is shown in Table 2.4.

The experiment is run at a repetition rate of 40 Hz in reference to the internal timing of the pulse generator, called $t_0$. Channel A controls the ion trap such that every 24.5 $\mu$s, the exit electrodes of the hexapole ion trap are pulsed allowing the packet of ions to exit. The injection into
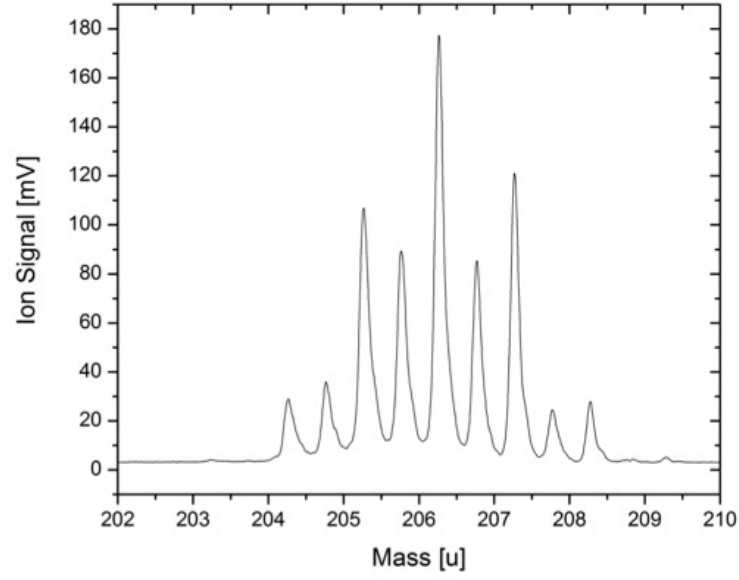
Figure 2.7: PtCl$_6$$^{2-}$ Mass Spectrum.

| Channel | Referenced to | Phase | Component | Width ($\mu$s) | Delay ($\mu$s) |
|---------|---------------|-------|-----------|----------------|----------------|
| A | t$_0$ | 1,2 | Ion Trap | 2-10 | 2000 |
| B | A | 1,2 | TOF Accelerator | 4-10 | 15-60 |
| C | B | 1, 2 | Mass Gate | 1 | 8-15 |
| D | B | 1,2 | Q-Switch and Detector | 2000 | 8-15 |
| E | D | 1 | Flashlamp | 10 | -215 |
| F | B | 1 | Signal Scope | 10 | 0 |
| G | B | 2 | Background Scope | 10 | 0 |

Table 2.4: Pulse timing output for experimental set-up.

the TOF-MS is initiated by a pulse to a set of fast high-voltage, push-pull switches (Behlke, GHTS 60), after the ions ejected from the ion trap have reached the acceleration region. If used, the mass gate is pulsed to ground at the appropriate time after the acceleration pulse. The D channel triggers the laser pulse and pulses the front plate of the MCP as described in the following section. The laser is pulsed at 20 Hz, half the repetition rate of the mass spectrometer, with irradiation of alternating mass-selected ion packets. This allows for correction of baseline fluctuations during the acquisition of a photodissociation spectrum as well as unimolecular decay of the parent species. One oscilloscope, recording the PD signal, is triggered to coincide with the laser-on cycle (channel F), while the other oscilloscope, monitoring the background signal, is triggered to collect data during the laser-off cycle (channel G).

### 2.6.2    Reflectron MCP

The reflectron MCP, used for parent and fragment signal detection, is adjacent to the path of the laser beam such that scattered light from the beam may hit the front of the MCP. At photon energies less than the work function of the MCP, the light will have no effect on the signal. At photon energies above the MCP's work function (greater than $\sim$3.9 eV or 315 nm) however, the laser will cause electrons to be ejected from the MCP surface, inducing a cascade of secondary electrons. This can deplete the charge on the MCP available for ion detection resulting in a reduced detection efficiency and MCP gain. The MCP may not recover from saturation until well after the arrival of the fragment ions. To combat this effect, a series of baffles were put in place to prevent light from reaching the MCP. The components nearby were bead blasted and coated with colloidal graphite to reduce scattering. Saturation of the MCP detector is further reduced by pulsing the front plate of the MCP up to approximately 75% of the back plate voltage while the laser beam passes. This reduces the voltage gradient across the detector and results in a reduced flow of secondary electrons away from the front of the MCP. The timing of pulsing the front plate up is controlled by the same channel that controls the laser timing ensuring that the front plate is pulsed up while the laser beam passes.

### 2.6.3    Correction for Baseline and Unimolecular Decay

In generating a photodissociation action spectrum, we wish to record a measure of the number of fragments formed as a result of photoirradiation only. It is possible, however, for fragments to form from the unimolecular decay of the parent species, independent of the photon energy. Unimolecular decay likely occurs as a result of collisional activation of vibrationally hot parent ions. Upon secondary mass separation in the reflectron and detection, these fragment ions will add to the photoinduced signal. Because the baseline of the ion signal and the unimolecular decay signal may fluctuate over the course of the acquisition of a spectrum, it is necessary to correct for both at each acquired data point. By running the mass spectrum at 40 Hz and the laser pulse at 20 Hz, we are able to alternate between acquiring a background signal and action signal. The background signal is subtracted from the action signal to ensure a zero background over all data points.

### 2.6.4    Fluence Measurements

In order to determine the fragment ion signal dependence on photon fluence, we may take measurement of the fragment signal as a function of average laser power. To obtain a fluence plot, we typically select the wavelength with highest observed cross section. Using a Labview program, we take an average of twenty data points with a two second pause between each data collection event. Plotting ion signal as a function of laser power controlled through the pump power applied, we should see a linear relationship for a one-photon process, as was the case in all systems studied for this thesis.

## 2.7    Data Analysis

### 2.7.1    Requirements for Photodissociation

In order to observe a photodissociation signal, four criteria must be met. First, the ion must be able to absorb a photon at the wavelength selected for irradiation. This is the essence of why this

technique may be used to gain analogous information to a solution UV/Vis absorption spectrum. Because the ability of the molecule to dissociate is related to the absorption cross section, we have access to similar information. Second, the absorption of the photon must result in fragmentation of least one bond within the molecule. As such, the photon energy must be higher than the dissociation energy along some pathway. Third, the excited electronic state that we access must be dissociative or readily couple to a dissociative state. This leads to the fourth criterion, dissociation must take place within the timescale of the experiment, that is in the time it takes for the molecule to travel from the laser interaction region to the reflectron, where mass separation takes place. If fragmentation takes place after mass separation, the fragment species will appear with the parent in any data acquisition.

### 2.7.2    Action Spectra

In taking gas-phase photodissociation data, our aim is to determine a measurement of the absorption cross section and fragment channel-specific photodissociation quantum yield as a function of photon energy. It is through measurement of these values that we may compare with similar values taken in solution and ascertain the parent ion's predisposition towards a particular fragmentation mechanism in the context of its overall chemistry.

When obtaining raw data, we are measuring the number of fragment ions of a particular m/z produced. The number of photoinduced fragment ions formed within the timescale of the experiment, $N(E)$, ideally should be directly related to the parent ion signal, $P_0$, the photon flux ($\phi_p$), as well as the absorption cross section ($\sigma(E)$) and the quantum yield for the fragmentation channel ($Q(E)$) according to:

$$N(E) = P_0 \cdot \phi_p \cdot \sigma(E) \cdot Q(E) \tag{2.12}$$

By rearranging this equation, we may obtain a measure of the product of the absorption cross section and the quantum yield which we define as the photodissoicaiotn cross section [1], $\Omega(E)$,

such that for each fragment ion of interest:

$$\sigma(E) \cdot Q(E) = \Omega(E) = \frac{N(E)}{P_0 \cdot \phi_p} \tag{2.13}$$

By monitoring raw photo fragment signal, normalized to parent ion signal and photon flux, we may directly obtain a measure of the product absorption cross section and quantum yield. In the current iteration of the experimental set-up, we cannot normalize to parent ion signal. Variation in parent ion signal over the period of taking a data set (usually 20 to 30 minutes, depending on the laser region) is very small (between 0 and 5% [1]), so we may correct for any discrepancies by averaging over multiple data sets and reversing the direction of photon energy in scanning.

Certain assumptions are built into this determination. We assume that all parent ions lie within the volume irradiated by the laser beam, which could allow us to normalize to parent ions based on the detected ion signal. While this may not be exactly true, it is likely that the number of ions in the irradiation volume is proportional to the parent ion signal. We further assume that within the irradiation volume, the density of parent ions and photon flux are both uniform. While this is not likely true in the case of parent ion density and certainly not true when considering the laser beam profile, inaccuracies as a result of this assumption are not considered dramatic in the context of the experiment. We also assume that each dissociation event is the result of absorbing only one photon. This assumption can be confirmed for each chemical system and fragment channel observed by determining the correlation between the fragment signal and photon flux as described in the fluence section. Finally, we are not able to obtain absolute branching ratios because the MCP detection efficiency is dependent upon ion kinetic energy, which will be different between parent and fragment ions of different masses.

## 2.8 References

[1] J. Marcum, <u>Electronic Photodissociation Spectroscopy of Electrosprayed Anions</u>. PhD thesis, University of Colorado Boulder, 2011.

[2] J. Marcum, A. Halevi, and J. Weber, "Photodamage to Isolated Mononucleotides: Photodissociation Spectra and Fragment Channels," <u>Physical Chemistry Chemical Physics</u>, vol. 11, pp. 1740–1751, 2009.

[3] M. Yamashita and J. B. Fenn, "Negative ion production with the electrospray ion source," <u>The Journal of Physical Chemistry</u>, vol. 88, no. 20, pp. 4671–4675, 1984.

[4] J. B. Fenn, M. Mann, C. K. Meng, S. F. Wong, and C. M. Whitehouse, "Electrospray ionization for mass spectrometry of large biomolecules," <u>Science</u>, vol. 246, no. 4926, pp. 64–71, 1989.

[5] G. Taylor, "Disintegration of water drops in an electric field," <u>Proceedings of the Royal Society of London. Series A. Mathematical and Physical Sciences</u>, vol. 280, no. 1382, pp. 383–397, 1964.

[6] A. Gomez and K. Tang, "Charge and fission of droplets in electrostatic sprays," <u>Physics of Fluids</u>, vol. 6, p. 404, 1994.

[7] E. Hoffmann, <u>Mass Spectrometry</u>. Wiley Online Library, 1996.

[8] M. A. Kelly, M. M. Vestling, C. C. Fenselau, and P. B. Smith, "Electrospray analysis of proteins: A comparison of positive-ion and negative-ion mass spectra at high and low pH," <u>Organic Mass Spectrometry</u>, vol. 27, no. 10, pp. 1143–1147, 1992.

[9] D. Gerlich, "Inhomogeneous, RF fields: a versatile tool for the study of processes with slow ions," <u>Advances in Chemical Physics</u>, vol. 82, pp. 1–176, 1992.

[10] R. M. Jones, D. Gerlich, and S. L. Anderson, "Simple radio-frequency power source for ion guides and ion traps," <u>Review of Scientific Instruments</u>, vol. 68, no. 9, pp. 3357–3362, 1997.

[11] A. Luca, S. Schlemmer, I. Cermák, and D. Gerlich, "On the combination of a linear field free trap with a time-of-flight mass spectrometer," <u>Review of Scientific Instruments</u>, vol. 72, no. 7, pp. 2900–2908, 2001.

[12] G. Riddle, "Electrostatic einzel lenses with reduced spherical aberration for use in field-emission guns," <u>Journal of Vacuum Science and Technology</u>, vol. 15, no. 3, pp. 857–860, 1978.

[13] W. Wiley and I. H. McLaren, "Time-of-flight mass spectrometer with improved resolution," <u>Review of Scientific Instruments</u>, vol. 26, p. 1150, 1955.

[14] C. W. Stoermer, S. Gilb, J. Friedrich, D. Schooss, and M. M. Kappes, "A high resolution dual mass gate for ion separation in laser desorption/ionization time of flight mass spectrometry," <u>Review of Scientific Instruments</u>, vol. 69, no. 4, pp. 1661–1664, 1998.

[15] B. Mamyrin, V. Karataev, D. Shmikk, and V. Zagulin, "The mass reflectron, a new non-magnetic time-of-flight mass spectrometer with high resolution," <u>Zhurnal Eksperimentalńoi i Teoreticheskoi Fiziki</u>, vol. 64, pp. 82–89, 1973.

[16] J. T. Verdeyen, <u>Laser Electronics</u>. Prentice Hall, Englewood Cliffs, NJ, 1989.

[17] R. W. Boyd, <u>Nonlinear Optics</u>. Academic press, 2003.

<div align="center">

**Chapter 3**

**Spectroscopy and Photochemistry of Sodium Chromate Ester Cluster Ions**

</div>

This chapter has been adapted with permission from:

## 3.1    Background

The chemistry of chromate is of tremendous scientific interest because of its many industrial and scientific applications as well as its biological and environmental hazards. From holograms to pigments to catalysts and photosensitizers [1–4], chromium compounds are used for a range of technologies. Consequently, their solution chemistry has been studied extensively, not only to improve their application but also to study their effects on the environment and to determine routes towards remediation of polluted areas.

Chromium was named for the variety of colors it can assume depending on its charge state and the other atoms in the molecule. In industry, it is used primarily for two of its most unique properties: its color and hardness. Since 1985, more than 300 million pounds of chromate species have been extracted and used for chromium plating, pigments, and as a chemical oxidizer [5].

Chromium(VI) is a well-documented carcinogen [6, 7] and environmental pollutant. It is thought that the mutagenic potency of chromate stems from its mobility across the cell membrane combined with the intermediates formed as Cr(VI) is reduced to Cr(V) and Cr(IV), as well as

the reactive organic radicals produced concurrently [8–10]. Due to the high solubility of Cr(VI), chromate pollution has been identified in tap water in 42 states [11]. In contrast, Cr(III), the most stable oxidation state of chromium, is biologically inert, insoluble in water, and thus geologically less mobile. There is also evidence that Cr(III) may support essential cell functions in mammals [12].

Because many Cr(III) compounds are insoluble in water and not a biological hazard, remediation of Cr(VI) by reduction to Cr(III) has been a subject of study by environmental chemists [13–16] but the mechanism by which this process occurs is still not well understood. In solution, chromium may exist in a number of species making remediation of all Cr(VI) extremely difficult. The form of chromium is also particularly sensitive to the pH of the solution [17]. There is significant evidence to indicate that sunlight plays an important role in natural degradation of Cr(VI) to Cr(III) [18,19] In chromate-polluted waters, a stratification exists wherein the concentration of Cr(VI) in the shallower, sunlit layer of water is much lower than in deeper water which experience reduced solar flux. As the Cr(VI) is reduced to Cr(III), it precipitates out of solution. As such, there has been a significant focus of research on chromate reduction as a primary step towards remediation. Other types of remediation largely focus on chemical adsorption [16, 20].

Obtaining a greater understanding of the molecular level picture by which chromate is reduced, specifically the process of photodinduced reduction, may help in designing better ways to monitor [21] and remove Cr(VI) from waterways and drinking supplies.

All chromate redox reactions have been found to be photosensitive, but some occur exclusively in the presence of light [22]. Chromate (VI) has a $d^0$ electron configuration. Its sensitivity towards light stems from the formation of coordination complexes in solution that can undergo ligand-to-metal charge transfer (LMCT), as a consequence of which chromium reduction may occur.

Chromates are important agents for the oxidation of organic species, but questions about the active mechanisms remain [23–26]. Many reaction mechanisms have been suggested to describe the chromate-induced oxidation of alcohols including the formation of cyclic chromate esters [27] and various electron transfer pathways [28]. Chromate esters have been of interest since they were first observed in the late 1800's [29], and much work has been done to improve our understanding of their

chemistry in solution. Experimental evidence suggests [30–34] that chromate esters form quickly in reactions of alcohols with what is thought to be the main reactive form of chromate, $HCrO_4^-$, especially at low pH. The chromate esters undergo a slow intramolecular redox reaction during which a Cr(V) [25,35] or Cr(IV) species is formed [36]. Chromium species in high oxidation states will continue to abstract electrons from reaction partners in solution until Cr(III), its most stable oxidation state, is formed [37]. It is widely believed that in strong acids, the slow redox step involves the transfer of two electrons [38], bypassing the Cr(V) oxidation state as well as the formation of an organic radical. Without the presence of excess acid, EPR data suggest that a one electron, outer sphere electron transfer mechanism occurs, resulting in the formation of Cr(V) and an organic radical [39,40]. Because of the reactivity of the intermediates formed (Cr(V) and Cr(IV) as well as organic oxyradicals), it is difficult to differentiate primary intermediates in solution, formed during the initial chromate ester redox reaction, from the cascade of secondary and tertiary products.

The presence of many different species in any solution makes the understanding of the molecular level properties of the key species from solution data alone challenging at best. Experiments on mass-selected ions are a powerful tool to investigate molecular level photochemical properties of ionic species [41–46] and thereby circumvent many of the problems caused by speciation in solution [47, 48]. In the present study, we perform photodissociation spectroscopy on chromate ester cluster ions isolated in the gas phase. We investigate the spectroscopic properties of $Na_n[CrO_3(OCH_3)]_{n+1}^-$ ions ($n = 1, 2$) as well as their fragmentation pathways to obtain molecular level information on the mechanisms involved in chromate photochemistry.

## 3.2    Computational Methods

Geometry optimizations of relevant species were performed using density functional theory [49] (DFT) as implemented in the TURBOMOLE suite of programs [50,51] (V5.9.1 and V6.2), employing the B3-LYP functional and def2-TZVP basis sets [52, 53] for all atoms. All geometry optimizations were performed without symmetry restrictions. The obtained DFT energies were corrected for zero-point energy by analytical calculation of harmonic frequencies using the

AOFORCE program [54]. We performed time-dependent density functional theory (TDDFT) calculations to obtain the absorption spectrum of the chromate ester monomer, $CrO_3(OCH_3)^-$, also using def2-TZVP basis sets and the B3-LYP functional. Estimates of threshold energies for various fragmentation pathways were calculated using a simple Hess's Law approach and subtracting zero-point energy-corrected internal energies of the reactants from those of the products. Threshold energies were also corrected for the internal energies of the parent species to more accurately compare computed threshold energies with experimental values according to,

$$U_{vib} = \sum_i \frac{h\nu_i}{(e^{h\nu_i/kT} - 1)} \tag{3.1}$$

where $h$ is Planck's constant, $\nu_i$ is the $i$th vibrational frequency, $k$ is the Boltzmann constant, and T is the temperature of the ions, assumed to be 300 K, given by the temperature of the hexapole ion trap where thermal equilibrium is established.

## 3.3    Results and Discussion

### 3.3.1    Mass Spectrometry

Electrospray ionization mass spectra of a solution of $Na_2Cr_2O_7$ in methanol/water (1:1) in anion mode show intense mass peaks around m/z = 285 u and 439 u (see Figure 3.1). Reaction products between Cr(VI) and methanol had been observed by Hedlam and Lay, but not definitively identified [55]. Later work by the O'Hair group [56] identified a peak at m/z = 131 u as the methyl chromate ester $CrO_3(OCH_3)^-$, but no chromate ester clusters were reported. The isotope patterns of the mass peaks observed in this study indicate that the lighter species contains two chromium atoms, the heavier species contains three chromium atoms, and all ions are singly charged. We will therefore refer to the mass of fragment ions rather than the mass-to-charge ratio in the remainder of this chapter. In order to clearly identify the composition of these ions, we sprayed the same dichromate salt from deuterated methanol ($CD_3OD$) and from ethanol/water mixtures. Electrospray from $CD_3OD$ resulted in a peak pattern for the lower (higher) mass signature that

Figure 3.1: Mass spectrum of chromate ester cluster ions $Na_n[CrO_3(OCH_3)]_{n+1}{}^-$ where n = 1,2, obtained by electrospray ionization of a solution of $Na_2Cr_2O_7 \cdot 2H_2O$ in methanol/water in anion mode.

was shifted by +6 u (+9 u), while spraying from ethanol/water mixtures shifted the pattern by +28 u (+42 u), indicating that the original ion contained two (three) methyl groups. We identify the two intense features observed in the mass spectrum as $Na_n[CrO_3(OCH_3)]_{n+1}^-$ where $n = 1$ for the lower mass feature and $n = 2$ for the heavier species. The most abundant masses in the isotope distribution are $(284.8 \pm 0.5)$ u and $(438.4 \pm 0.5)$ u, in excellent agreement with the calculated masses of 284.8 u and 438.8 u. In the remainder of this chapter, we refer to the lower mass species as "chromate ester dimer" or simply "dimer", and the heavier species as "trimer". Our findings are reminiscent of results by Nagy-Felsobuki and coworkers [57] who observed polyoxochromate cluster species in ESI-MS experiments. The calculated lowest energy structures of the dimer and trimer ions are shown in Figure 3.2.



Figure 3.2: Calculated geometries of the chromate ester dimer (A) and trimer (B) parent anions. Na: grey; Cr: yellow; O: red; C: black; H: white.

It is worth noting that while while we also observed the methyl chromate ester monomer in the mass spectrum, $CrO_3(OCH_3)^-$, we did not detect photodissociation products from the this parent ion in tests with photon energies up to 5.6 eV. The lack of photoproduct could be a result of

the low kinetic energy of photoproduct produced or that light-induced fragmentation is hindered in the monomer in contrast to the cluster. Evidence for this last point is supported by the concerted fragmentation mechanism seen in the dimer and trimer, as discussed later in this chapter. O'Hair and coworkers [56] report collision-induced dissociation of this species, yielding $CrO_2(OH)^-$ product ions, but they did not report threshold energies for the observation of this process.

The dimer parent ion is calculated to be in a singlet ground state (lower than the triplet by 1.6 eV). Similarly, the lowest energy singlet state of the trimer parent ion is 1.8 eV more stable than the lowest energy triplet state. The individual anionic chromate ester units are held together by $Na^+$ counter-ions. In the dimer, the oxygen atoms of the methoxy groups point towards each other. Likewise, we observe that two of the methoxy groups are pointing at each other across the gaps occupied by the $Na^+$ counter-ions in the trimer. The proximity of these groups may play an important role in the fragmentation processes.

### 3.3.2    Photodissocation of the Chromate Ester Dimer Anion

The photodissociation spectra were acquired using the ESI-TOF instrument described in the Experimentation chapter. A solution of approximately 10 mM $Na_2Cr_2O_7 \cdot 2H_2O$ (Sigma-Aldrich, ACS Reagent, 99.5%) in 1:1 methanol/water was electrosprayed to produce the chromate ester ions of interest. The only fragment channel observed upon irradiation with photons in the energy range of 2 to 5.6 eV, of the dimer is the formation of a species of m = 223 u. A search for other fragments was conducted within the peak regions at 2.75 eV, 3.5 eV and 4.7 eV, but no other fragments were observed. Irradiation of the parent ions $Na[CrO_3(OCD_3)]_2^-$ (sprayed from deuterated methanol/water) and $Na[CrO_3(OC_2H_5)]_2^-$ (sprayed from ethanol/water) resulted in fragment ions with the same mass. Based on this finding, we identify the fragment ion as $NaCr_2O_6^-$, which in principle amounts to the net loss of two methoxy units from the dimer parent ion.

The corresponding photodissociation action spectrum is shown in Figure 3.3, along with the UV/Vis absorbance spectrum of a solution of $Na_2Cr_2O_7 \cdot 2H_2O$ (Sigma-Aldrich, ACS Reagent, 99.5%) dissolved in a 1:1 mixture of methanol and water, acquired using a Varian Cary 500 Scan

UV-visible-NIR spectrometer (version 8.01) with a 10 mm path length, 1 nm step size, 2 nm resolution, and integration time of 0.1 s.

The photodissociation spectrum shows the same features as the UV/vis absorption spectrum of the $Na_2Cr_2O_7$ solution. Interestingly, the spectrum is characteristic for species related to chromate, $CrO_4{}^{2-}$, rather than dichromate, $Cr_2O_7{}^{2-}$ [58,59]. The spectral signature of Cr(V), a peak at about 1.65 eV (750 nm), is not observed nor is that of Cr(III), expected at 2.18 eV (570 nm). The observation of species more closely related to chromate in the sample solution is due to the following equilibrium:

$$Cr_2O_7^{2-} + H_2O \rightleftharpoons 2CrO_4^{2-} + 2H^+ \tag{3.2}$$

The chromate ions thus formed may react either in solution or during the electrospray process to form the chromate ester based species observed in the ESI mass spectra. We note that the overall shape of the UV/vis spectrum of the sample solution does not change significantly upon changing the concentration from 50 mM to 50 $\mu$M. Assuming that the chromophore species in solution are predominantly monomeric chromate based ions, it is interesting to compare the experimental UV/vis spectrum with the calculated spectrum of a chromate ester monomer anion, $CrO_3(OCH_3)^-$. This calculated spectrum (shown in Figure 3.3) shows remarkable agreement with the experimental photodissociation and UV/vis absorption spectra and allows assignment of the observed transitions. The electronic excitations of the chromate ester in the energy range probed here are all ligand-to-metal charge transfer (LMCT) transitions, as expected for a $d^0$ Cr(VI) complex. Some of the features are calculated to be up to 0.4 eV higher in energy compared to the experimental spectrum. However, the overall pattern recovers the experimental photodissociation spectrum well. The main contributions to the electronic transitions in this energy range are given by charge transfer from $2p$ oxygen atomic orbitals to the nearest chromium atom. The band calculated at around 3.88 eV involves the oxygen orbitals on the chromate ester bridge, while the transitions at 3.14 eV and 4.50 eV originate mostly on the other three oxygen ligands. It is unclear whether the transfer

Figure 3.3: Top: Photodissociation spectrum of the chromate ester dimer obtained by monitoring the m = 223 u fragment channel as a function of photon energy. Open circles represent photodissiociation action data points. The full line shows the UV/Vis absorbance spectrum of a 0.5 mM solution of $Na_2Cr_2O_7$ in a methanol/water mixture (1:1). Bottom: Calculated excitation energies of the chromate ester monomer $CrO_3(OCH_3)^-$ from TDDFT calculations. The oscillator strengths of individual transitions are given by the vertical bars. The full line represents a convolution of the excited state spectrum with a Gaussian (0.2 eV FWHM).

of electron density away from the organic portion of the molecule is substantial enough to sever the chromate ester bridge directly. Alternatively, fast relaxation into lower electronic states may eventually promote the fragmentation reaction via a vibrationally hot ion. The similarity of the UV/vis absorption spectrum and the photodissociation spectrum suggests that there is little to no specificity with respect to the excited state, rendering direct bond cleavage on the excited state surface unlikely. The similarity also indicates that the fragmentation time is short compared to the 20 $\mu$s observation window in our experiment (i.e. the time between irradiation and the second mass separation in the reflectron). The fluence dependence of the observed fragment ion intensity confirms that one photon is sufficient to initiate the fragmentation process.

The remarkable similarity between the gas-phase and solution electronic spectra and the minimal solvatochromic shifts show that the electronic environment of the orbitals involved in transitions resulting in photodissociation are only minimally perturbed by the presence of solvent or counterions.

Interestingly, we did not observe the formation of either methoxy anion or dimethyl peroxide anion which would result if one or both of the chromium centers was not reduced during fragment formation (i.e. the charge departing with the organic fragment). It is possible that the detection efficiency for these lighter fragments is insufficient to allow observation, due to their low kinetic energy upon fragmentation. Similarly, we do not observe the formation of an ionic fragment corresponding to the reduction of only one chromium atom (i.e. loss of only one methoxy group or of a formaldehyde molecule).

Geometry optimization of the product anion, starting by removal of the methoxy groups from the parent anion, leads to a chromium(V) trioxide dimer dianion in a complex with a sodium counter cation. Our calculations indicate that loss of the methoxy moieties from the parent ion results in the formation of a cohesive chromium oxide framework rather than two independent chromium oxide ions (see Figure 3.4). The spin state of the fragment ion can be a singlet or a triplet, and the triplet state is calculated to be lower by 0.6 eV.

The relative positions of the two methoxy groups in the parent ion may necessary for the

Figure 3.4: Calculated structure of the $Na(CrO_3)_2^-$ photodissociation product ion of the chromate ester dimer parent ion. Na: grey; Cr: yellow; O: red.

formation of the fragment, since their proximity may be necessary to cooperatively induce oxidation of the organic group and concomitant reduction of the chromates.

### 3.3.3    Photodissocation of the Chromate Ester Trimer Anion

Electronic excitation of the trimer anion results in the observation of four fragment ion channels with masses 223 u, 285 u, 347 u and 377 u. The fragment with m = 223 u is identical to the $Na(CrO_3)_2^-$ photofragment generated upon excitation of the dimer parent ion, and the fragment with m = 285 u is identical with the dimer parent ion, $Na[CrO_3(OCH_3)]_2^-$. The calculated structures of the other two fragment ions are shown in Figure 3.5.

The photodissociation action spectra for these fragment ions are shown in Figure 3.6. Different fragment channels are active in different photon energy regions, but the overall shapes of the spectra recover the bands of the UV/vis absorption spectrum, similar to the dimer photodissociation action spectrum discussed above.

The formation of the fragment with m = 377 u corresponds to the loss of two of the parent ions and three methoxy units:

$$Na_2[CrO_3(OCH_3)]_3^- \xrightarrow{h\nu} Na_2(CrO_3)_2[CrO_3(OCH_3)]^- + (2O, 2C, 6H) \tag{3.3}$$

The third chromate ester unit is not reduced in this fragment channel. The fragmentation threshold occurs at the onset of absorbance of the chromate species, similar to the dimer parent ion case. Fragment action for this channel vanishes at ca. 4 eV, probably indicating that energy

Figure 3.5: Calculated geometries of fragment ions from the trimer parent ion. A: fragment mass 347 u. B: fragment mass 377 u. Na: grey; Cr: yellow; O: red; C: black; H: white.

Figure 3.6: Top panel: UV/Vis absorbance of 0.5 mM solution of $Na_2Cr_2O_7$ in a methanol/water mixture (1:1). Lower panels: Normalized photodissociation spectra of the four fragment channels observed from the chromate ester trimer. The fragment mass for each channel is shown.

deposited into the parent ion is too large for this fragment ion to survive without further reactions. In the second fragment channel (m = 347 u), all three of the chromate ester units are reduced:

$$\text{Na}_2[\text{CrO}_3(\text{OCH}_3)]_3^- \xrightarrow{h\nu} \text{Na}_2(\text{CrO}_3)_2[\text{CrO}_2\text{OH}]^- + (3\text{O}, 3\text{C}, 8\text{H}) \qquad (3.4)$$

The calculated structure of the product ion closely matches that of bulk chromium trioxide [60], suggesting the continuation of the polymerization reaction found for the dimer parent ion. The position of the H atom as shown represents the lowest energy isomer. Although the other isomers are higher in energy by 0.65 eV and more, we note that the H atom could be kinetically trapped at other oxygen atoms if the primary fragmentation reactions form higher energy isomers. The fragmentation reaction is accessible across the whole observed absorption spectrum. Comparison of the photodissociation action spectrum with the UV/vis absorption spectrum of the solution shows that the features below ca. 4 eV photon energy are suppressed. This may be due to competition with partial reduction channel which disappears at roughly the same photon energy. The fragment with m = 285 u corresponds to the loss of a neutral chromate ester sodium salt unit, resulting in the formation of the chromate ester dimer ion:

$$\text{Na}_2[\text{CrO}_3(\text{OCH}_3)]_3^- \xrightarrow{h\nu} \text{Na}[\text{CrO}_3(\text{OCH}_3)]_2^- + \text{Na}[\text{CrO}_3(\text{OCH}_3)] \qquad (3.5)$$

While the overall spectrum looks very similar to that of other fragment channels, no reductive fragmentation occurs, suggesting that specific excitations do not predetermine the fragmentation channel, but that fragmentation rather occurs via rapid relaxation into vibrationally hot lower electronic states. This is consistent with our interpretation of the dimer photodissociation spectrum. Similar to the fragmentation of the dimer parent ion, a fragment with mass m = 223 u is formed, corresponding to a combination of chromium reduction and loss of a neutral salt unit,

$$\text{Na}_2[\text{CrO}_3(\text{OCH}_3)]_3^- \xrightarrow{h\nu} \text{Na}(\text{CrO}_3)_2^- + \text{Na}[\text{CrO}_3(\text{OCH}_3)] + (2\text{O}, 2\text{C}, 6\text{H}) \qquad (3.6)$$

The fragment action in this channel increases strongly at ca. 4 eV. Loss of flux at lower

energies is probably due to competition with the partial reduction channel (m = 377 u), similar to the suppression of the lower energy signatures in the full reduction channel (see above).

## 3.4    Organometallic Redox Mechanism

Electron transfer reactions of chromate are thought to occur either through a covalent bond (inner-sphere mechanism) with significant molecular rearrangement, or by a Marcus-type (outer-sphere) mechanism without significant change to the geometry and environment of the redox pair. Marcus Theory is most often used to describe redox reactions in solution. The rate of electron transfer results from the thermodynamic driving force between the redox pair, that is the difference in the redox potentials of the electron-exchanging sites [61].

The prevalence of one mechanism over the other is determined by the strength of the chromate ester bridge formed between the chromate and the electron donor [35]. For an aliphatic chromate ester (as is the case here), the inner sphere mechanism can be characterized as a two-electron reduction of the metal from Cr(VI) to Cr(IV). This involves cleaving the CO bond of the chromate ester bridge concomitant with formation of a Cr-O-H bond and oxidation of the electron donor to a ketone or aldehyde (Figure 3.7). Starting from the chromate ester, this reduction may be either thermally or photoinduced.



Figure 3.7: Inner sphere mechanism of a methyl chromate ester. The metal center is reduced from Cr(VI) to Cr(IV).

In contrast, an outer sphere process, observed only upon photoexcitation, results in transfer of one electron from the alkoxy residue to the metal (Figure 3.8), leading to production of an organic radical along with Cr(V) [35].

48



Figure 3.8: Outer sphere mechanism of a methyl chromate ester. The metal center is reduced from Cr(VI) to Cr(V).

In solution, the Cr(V) species may quickly oxidize available reaction partners [57]. The reactivity of the species produced makes it difficult to study them in solution, although much work has been done to describe these reactions more completely. In the case of the chromate ester dimer, we observe a net transfer of two electrons, one for each methoxy unit lost. In principle, the reactions that could be at play for the case of the dimer may take place as described in one of the following two ways: In the first scenario, the dimer undergoes an outer shell one-electron transfer onto one chromate ester unit, leading to the formation of a transient methoxy radical. This radical subsequently reacts with the second chromate ester, abstracting its methoxy unit, thus both chromium centers are thus reduced to Cr(V):

$$\mathrm{Na[Cr^{VI}O_3(OCH_3)]_2^-} \xrightarrow{h\nu} \mathrm{Na(Cr^VO_3)[Cr^{VI}O_3(OCH_3)]...CH_3O} \rightarrow \mathrm{Na(Cr^VO_3)_2^- + (CH_3O)_2} \quad (3.7)$$

The calculated fragmentation threshold for the dimethyl peroxide product, correcting for the internal energy of the room temperature parent ions, is 2.8 eV for a singlet fragment ion (2.3 eV for the triplet). In contrast, the formation of two isolated methoxy radicals (assuming no additional barrier) is about 1.66 eV [62, 63] higher, resulting in a threshold of $\sim$4.0 eV for a triplet fragment ion and $\sim$4.5 eV for a singlet fragment, both of which are incompatible with the experimentally observed onset of the photodissociation spectrum. Assuming that no spin flip occurs, the $\mathrm{Na(Cr^VO_3)_2^-}$ product ion will be a singlet, but we cannot unambiguously rule out a spin flip in this process. The calculated threshold energies are consistent with either fragment multiplicity. Alternatively, an inner shell two-electron transfer could take place via intramolecular H-transfer from the methoxy group to form formaldehyde and a $\mathrm{HCrO_3^-}$ ion with a Cr(IV) metal center. The $\mathrm{HCr^{IV}O_3^-}$ ion would then react with the second chromate ester unit to form methanol.

During this process, the two chromium centers comproportionate to Cr(V):

$$\mathrm{Na[Cr^{VI}O_3(OCH_3)]_2^-} \xrightarrow{h\nu} \mathrm{Na(Cr^{IV}O_2OH)[Cr^{VI}O_3(OCH_3)]^-} + \mathrm{CH_2O} \tag{3.8}$$

$$\mathrm{Na(Cr^{IV}O_2OH)[Cr^{VI}O_3(OCH_3)]^-} \rightarrow \mathrm{Na(Cr^VO_3)_2^-} + \mathrm{CH_3OH} \tag{3.9}$$
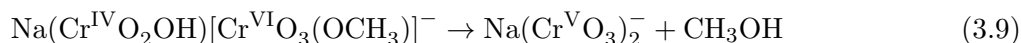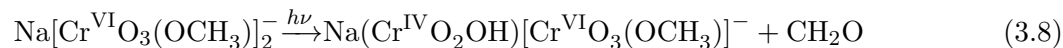
In the initial process, shown in equation (1.8), electron transfer leads to formation of formaldehyde and a Cr(IV) atom, with a threshold calculated to be only ca. 0.9 eV, which is the lowest threshold energy of any of the processes in our calculations. However, the product ion is in a triplet and therefore requires a spin flip process.

In the case of full reduction of the trimer parent ion, the formation of the m = 347 u fragment suggests that the last chromate ester reacts by formaldehyde formation. This is evidence for a two-electron inner sphere mechanism in this process and is consistent with the collision-induced dissociation results of O'Hair and coworkers [56]. This photoabsorption and subsequent reduction, which may be thought of formally as a hydride transfer presents the most striking evidence for a two-electron process like that suggested to occur in solution. However, we note that we cannot completely rule out that the outer sphere mechanism may contribute during dimer fragmentation. Formally, this channel corresponds to two of the Cr centers being reduced to Cr(V), while the last one is in oxidation state (VI). The fragmentation mechanism of the clusters is not clear and cannot be determined by the photofragment mass spectra. However, since all fragmentation processes are triggered by absorption of just one photon, the second and third reduction steps are likely to be the result of a vibrationally hot intermediate.

The geometry optimization of the full photoreduction fragment bears a striking resemblance to the bulk form of Cr(III) oxide, the most naturally abundant chromium compound. This may suggest that the central Cr has a formal charge of 3+, rather than all three chromiums having the same 5+ charge. By extension, it may be possible for one photon to set off a chain reaction in larger gas-phase sodium chromate ester clusters resulting in continued polymerization of the

species. Cr(III) oxide would be a particularly good end product for remediation techniques given its insolubility in water, imperviousness to both acids and bases, and its biological inertness [64].

Finally, the absence of the observation of photofragment ions from the monomer parent ion, $Cr^{VI}O_3(OCH_3)^-$, is puzzling. While we cannot draw too firm a conclusion from the lack of evidence of photofragmentation, it may indicate that the barrier for dissociation of a bare chromate ester ion is significantly lowered in clusters and in the condensed phase, possibly due to solvation effects or caused by the presence of a neighboring reaction partner (here a chromate ester within the cluster). Another possibility is that the initial redox step forming Cr(IV) requires a spin-flip. This process could be mediated by the presence of a collision partner (i.e. in the cluster, in the condensed phase or even in collisional activation [56]), which is absent for the monomer.

## 3.5    Summary and Conclusions

We have identified chromate ester cluster ions $Na_n[CrO_3(OCH_3)]_{n+1}^-$ as prominent species in ESI mass spectrometry of a solution of $Na_2Cr_2O_7$ in a methanol/water mixture, notably the dimer and trimer anions, $Na[CrO_3(OCH_3)]_2^-$ and $Na_2[CrO_3(OCH_3)]_3^-$.

The photodissociation spectra of these ions are very similar to the UV/vis absorption spectrum of the sample solution with solvatochromic shifts less than 0.1 eV. The dominant bands in the electronic spectra can be assigned to LMCT transitions shifting electron density from the oxygen atoms onto the Cr centers [65]. The similarity of UV/vis, and the dimer and trimer photodissociation spectra suggests that solvation and clustering does not significantly change the observed LMCT bands.

Photoexcitation of the dimer parent ion results in reductive fragmentation involving the cleavage of both chromate ester bonds and concomitant loss of both methoxy residues, resulting in the formation of a $Na(CrO_3)_2^-$ ion with polymerization of the chromium(V) trioxide subunits. Photoexcitation of the trimer ion leads to reduction of two or all three of the metal centers from Cr(VI) to Cr(V), to (non-reductive) evaporation of neutral chromate ester salt units, or to a combination of reductive and non-reductive processes. The observation of complete reduction of the

trimer parent ion consistent with formaldehyde formation suggests that the redox reaction occurs as a two-electron, inner sphere transfer process.

All reductive pathways observed involve absorption of a photon by the largely ligand-based 2p orbitals. In those pathways resulting in reductive fragmentation, absorption of the photon then results in a LMCT in one of the chromate ester monomers present in the cluster. This electronic transition is followed by a dramatic change in geometry, resulting in reduction in the adjacent chromate ester and bridge formation between the metal centers. This process may possibly suggest that a single photon may induce a reductive chain reaction leading to a structure similar to that observed in bulk $Cr^{III}_2O_3$.

## 3.6    References

[1] C. Pizzocaro, C. Lafond, and M. Bolte, "Dichromated polyvinylalcohol: key role of chromium (V) in the properties of the photosensitive material," <u>Journal of Photochemistry and Photobiology A: Chemistry</u>, vol. 151, no. 1, pp. 221–228, 2002.

[2] J. M. Jehng, I. E. Wachs, B. M. Weckhuysen, and R. A. Schoonheydt, "Surface chemistry of silica-titania-supported chromium oxide catalysts," <u>Journal of the Chemical Society, Faraday Transactions</u>, vol. 91, pp. 953–961, 1995.

[3] H. Guo, C. Dong, D. Kim, D. Urabe, J. Wang, J. Kim, X. Liu, T. Sasaki, and Y. Kishi, "Toolbox Approach to the Search for Effective Ligands for Catalytic Asymmetric Cr-Mediated Coupling Reactions," <u>Journal of the American Chemical Society</u>, vol. 131, no. 42, pp. 15387–15393, 2009. PMID: 19795862.

[4] C. Pizzocaro, M. Bolte, and M. Hoffman, "Polymerization of acrylamide photosensitized by the tris-(bipyridine)chromium(III) ion in aqueous solution," <u>Polyhedron</u>, vol. 12, no. 8, pp. 855 – 858, 1993.

[5] J. Speight, "Ullmann's encyclopedia of industrial chemistry," <u>Petroleum Science and Technology</u>, vol. 17, no. 3-4, pp. 445–445, 1999.

[6] P. Connett and K. Wetterhahn, <u>Metabolism of the carcinogen chromate by cellular constituents</u>, vol. 54 of <u>Inorganic Elements in Biochemistry</u>. Springer Berlin Heidelberg, 1983.

[7] A. Levina, L. Zhang, and P. Lay, "Structure and Reactivity of a Chromium(V) Glutathione Complex," <u>Inorganic Chemistry</u>, vol. 42, no. 3, pp. 767–784, 2003.

[8] M. I. Frascaroli, S. Signorella, J. C. Gonzalez, M. F. Mangiameli, S. Garcia, E. R. de Celis, L. Piehl, L. F. Sala, and A. M. Atria, "Oxidation of 2-amino-2-deoxy-d-glucopyranose by Hypervalent Chromium: Kinetics and Mechanism," <u>Polyhedron</u>, vol. 30, no. 11, pp. 1914 – 1921, 2011.

[9] A. Levina and P. Lay, "Mechanistic studies of relevance to the biological activities of chromium," <u>Coordination Chemistry Reviews</u>, vol. 249, pp. 281 – 298, 2005. Inorganic Reaction Mechanisms, an appreciation of Henry Taube in his 90th year.

[10] K. Jennette, K. Wetterhahn, "Microsomal Reduction of the Carcinogen Chromate Produces Chromium(V)," <u>Journal of the American Chemical Society</u>, vol. 104, no. 3, pp. 874–875, 1982.

[11] R. Sutton, "Chromium-6 in U.S. Tap Water," tech. rep., Environmental Working Group, 12 2010.

[12] W. Mertz, "Chromium in Human Nutrition: A Review," <u>The Journal of Nutrition</u>, vol. 123, no. 4, pp. 626–633, 1993.

[13] S. Ponder, J. Darab, and T. Mallouk, "Remediation of Cr(VI) and Pb(II) Aqueous Solutions Using Supported, Nanoscale Zero-Valent Iron," <u>Environmental Science And Technology</u>, vol. 34, no. 12, pp. 2564–2569, 2000.

[14] D. Blowes, C. Ptacek, and J. Jambor, "In-Situ Remediation of Cr(VI)-Contaminated Groundwater Using Permeable Reactive Walls: Laboratory Studies," Environmental Science And Technology, vol. 31, no. 12, pp. 3348–3357, 1997.

[15] D. Mohan and C. Pittman Jr., "Activated carbons and low cost adsorbents for remediation of tri- and hexavalent chromium from water," Journal of Hazardous Materials, vol. 137, no. 2, pp. 762 – 811, 2006.

[16] R. Powell, R. Puls, S. Hightower, and D. Sabatini, "Coupled Iron Corrosion and Chromate Reduction: Mechanisms for Subsurface Remediation," Environmental Science And Technology, vol. 29, no. 8, pp. 1913–1922, 1995.

[17] R. Tandon, P. Crisp, J. Ellis, and R. Baker, "Effect of pH on chromium (VI) species in solution," Talanta, vol. 31, no. 3, pp. 227–228, 1984.

[18] K. Abu-Saba, D. Sedlak, and A. Flegal, "Indirect reduction of hexavalent chromium by copper in the presence of superoxide," Marine Chemistry, vol. 69, pp. 33 – 41, 2000.

[19] R. Kieber and G. Helz, "Indirect Photoreduction of Aqueous Chromium(VI)," Environmental Science And Technology, vol. 26, no. 2, pp. 307–312, 1992.

[20] M. Ghiaci, R. Kia, A. Abbaspur, and F. Seyedeyn-Azad, "Adsorption of chromate by surfactant-modified zeolites and MCM-41 molecular sieve," Separation and Purification Technology, vol. 40, no. 3, pp. 285–295, 2004.

[21] R. Güell, C. Fontàs, V. Salvadó, and E. Anticó, "Development of a selective optical sensor for Cr(VI) monitoring in polluted waters," Analytica Chimica Acta, vol. 594, no. 2, pp. 162–168, 2007.

[22] M. Mitewa, A. Malinovski, P. Bontchev, and K. Kabassanov, "ESR study on chromium(V) complexes formed in the process of photochemical oxidation of diethylene glycol by dichromate," Inorganica Chimica Acta, vol. 8, no. 0, pp. 17 – 23, 1974.

[23] E. Pérez-Benito and E. Rodenas, "Methanol and ethanol oxidation by chromium (VI) in aqueous perchloric acid," Transition Metal Chemistry, vol. 18, no. 3, pp. 329–334, 1993.

[24] S. Chen, S. Huang, P. Chiang, J. Liu, W. Kuan, J. Huang, J. Hung, Y. Tzou, C. Chen, and M. Wang, "Influence of chemical compositions and molecular weights of humic acids on Cr(VI) photo-reduction," Journal of Hazardous Materials, vol. 197, no. 0, pp. 337 – 344, 2011.

[25] J. C. González, S. Garcıa, N. Mamana, L. F. Sala, and S. Signorella, "Evidence for the involvement of Cr(II) and free radicals as intermediates in the reduction of $HCrO_4^-$ by saccharides, alcohols and hydroxyacids," Inorganic Chemistry Communications, vol. 9, pp. 437–440, 2006.

[26] T. Waters, X. Wang, S. Li, B. Kiran, D. Dixon, and L. Wang, "Electronic Structure of the Hydroxo and Methoxo Oxometalate Anions $MO_3(OH)^-$ and $MO_3(OCH_3)^-$ (M = Cr, Mo, and W)," The Journal of Physical Chemistry A, vol. 109, no. 51, pp. 11771–11780, 2005.

[27] D. Lee and T. Chen, "The oxidation of alcohols by permanganate. A comparison with other high-valent transition-metal oxidants," The Journal of Organic Chemistry, vol. 56, no. 18, pp. 5341–5345, 1991.

[28] P. Cieśla, P. Kocot, P. Mytych, and Z. Stasicka, "Homogeneous photocatalysis by transition metal complexes in the environment," Journal of Molecular Catalysis A: Chemical, vol. 224, no. 1, pp. 17–33, 2004.

[29] E. Beckmann, "Untersuchungen in der Campherreihe," Justus Liebigs Annalen der Chemie, vol. 250, no. 3, pp. 322–375, 1889.

[30] U. Kläning, "Complexes of acid chromate ion with alcohols or acetaldehyde," Acta Chemica Scandinavica, vol. 11, pp. 1313–1316, 1957.

[31] U. Kläning, "The photoinduced oxidation of 2-propanol by acid chromate," Acta Chemica Scandinavica, vol. 12, no. 5, p. 2, 1958.

[32] N. Brasch, D. Buckingham, A. Evans, and C. Clark, "$^{17}$O NMR Study of Chromium(VI) Ions in Water," Journal of the American Chemical Society, vol. 118, no. 34, pp. 7969–7980, 1996.

[33] W. Dehn, "Colorimetric studies on the nature of chromate solutions," Journal of the American Chemical Society, vol. 36, no. 5, pp. 829–847, 1914.

[34] J. Chlistunoff and K. Johnston, "UV/Vis Spectroscopic Determination of the Dissociation Constant of Bichromate from 160 to 400 nm," The Journal of Physical Chemistry B, vol. 102, no. 20, pp. 3993–4003, 1998.

[35] P. Mytych, A. Karocki, and Z. Stasicka, "Mechanism of photochemical reduction of chromium(VI) by alcohols and its environmental aspects," Journal of Photochemistry and Photobiology A: Chemistry, vol. 160, no. 3, pp. 163 – 170, 2003.

[36] U. Klaning and M. Symons, "Photoinduced oxidation of 2-propanol by acid chromate," Proceedings of the Chemical Society, London, pp. 95–96, 1959.

[37] J. Kotas and Z. Stasicka, "Chromium occurrence in the environment and methods of its speciation," Environmental Pollution, vol. 107, no. 3, pp. 263 – 283, 2000.

[38] G. Haight, G. Jursich, M. Kelso, and P. Merrill, "Kinetics and mechanisms of oxidation of lactic acid by chromium(VI) and chromium(V)," Inorganic Chemistry, vol. 24, no. 18, pp. 2740–2746, 1985.

[39] D. Dey, J. Dkhar, and M. Mahanti, "Kinetics of oxidation of primary alcohols by quinolinium dichromate," Oxidation Communications, vol. 21, no. 1, pp. 62–67, 1998.

[40] M. Mitewa and P. Bontchev, "Chromium(V) coordination chemistry," Coordination Chemistry Reviews, vol. 61, no. 0, pp. 241 – 272, 1985.

[41] X. Wang, X. Yang, and L. Wang, "Probing solution-phase species and chemistry in the gas phase," International Reviews in Physical Chemistry, vol. 21, no. 3, pp. 473–498, 2002.

[42] M. Perera, P. Ganssle, and R. Metz, "Microsolvation of $Co^{2+}$ and $Ni^{2+}$ by Acetonitrile and Water: Photodissociation Dynamics of $M^{2+}(CH_3CN)_n(H_2O)_m$," Physical Chemistry Chemical Physics, vol. 13, pp. 18347–18354, 2011.

[43] A. Kamariotis, O. Boyarkin, S. Mercier, R. Beck, M. Bush, E. Williams, and R., "Infrared Spectroscopy of Hydrated Amino Acids in the Gas Phase: Protonated and Lithiated Valine," Journal of the American Chemical Society, vol. 128, no. 3, pp. 905–916, 2006. PMID: 16417381.

[44] J. Friedrich, S. Gilb, O. Ehrler, A. Behrendt, and M. Kappes, "Electronic photodissociation spectroscopy of isolated $IrX_6^{2-}$ (X=Cl,Br)," The Journal of Chemical Physics, vol. 117, no. 6, p. 2635, 2002.

[45] M. Lykkegaard, H. Zettergren, M. Kirketerp, A. Ehlerding, J. Wyer, U. Kadhane, and S. Nielsen, "Photodissociation of Isolated Ferric Heme and Heme-His Cations in an Electrostatic Ion Storage Ring," The Journal of Physical Chemistry A, vol. 113, no. 8, pp. 1440–1444, 2009.

[46] T. Tabarin, A. Kulesza, R. Antoine, R. Mitrić, M. Broyer, P. Dugourd, and V. Bonačić-Kouteckỳ, "Absorption enhancement and conformational control of peptides by small silver clusters," Physical review letters, vol. 101, no. 21, p. 213001, 2008.

[47] H. Zhai, X. Huang, T. Waters, X. Wang, R. O'Hair, A. Wedd, and L. Wang, "Photoelectron Spectroscopy of Doubly and Singly Charged Group VIB Dimetalate Anions: $M_2O_7^{2-}$, $MM'O_7^{2-}$, and $M_2O_7^{-}$ (M, M' = Cr, Mo, W)," The Journal of Physical Chemistry A, vol. 109, no. 46, pp. 10512–10520, 2005. PMID: 16834306.

[48] J. Marcum, A. Halevi, and J. Weber, "Photodamage to Isolated Mononucleotides: Photodissociation Spectra and Fragment Channels," Physical Chemistry Chemical Physics, vol. 11, pp. 1740–1751, 2009.

[49] R. Parr and W. Yang, Density-Functional Theory of Atoms and Molecules, vol. 16 of International Series of Monographs on Chemistry. Oxford University Press, 1989.

[50] F. Weigend, M. Hser, H. Patzelt, and R. Alrichs, "Electronic structure calculations on workstation computers: The program system turbomole," Chemical Physics Letters, vol. 162, no. 3, pp. 165 – 169, 1989.

[51] O. Treutler and R. Ahlrichs, "Efficient molecular numerical integration schemes," The Journal of Chemical Physics, vol. 102, no. 1, pp. 346–354, 1995.

[52] F. Weigend and M. Hser, "RI-MP2: optimized auxiliary basis sets and demonstration of efficiency," Chemical Physics Letters, vol. 294, pp. 143 – 152, 1998.

[53] F. Weigend and R. Ahlrichs, "Balanced basis sets of split valence, triple zeta valence and quadruple zeta valence quality for H to Rn: Design and assessment of accuracy," Physical Chemistry Chemical Physics, vol. 7, no. 18, pp. 3297–3305, 2005.

[54] R. Bauernschmitt and R. Ahlrichs, "Treatment of electronic excitations within the adiabatic approximation of time dependent density functional theory," Chemical Physics Letters, vol. 256, pp. 454 – 464, 1996.

[55] H. Headlam and P. Lay, "EPR Spectroscopic Studies of the Reduction of Chromium(VI) by Methanol in the Presence of Peptides. Formation of Long-Lived Chromium(V) Peptide Complexes," Inorganic Chemistry, vol. 40, no. 1, pp. 78–86, 2001.

[56] S. Feyel, T. Waters, R. O'Hair, and A. Wedd, "Gas-Phase Oxidation of Alkoxo Ligands in Bis(peroxo) $[MO(O_2)_2(OR)]^-$ and Trisoxo $[MO_3(OR)]^-$ Anions (M = Cr, Mo, W)," Journal of the Chemical Society, Dalton Transactions, vol. 0, pp. 4010–4016, 2004.

[57] F. Sahureka, R. Burns, and E. von Nagy-Felsobuki, "Electrospray identification of new poly-oxochromate species," Inorganica Chimica Acta, vol. 332, no. 1, pp. 7 – 17, 2002.

[58] Z. Staszak, A. Wojciechowska, and M. Cieslak-Golonka, "Spectroscopic Investigation of Electronic States of the $CrO_4{}^{2-}$ Ion in the Visible and Ultraviolet Absorption Region," Polish Journal of Chemistry, vol. 83, no. 3, pp. 503–513, 2009.

[59] N. Kondratenko and V. Sherstyuk, "Spectroscopic characteristics of chromium(VI) oxy anions in aqueous solutions," Teoreticheskaya i Eksperimental'naya Khimiya, vol. 22, no. 6, pp. 686–693, 1986.

[60] A. Byström and K.-A. Wilhelmi, "The crystal structure of chromium trioxide," Acta Qiemica Scandinavica, vol. 4, pp. 1131–1141, 1950.

[61] R. Marcus, "Electron transfer reactions in chemistry theory and experiment," Journal of Electroanalytical Chemistry, vol. 438, no. 1, pp. 251–259, 1997.

[62] W. Tsang, Heats of Formation of Organic Free Radicals by Kinetic Methods, vol. 4 of Structure Energetics and Reactivity in Chemistry Series (SEARCH series). Springer Netherlands, 1996.

[63] G. Paul and P. Kebarle, "Thermodynamics of the association reactions hydroxide + water = $(HOHOH)^-$ and methoxy(1-) + methanol = $(CH_3OHOCH_3)^-$ in the gas phase," The Journal of Physical Chemistry, vol. 94, no. 12, pp. 5184–5189, 1990.

[64] N. Greenwood, A. Earnshaw, and A. Earnshaw, Chemistry of the Elements. Pergamon Press Oxford, 1984.

[65] Z. Staszak, A. Wojciechowska, and M. Cieslak-Golonka, "Coordination geometry of Cr(VI) species: Structural and spectroscopic characteristics," Coordination Chemistry Reviews, vol. 249, pp. 2391 – 2407, 2005.

## Chapter 4

## UV Spectroscopy of Permanganate Ions *in Vacuo*

This chapter has been adapted with permission from:

- Jørgen Houmøller, Sydney H. Kaufman, Kristian Støchkel, Lokesh C. Tribedi, Steen Brøndsted Nielsen, J. Mathias Weber. *On the Photoabsorption by Permanganate Ions in Vacuo and the Role of a Single Water Molecule. New Experimental Benchmarks for Electronic Structure Theory.* ChemPhysChem, 2013. **14**: p. 1133 –1137. Copyright 2013 Wiley-VHC Verlag GmbH and Company.

## 4.1    Background

The permanganate anion, $MnO_4^-$, is a very well studied species. Its bright purple color and well-resolved electronic absorption spectrum, exhibiting vibronic transitions visible even in room temperature solutions, make it suitable for teaching chemistry. The high (7+) oxidation state of the manganese metal makes it a widely-used tool in the oxidation of organic species. Like many of the species examined in this thesis, despite its chemical ubiquity, there remains much more we can learn about the isolated permanganate ion which can shed light upon its nature and chemistry in solution.

Potassium permanganate, $KMnO_4$, in particular, has a rich history. It was initially discovered and isolated as early as 1659 by Johann Rudolf Glauber who observed a green solution (now known to be the $MnO_4^{2-}$ manganate ion) turning red, then violet over time [1]. Potassium permanganate was subsequently used as a disinfectant, marketed as Condy's fluid by Edward Bellman Condy in the

1800's [2], as a component in photographic flash bulbs and more recently as a propellant in rockets and torpedoes. It is now largely used for its strong oxidizing capabilities and ability to oxidize without forming hazardous byproducts [3], as occurs when chromate is used (see Chapter 3 on Chromate Ester Photochemistry). For this reason, it has become a focus for green chemistry [4,5].

The central manganese atom is in a 7+ oxidation state with a $d^0$ electron configuration, tetrahedrally bound to the four surrounding oxygen ligands. This calculated structure is shown in Figure 4.1.
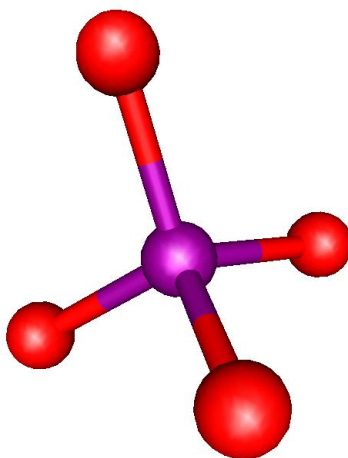


Figure 4.1: Calculated geometry of tetrahedral, ground state permanganate anion using def2-TZVP basis set and B3-LYP functional.

These four bonds exhibit strong $\pi$-bonding character [6]. Since the first lattice spectra of permanganate were taken in the late 1930s by Teltow [7,8], then with improved resolution in 1967 by Ballhausen [9], it has been a model system for understanding the spectroscopy of transition-metal complexes and much experimental data on its spectral features has been collected [9–14]. Its pervasiveness has also made it the focus of computational chemists who have found it to be a challenging target [15]. The results of these calculations have often not agreed well with experimental results, specifically in predicting electronic excitation energies. The source of the observed

discrepancy is the strong vibronic coupling and shift in geometry that permanganate undergoes following excitation [16]. Its ground state has $T_d$ symmetry, but upon excitation, the molecule shifts to lower symmetry as a result of Jahn-Teller distortion, thus the vibrational character of the lower symmetry structures must be considered in order to determine the energetic minima of the excited species. This task has proved challenging, and full agreement on the assignment of all excitations has not yet been reached, even as the spectral assignment for other similar tetroxo $d^0$ metallate species has been accomplished [17].

Because quantum mechanical calculations are often carried out on isolated molecules rather than taking solvation into account, it is worthwhile to obtain an excitation spectrum of isolated permanganate in the gas-phase in order to obtain a spectrum which should more closely resemble calculated results. As in the chromate chapter, a greater understanding of how the isolated permanganate interacts with light may also shed light upon the photoinduced redox reactions [18–21].

There have been only a handful of gas-phase studies on permanganate anion including study via electrospray ionization by Lau et al. [22]. In this collision-induced dissociation (CID) study, they observed permanganate dissociating into $MnO_3^-$ and $MnO_2^-$. It was assumed that $MnO_4^-$ dissociates by successive loss of individual oxygen atoms. CID is a slow heating process, meaning the lowest energy fragmentation pathway should be predominately observed, in this case being $MnO_3^-$. A study photoelectron spectroscopy and calculations performed by Wang and co-workers [23] determined that permanganate ion has an electron affinity of $4.80 \pm 0.10$ eV. Because of its electronic structure, the neutral $MnO_4$ has a hole in its valence shell, creating chemistry similar to a halogen as a result of its high electron affinity, making it act like a so called "super halogen" [24]. As a result, ionic fragmentation pathways will be accessible in the current experiment, but electron detachment will not.

In this study, it was our aim to obtain a gas-phase spectrum of the excited permanganate by observing the photofragments produced from $MnO_4^-$ upon irradiation with UV photons. A concurrent visible light photofragment experiment on $MnO_4^-$ as well as permanganate solvated by a single water molecule, $MnO_4 \cdot H_2O^-$ was performed in the laboratory of Dr. Steen Nielsen in

Aarhus, Denmark and combined with the study presented in this chapter for publication [25].

## 4.2    Computational Methods

Calculations were performed to determine the optimized geometry of the parent, $MnO_4^-$ as well as $MnO_3^-$ and $MnO_2^-$ photofragments and associated threshold energies. Geometry optimizations, initially performed without symmetry restrictions, then with $T_d$ symmetry, were performed using density functional theory (DFT) [26] with TURBOMOLE (V5.9.1 and V6.2) [27, 28] employing the B3-LYP functional and def2-TZVP basis sets [29, 30] for all atoms. The obtained DFT energies were corrected for zero-point energy by analytical calculation of harmonic frequencies using the AOFORCE program [31]. Estimates of threshold energies for various fragmentation pathways were calculated using a simple Hess's Law approach and subtracting zero-point energy-corrected internal energies of the reactants from those of the products. Threshold energies were also corrected for the internal energies of the parent species to more accurately compare computed threshold energies with those occurring within the experiment. The internal vibrational energy was calculated as:

$$U_{vib} = \sum_i \frac{h\nu_i}{(e^{h\nu_i/kT} - 1)} \tag{4.1}$$

where $h$ is Planck's constant, $\nu_i$ is the $i$th vibrational frequency, $k$ is the Boltzmann constant, and T is the temperature of the ions, assumed to be 300 K, given by the temperature of the hexapole ion trap where thermal equilibrium is established. The internal rotational energy was similarly calculated as:

$$U_{rot} = \frac{3}{2}kT \tag{4.2}$$

## 4.3    Results

The photodissociation spectra were acquired using the ESI-TOF instrument described in the instrumentation chapter. A solution of $\sim$10 mM $KMnO_4$(Sigma-Aldrich, ACS Reagent, $\geq$99.0%) in 1:1 methanol/water was electrosprayed to produce the ions of interest as described in the Experimentation Chapter. Upon irradiated by photons with energies ranging from 3 to 5.6 eV, the

permanganate ion predominantly undergoes loss of one neutral oxygen atom to form $MnO_3^-$ (structure shown in Figure 4.2).
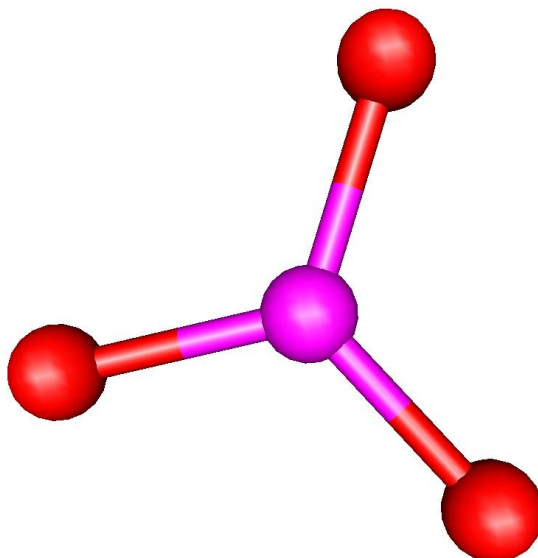


Figure 4.2: Calculated geometry of $MnO_3^-$ photofragment using def2-TZVP basis set and B3-LYP functional.

A UV/vis absorption spectrum of $\sim 100\mu M$ $KMnO_4$ (Sigma-Aldrich, ACS Reagent, $\geq 99.0\%$) in water was acquired using a Varian Cary 500 Scan UV-visible-NIR spectrometer (version 8.01) with a 10 mm path length, 1 nm step size, 2 nm resolution, and integration time of 0.1 s. The obtained UV/Vis and photodissociation spectra of permanganate are shown in Figure 4.3.

Measurement of the laser power dependance of the fragmentation yield (fluence), shown in Figure 4.4, indicates a linear relationship, that is that the absorbance of one photon leads to photodissociation and loss of atomic oxygen.

The formation of $MnO_2^-$ was also observed, but the signal was too weak to obtain a photodissociation spectrum, whose structure is shown in Figure 4.5).

The calculated threshold energy for loss of an oxygen atom is 3.5 eV, above the observed onset of fragmentation observed for the $MnO_3^-$. The calculated threshold for for an additional loss
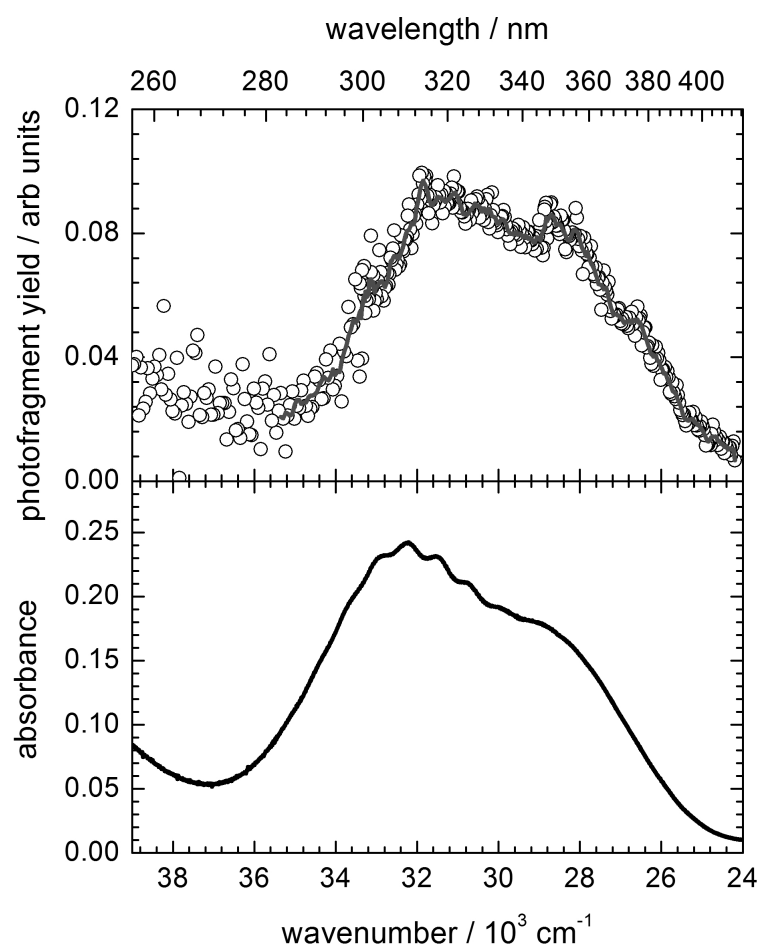
Figure 4.3: Photodissociation spectrum (top) and UV/Vis absorbance spectrum (bottom) of permanganate.
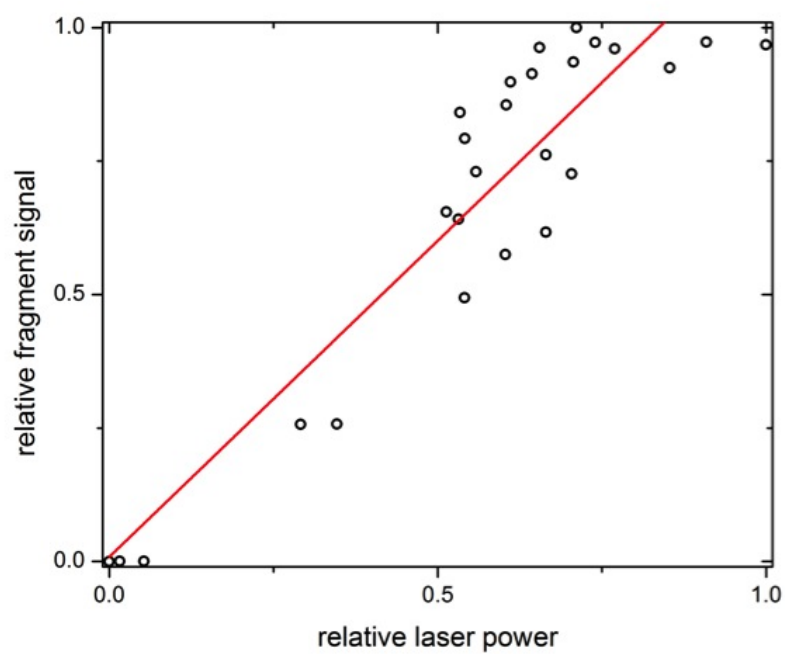
Figure 4.4: Power-dependence: Yield of $MnO_3^-$ after photoexcitation of $MnO_4^-$ at $\lambda = 311$ nm
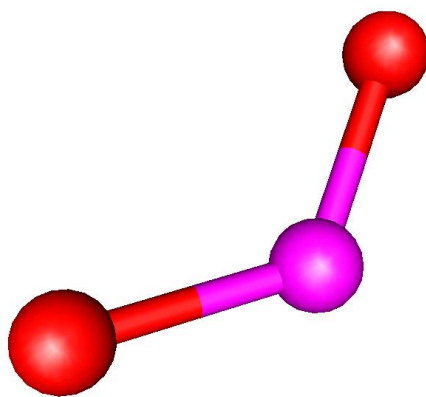


Figure 4.5: Calculated geometry of $MnO_2^-$ photofragment using def2-TZVP basis set and B3-LYP functional.

of oxygen from $MnO_3^-$ to form $MnO_2^-$ is 6.35 eV, well above the energy region explored in this study. In order to determine the threshold energy for fragmentation, it is instructive to examine photodissociation data taken in the visible spectral region. The spectra obtained by Houmøller et al. are shown in Figure 4.6 [25].

This work shows an onset of fragmentation for $MnO_3^-$ at approximately 2.0 eV and $MnO_2^-$ at only slightly higher energy, around 2.10 eV. Fluence measurements indicate absorption of two photons are necessary for both fragmentation processes. Based on the onset of fragmentation with two photon, 4.2 eV, it should be possible to observe an $MnO_2^-$ signal within the energetic limits of the experiment. Despite this, $MnO_2^-$ is not observed in any substantial quantity in our experimental setup even at photon energy about 4.0 eV.

The calculated threshold for the formation of $MnO_2^-$, via the following reaction:

$$MnO_4^- \xrightarrow{h\nu} + MnO_2^- + 2O^{\cdot} \tag{4.3}$$

is ∼6.3 eV owing to the energetic instability of the oxygen radicals formed. By contrast, the loss of molecular oxygen, according to the following:

$$MnO_4^- \xrightarrow{h\nu} + MnO_2^- + O_2 \tag{4.4}$$

has a calculated threshold energy of 4.7 eV, lower by 1.6 eV as it forgoes the formation of two unstable oxygen radicals. This mechanism, which will be discussed in greater detail later in this chapter, falls within the energy range which should be observable by both the two-photon visible (Aarhus) and UV (Boulder) experimental set-ups.

## 4.4    Discussion

### 4.4.1    Electronic Transitions

Beginning with the earliest well-resolved spectrum of permanganate, carried out by Ballhausen in 1967 [9], three regions of spectroscopic activity of interest were identified as outlined in Table 4.1.
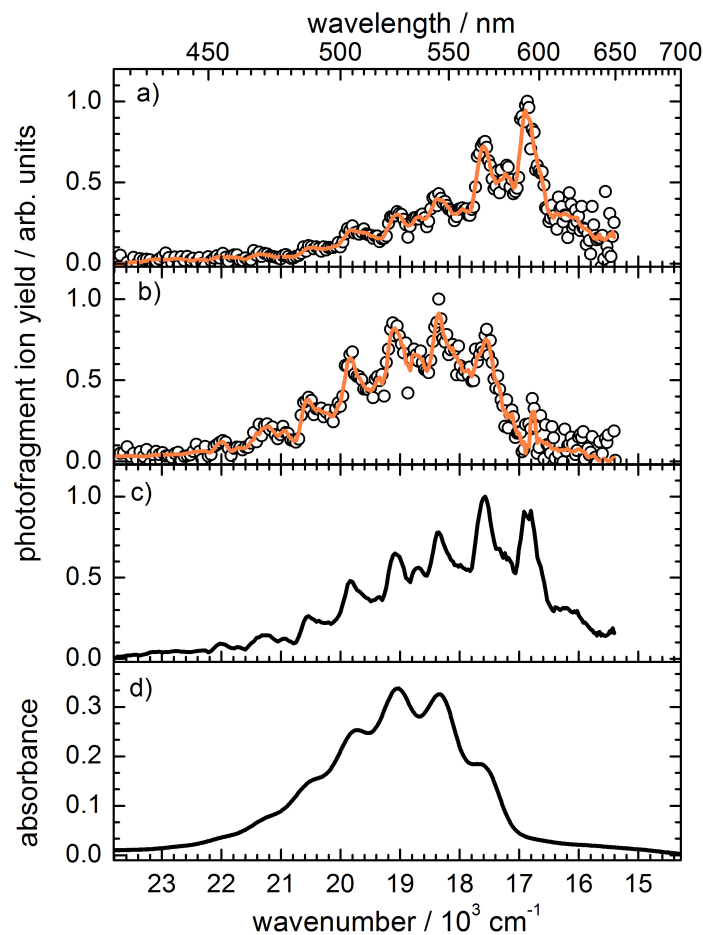
Figure 4.6: Permangate spectra obtained by the research group of Prof. Steen Nielsen at the University of Aarhus, Denmark. The top two traces show photo fragment action yield of (a) $MnO_3^-$ and (b) $MnO_2^-$ from $MnO_4^-$ parent. The orange curves are based on a Savitzky-Golay smoothing filter using five and three successive data points, respectively. (c) Sum of the two orange curves from (a) and (b). (d) Absorption spectrum of an aqueous solution of $KMnO_4$ (100 $\mu M$ concentration). The details of this experiment may be found in [25].

| Region | State | Vertical Excitation Energy [9] | Adiabatic Transition Energy [25] | Transition | Percentage of Contribution [17] | Geometry of Excited State [17] |
|--------|-------|-------------------------------|----------------------------------|------------|--------------------------------|-------------------------------|
| 1 | $1T_2$ | 2.34 eV | 2.08 | $1t_1 \rightarrow 2e$ | 88 | $C_{3v}$ |
|   |        |         |      | $2t_2 \rightarrow 2e$ | 4 |  |
| 2 | $2T_2$ | 3.5 eV | 3.74 | $2t_2 \rightarrow 2e$ | 66 | $C_{2v}$ |
|   |        |         |      | $1t_1 \rightarrow 3t_2$ | 32 |  |
| 3 | $3T_2$ | 4.09 eV | 3.96 | $1t_1 \rightarrow 3t_2$ | 52 | $D_{2d}$ |
|   |        |         |      | $2t_2 \rightarrow 2e$ | 20 |  |

Table 4.1: Observed regions of electronic transitions of $MnO_4^-$ in dilute crystal as obtained in [9], values *in vacuo* as obtained in [25], and MO contributions and excited state geometries as calculated in [17].

The lowest energy, at $\sim$2.25 eV as been identified with reasonable certainty as being the HOMO to LUMO transition, ($1t_1 \rightarrow 2e$) belonging to the $1^1T_2$ state. The spectrum, obtained by Nielsen and co-workers, in Figure 4.6 [25], shows this transition. The vibronic progression matches well that seen in earlier experiments as well as calculation [9, 16, 17]. Identification of the source of the second and third bands, whose electronic region are also the subject of study in this chapter, have found much less success. As mentioned, while the tetrahedral ground state of the permanganate ion parent is well understood, its geometric changes upon excitation make assigning the origin of peaks difficult. The calculated MOs of the ground state, tetrahedral $MnO_4^-$ are shown in Figure 4.7.

Despite the formal $d^0$ of the central metal, previous population analysis computation has established that excitation does not result in a pure ligand-to-metal charge transfer (LMCT), but rather a rearrangement of the electron density throughout the molecule [36]. Upon excitation, permanganate undergoes distortion to $C_{3v}$, $C_{2v}$, or $D_{2d}$ symmetry, as a result from elongation of Mn-O bonds, depending on the excitation [17]. In recent computational work by Jose et al. [17], the excited state geometries were optimized, while constraining them to $T_d$ symmetry, then allowed to naturally distort along the vibrational coordinates calculated to a minimum on the potential energy surface.

Our UV solution absorbance and photodissociation spectra of the second and third bands, beginning at $\sim$3 eV exhibit far less vibronic resolution than that observed in the visible region. The second band, of the $2^1T_2$ state, centered around 3.3 eV is believed to result from the $2t_2 \rightarrow 2e$ transition and results in a geometry distortion to $C_{2v}$ symmetry. This bend shows a shift of about 0.09 eV from that seen in the crystal spectrum by Holt and Ballhausen [9]. The highest energy transition we observe, which overlaps with the transition centered around 4.1 eV, results largely from the $1t_2 \rightarrow 2e$ transition. Electronic structure calculations performed by Jose et al. predict vertical transition energies for the second and third electronic bands which are too high by 0.6 eV and 1.2 eV, respectively [17].

In comparing the solution and gas-phase spectra of permanganate in the UV, very little
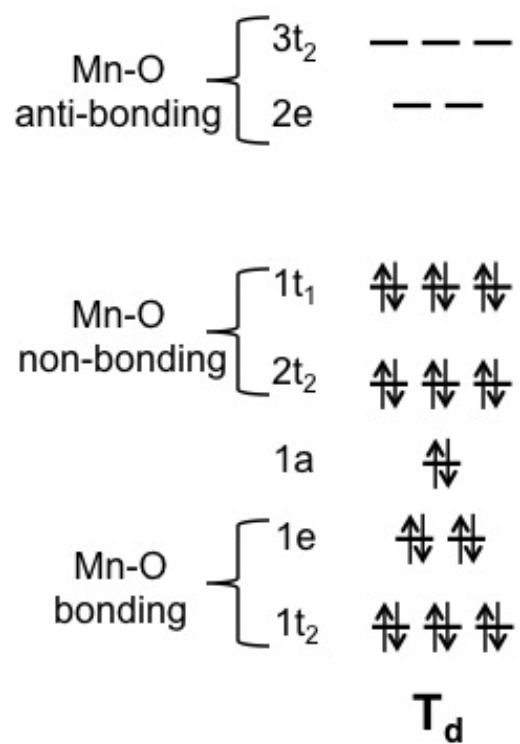
Figure 4.7: Ground state, tetrahedral, molecular orbital diagram of permanganate anion, $MnO_4{}^-$ [15–17, 32–35]

solvatochromic shift is observed. Upon full solvation, the 2nd electronic transition is not shifted at all and the third transition is shifted to the blue by ∼0.05 eV. In comparing this to the dilute crystal spectrum taken by Holt et al., we see the aqueous absorbance spectrum matches that of the isolated molecule much more closely than the crystal spectrum [9]. A table of the solvatochromatic shifts, including those for the first, visible transition from data taken in Aarhus are shown in Table 4.2.

| Band | 1st | 2nd | 3rd |
|---|---|---|---|
| aqueous solution | 0.10 | N/A | 0.05 |
| dilute crystal | 0.15 | 0.09 | 0.16 |

Table 4.2: Solvatochromatic shifts of the three lowest energy electronic bands of $MnO_4^-$ in eV, defined as the observed energy center of the transition in the gas-phase subtracted from that in solution, in eV. Electronic bands are identified in the text. For the first transition in the gas-phase, the experimental value is taken from [25]. All dilute crystal values are cited from [9]. The uncertainty is ∼0.01 eV.

These values indicate that the chemical environment of the ion in the dilute crystal is more perturbing than that in solution. The blue shift is also contrary to calculations performed using a conductor-like screening model (COSMO) to recreate the dielectric environment of a molecule in solution, which predicts a red shift [16].

### 4.4.2    The Permanganate Oxidation Mechanism

Computational studies on permanganate's photochemical oxidizing mechanism have been previously performed by Nakai et al. [37]. Permanganate has long been known to decompose photochemically in solution, resulting in the production of molecular oxygen [18–21] by the following reaction:

$$MnO_4^- \xrightarrow{h\nu} + MnO_2^- + O_2 \tag{4.5}$$

The yield of this reaction is seen to be highly wavelength-dependent as well as showing dependence on temperature especially at longer wavelengths [19], presumably to allow access to excited

vibrational states necessary for decomposition to occur. This led to the conclusion that electronic excitation is followed by internal conversion to a vibrationally excited state, then by unimolecular decay with charge transfer occurring during one of these steps. The observed temperature dependence thus allows for reduction induced by with photons below the threshold energy of the process by increasing the available number of ions with sufficient vibrational energy to result in decomposition. Experimental evidence also showed that neither O, $O^-$, nor $O_2{}^-$ is formed during photodecomposition. This mechanism seems to exclusively involve the photoreduction of $Mn^{VII}$ to $Mn^{III}$, with an ensuing shift of four electrons. Zimmerman et al. also determined that the resulting $O_2$ came from the permanganate reactant and not from surrounding solvent [19].

Other explanations have been offered for the characteristics of this process including the possibility of a photoaquation step followed by decomposition, electron photodetachment, or coupling between specific electronic excitations and the product state [38], but Zimmerman's explanation has held. In a slightly more recent study by Lee et al. [21], further details of the oxidation mechanism were postulated. Based on spectroscopic and kinetic observations, Lee suggested that irradiation results in an intermediate with high oxidative potential. That intermediate may undergo either relaxation back to permanganate, decomposition to $MnO_2{}^-$ and $O_2$, or oxidize the nearest species with a removable electron. Lee further suggested a Mn(V) peroxo complex, shown in Figure 4.8, which could account for the formation of molecular oxygen and the long lifetime of the intermediate as suggested by the species' preference for oxidation or dissociation rather than relaxing back to the parent permanganate.

The long lifetime of the excited intermediate may result from a symmetry or Woodward-Hoffman barrier [39], the result of an avoided crossing of two electronic energy levels of the same symmetry. This can occur if an excitation leads to a dramatic distortion in geometry such that the ground state orbital is higher in energy than that of the excited electron resulting in an avoided crossing which prevents interconversion between the excited and ground state species [21]. Further, the formation of a Mn(V) peroxo intermediate followed by dissociation into $MnO_2{}^-$ and $O_2$ is in keeping with the observation that reduction tends to happen in steps of one or two, rather than
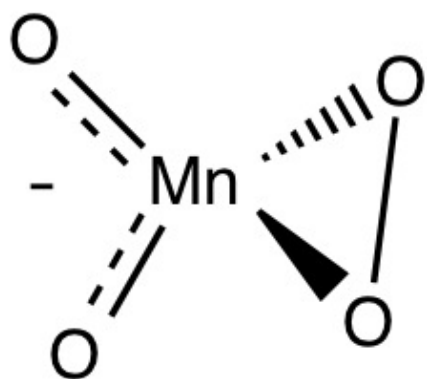
Figure 4.8: Oxidative intermediate postulated to form upon irradiation from permanganate ion by [21]

four [40].

Lee et al. also suggest that the intermediate takes the form of a monohapto dioxygen, three-coordinated manganese compound, as shown in Figure 4.9, evidence for which has been observed in earlier work on manganese(II) porphyrins [41].
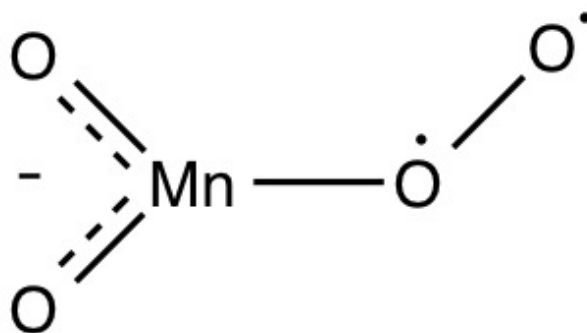


Figure 4.9: Oxidative intermediate postulated to form upon irradiation from permanganate ion by [41]

In this case, it is assumed that solvation of the vacant tetrahedral site will act as a the barrier to relaxation back to the parent. In the gas-phase, where solvation of this site is not possible, enough vibrational energy may exist within the molecule after electronic excitation/relaxation to allow dissociation of the O-O bond.

Experimental evidence suggests that two photons are required to cause fragmentation into $MnO_2^-$ in the visible and possibly the UV region in the gas-phase as well [25]. This would indicate that either the photoinduced reactions previously observed in solution are also the result of a two photon process or the addition of solvent stabilizes the presumed peroxo Mn(V) transition state sufficiently to result in fragmentation of $O_2$. Zimmerman also observed that the quantum yield of oxygen evolved, which shows dependence on wavelength and temperature, was not dependent on the solution composition or the intensity of light used. These observations also lend credence to the importance of solvent stabilization for permanganate-induced oxidation of organic species.

In the gas-phase, it would seem that excitation results in a LMCT followed by cleavage of a single Mn-O bond, despite the instability of the oxygen radical that results. It is possible that in

solution, when the same LMCT leads to bond cleavage, the solvent shell hinders the escape of the oxygen radical, allowing time for one of the structures shown in Figures 4.8 or 4.9 to form.

## 4.5    Conclusions

In conclusion, we have measured the UV electronic spectra of isolated permanganate ions using gas-phase photodissociation spectroscopy, focusing on the previously established [9] second and third lowest energy transitions observed. We observe a very slight blue shift upon full solvation of the ion, less than that seen in the dilute crystal spectrum, which has acted as the benchmark for calculations until now. This observation highlights the need for unperturbed electronic excitation values when comparing with computations.

This study of the dissociation of isolated permanganate ion may also help to shed light on the vital role that solution plays in photoinduced oxidation of organic species. Based on previous studies of this mechanism and the manganese-based products of these reactions, the formation of $MnO_2^-$ species might have seemed likely, despite its high calculated threshold energy. This may indicate that the stabilizing effects of solvent may be necessary for the formation of the intermediate resulting in the production of $MnO_2^-$ and the concurrent oxidation of the organic species.

## 4.6    References

[1] M. E. Weeks, <u>Discovery of the Elements</u>. Kessinger Publishing, 2003.

[2] W. Hugo, "A brief history of heat and chemical preservation and disinfection," <u>Journal of Applied Microbiology</u>, vol. 71, no. 1, pp. 9–18, 1991.

[3] J. Speight, "Ullmann's encyclopedia of industrial chemistry," <u>Petroleum Science and Technology</u>, vol. 17, no. 3-4, pp. 445–445, 1999.

[4] S. Dash, S. Patel, and B. K. Mishra, "Oxidation by permanganate: Synthetic and mechanistic aspects," <u>Tetrahedron</u>, vol. 65, no. 4, pp. 707–739, 2009.

[5] H. Raj Pant, B. Pant, H. Joo Kim, A. Amarjargal, C. Hee Park, L. D. Tijing, E. Kyo Kim, and C. Sang Kim, "A green and facile one-pot synthesis of Ag-ZnO/RGO nanocomposite with effective photocatalytic activity for removal of organic pollutants," <u>Ceramics International</u>, pp. 5083–5091, 2012.

[6] F. A. Cotton, G. Wilkinson, C. A. Murillo, and M. Bochmann, <u>Advanced Inorganic Chemistry</u>, vol. 5. Wiley New York, 1988.

[7] J. Teltow, "Absorption spectrum of the permanganate ion in various crystal lattices," <u>Zeitschrift für Physikalische Chemie</u>, vol. B40, pp. 397–430, 1938.

[8] J. Teltow, "Absorption spectra of permanganate, chromate, vanadate and manganate ion in crystals," <u>Zeitschrift für Physikalische Chemie</u>, vol. B43, pp. 198–212, 1939.

[9] S. L. Holt and C. Ballhausen, "Low temperature absorption spectra of $KMnO_4$ in $KClO_4$," <u>Theoretica Chimica Acta</u>, vol. 7, no. 4, pp. 313–320, 1967.

[10] G. Den Boef, H. Van Der Beek, and T. Braaf, "Absorption spectra in the visible and UV region of potassium permanganate and potassium manganate in solution and their application to the analysis of mixtures of these compounds," <u>Recueil des Travaux Chimiques des Pays-Bas</u>, vol. 77, no. 11, pp. 1064–1070, 1958.

[11] M. Wolfsberg and L. Helmholz, "The Spectra and Electronic Structure of the Tetrahedral Ions $MnO_4^-$, $CrO_4^-$, and $ClO_4^-$," <u>The Journal of Chemical Physics</u>, vol. 20, p. 837, 1952.

[12] C. Ballhausen and A. D. Liehr, "Intensities in inorganic complexes: Part II. Tetrahedral complexes," <u>Journal of Molecular Spectroscopy</u>, vol. 2, no. 1, pp. 342–360, 1958.

[13] C. Ballhausen, "A vibrational analysis of the $MnO_4^-$ bands," <u>Theoretica Chimica Acta</u>, vol. 1, no. 4, pp. 285–293, 1963.

[14] A. Viste and H. B. Gray, "The electronic structure of permanganate ion," <u>Inorganic Chemistry</u>, vol. 3, no. 8, pp. 1113–1123, 1964.

[15] M. A. Buijse and E. J. Baerends, "Analysis of nondynamical correlation in the metal–ligand bond. Pauli repulsion and orbital localization in MnO," <u>The Journal of Chemical Physics</u>, vol. 93, p. 4129, 1990.

[16] J. Neugebauer, E. J. Baerends, and M. Nooijen, "Vibronic structure of the permanganate absorption spectrum from time-dependent density functional calculations," The Journal of Physical Chemistry A, vol. 109, no. 6, pp. 1168–1179, 2005.

[17] L. Jose, M. Seth, and T. Ziegler, "Molecular and Vibrational Structure of Tetroxo $d^0$ Metal Complexes in their Excited States. A Study Based on Time-Dependent Density Functional Calculations and Franck–Condon Theory," The Journal of Physical Chemistry A, vol. 116, no. 7, pp. 1864–1876, 2012.

[18] J. H. Mathews and L. H. Dewey, "A quantitative study of some photochemical effects produced by ultra-violet light," The Journal of Physical Chemistry, vol. 17, no. 3, pp. 211–218, 1913.

[19] G. Zimmerman, "Photochemical decomposition of aqueous permanganate ion," The Journal of Chemical Physics, vol. 23, p. 825, 1955.

[20] U. Kläning and M. Symons, "Structure and reactivity of the oxyanions of transition metals. Part VI. Photolysis of chromate, permanganate, and related compounds in rigid media at low temperatures," Journal of the Chemical Society, pp. 3269–3272, 1959.

[21] D. G. Lee, C. R. Moylan, T. Hayashi, and J. I. Brauman, "Photochemistry of aqueous permanganate ion," Journal of the American Chemical Society, vol. 109, no. 10, pp. 3003–3010, 1987.

[22] T.-C. Lau, J. Wang, K. W. M. Siu, and R. Guevremont, "Electrospray tandem mass spectrometry of oxo complexes of chromium, manganese and tuthenium," Journal of the Chemical Society, Chemical Communications, no. 12, pp. 1487–1488, 1994.

[23] G. L. Gutsev, B. Rao, P. Jena, X.-B. Wang, and L.-S. Wang, "Origin of the unusual stability of $MnO_4{}^-$," Chemical Physics Letters, vol. 312, no. 5, pp. 598–605, 1999.

[24] G. L. Gutsev, P. Jena, and R. J. Bartlett, "Structure and stability of $BF_3{\cdot}F$ and $AlF_3{\cdot}F$ superhalogens," Chemical Physics Letters, vol. 292, no. 3, pp. 289–294, 1998.

[25] J. Houmøller, S. H. Kaufman, K. Støchkel, L. C. Tribedi, S. Brøndsted Nielsen, and J. M. Weber, "On the photoabsorption by permanganate ions in vacuo and the role of a single water molecule. new experimental benchmarks for electronic structure theory," ChemPhysChem, pp. 1133–1137, 2013.

[26] R. Parr and W. Yang, Density-Functional Theory of Atoms and Molecules, vol. 16 of International series of monographs on chemistry. Oxford University Press, 1989.

[27] F. Weigend, M. Hser, H. Patzelt, and R. Alrichs, "Electronic structure calculations on workstation computers: The program system turbomole," Chemical Physics Letters, vol. 162, no. 3, pp. 165 – 169, 1989.

[28] O. Treutler and R. Ahlrichs, "Efficient molecular numerical integration schemes," Journal of Chemical Physics, vol. 102, no. 1, pp. 346–354, 1995.

[29] F. Weigend and M. Hser, "RI-MP2: optimized auxiliary basis sets and demonstration of efficiency," Chemical Physics Letters, vol. 294, pp. 143 – 152, 1998.

[30] F. Weigend and R. Ahlrichs, "Balanced basis sets of split valence, triple zeta valence and quadruple zeta valence quality for H to Rn: Design and assessment of accuracy," Physical Chemistry Chemical Physics, vol. 7, no. 18, pp. 3297–3305, 2005.

[31] R. Bauernschmitt and R. Ahlrichs, "Treatment of electronic excitations within the adiabatic approximation of time dependent density functional theory," Chemical Physics Letters, vol. 256, pp. 454 – 464, 1996.

[32] S. Van Gisbergen, J. Groeneveld, A. Rosa, J. Snijders, and E. Baerends, "Excitation Energies for Transition Metal Compounds from Time-Dependent Density Functional Theory. Applications to $MnO_4^-$, $Ni(CO)_4$, and $Mn_2(CO)_{10}$," The Journal of Physical Chemistry A, vol. 103, no. 34, pp. 6835–6844, 1999.

[33] P. Boulet, H. Chermette, C. Daul, F. Gilardoni, F. Rogemond, J. Weber, and G. Zuber, "Absorption spectra of several metal complexes revisited by the time-dependent density-functional theory-response theory formalism," The Journal of Physical Chemistry A, vol. 105, no. 5, pp. 885–894, 2001.

[34] G. Menconi and N. Kaltsoyannis, "Time dependent DFT study of the electronic transition energies of $RuO_4$ and $OsO_4$," Chemical physics letters, vol. 415, no. 1, pp. 64–68, 2005.

[35] M. Seth, T. Ziegler, and J. Autschbach, "Application of magnetically perturbed time-dependent density functional theory to magnetic circular dichroism. III. Temperature-dependent magnetic circular dichroism induced by spin-orbit coupling," The Journal of Chemical Physics, vol. 129, p. 104105, 2008.

[36] T. Ziegler, A. Rauk, and E. Baerends, "The electronic structures of tetrahedral oxo-complexes. The nature of the charge transfer transitions," Chemical Physics, vol. 16, no. 2, pp. 209–217, 1976.

[37] H. Nakai and H. Nakatsuji, "Mechanism of photochemical reaction of permanganate ion," Journal of Molecular Structure: THEOCHEM, vol. 311, pp. 141–151, 1994.

[38] A. W. Adamson, W. L. Waltz, E. Zinato, D. W. Watts, P. D. Fleischauer, and R. D. Lindholm, "Photochemistry of transition-metal coordination compounds," Chemical Reviews, vol. 68, no. 5, pp. 541–585, 1968.

[39] R. Woodward and R. Hoffmann, "Stereochemistry of electrocyclic reactions," Journal of the American Chemical Society, vol. 87, no. 2, pp. 395–397, 1965.

[40] F. Basolo and R. Pearson, Mechanisms of Inorganic Reactions. Wiley, New York, 1967.

[41] B. M. Hoffman, C. J. Weschler, and F. Basolo, "The dioxygen adduct of meso-tetraphenylporphyrinmanganese (II), a synthetic oxygen carrier," Journal of the American Chemical Society, vol. 98, no. 18, pp. 5473–5482, 1976.

# Chapter 5

# Electronic Spectroscopy of Isolated Copper Nitrate Association Complexes

## 5.1    Background

Copper nitrate complexes are well studied and used from industry to teaching labs. In solution, copper nitrate forms a range of complexes including hydrates and ionic association complexes [1, 2]. It is this assortment of species in solution that makes copper nitrate interesting but also difficult to study. In the limit of saturation, that is at the onset of crystal formation and crystal dissolution, one can expect the species present will go beyond simple binary species instead forming charged salt clusters, $[M_xL_y]$. A similar process occurs in the formation of aerosol particles during nucleation and drying [3, 4] in the atmosphere. While it is difficult to elucidate the detailed chemistry of such association complexes or clusters in the condensed phase, salt cluster ions can be generated by electrospray ionization [5] making them accessible for gas-phase studies. In the current chapter, we focus on the electronic and photochemical properties of a copper nitrate association complex, $Cu(NO_3)_3{}^-$.

We chose to study copper nitrate anionic clusters for a few reasons. First, as with many of the species explored in this thesis, copper nitrate is a precursor to a family of interesting nanoparticle structures specifically, copper and copper oxides [6]. Most methods for generating nanoparticles, copper and otherwise, focus on chemical reduction of metal salts in solution [7]. Newer methods are being developed that focus on gas-phase generation of nanoparticles including laser-induced photoreduction [8]. By performing photoreduction rather than bulk chemical reduction, it may be possible to more closely control the design and synthesis of nanoparticles and avoid excessive use

of reductive chemicals which may be costly and polluting.

The gas-phase structure of neutral Cu(II) nitrate was established by electron diffraction in the 1960s [9]. Cu(II) complexes formally possess a $d^9$ electron configuration, making a fundamental understanding of their geometric and electronic structures particularly interesting to study. In crystals, they are known to adopt a variety of geometries between the limits of a square and a tetrahedron [10]. For example, many different structures are found for the $CuCl_4^{2-}$ dianion depending on the counterion [11]. In solution, Cu(II) ions are usually six-fold coordinated to solvent molecules, anionic ligands, or combinations thereof (in Jahn-Teller distorted tetragonal bipyramids) [12]. In the case of copper nitrate solutions, nitrate can displace water ligands in the coordination shell to form $CuNO_3^+$ cations. Electrospray ionization of nitrate solutions has been shown previously [13,14] to produce clusters containing an excess moiety of $NO_3^-$, which represent the anionic forms of association complexes. Because of the breadth of uses for copper nitrate and related species in solution, it may be desirable to tailor the equilibrium to promote the formation of one particular copper nitrate species [15]. Despite copper nitrate's ubiquity and chemical history, an understanding of its intrinsic geometry and electronic structure remains elusive in the gas-phase.

Presently, we use electrospray ionization mass spectrometry coupled with ultraviolet photodissociation spectroscopy to study $Cu(NO_3)_3^-$ anions in the gas-phase and discuss these complexes in the framework of a molecular orbital approach. In addition, we employ several quantum chemical methods to elucidate the electronic and geometric structures of the parent and fragment ions as well as the electronic excitation spectrum of the parent ion.

## 5.2    Computational Methods

Geometry optimizations were performed for the parent and fragment ions using the TURBO-MOLE V5.9.1 and V6.2 suites of programs [16]. We employed density functional theory (DFT) [17] with the PBE0 hybrid functional [18] as well as second-order Møller-Plesset perturbation theory applying the resolution-of-identity approximation for the evaluation of two-electron integrals (RI-MP2) [19]. Basis sets of triple-zeta quality (def2-TZVPP) [19, 20] were used for all atoms and

calculations. Geometry optimizations were performed initially on all relevant species without symmetry restrictions from a number of starting geometries. The obtained RI-MP2 and DFT calculated ground state energies were corrected for zero point energies obtained the NUMFORCE program in the case of RI-MP2 and using AOFORCE for DFT calculations. After inspection of the parent ion geometry obtained without symmetry restriction, geometry optimizations were again performed, this time restricting the molecule to $C_2$ symmetry. The resulting total energies differed by less than 1 meV from those obtained without symmetry restrictions. We therefore assume that the $Cu(NO_3)_3^-$ parent ion is of $C_2$ symmetry (see below). The orbital character of the electronic excitations was determined using time-dependent density functional theory (TDDFT) [21,22] utilizing the PBE0 functional and def2-TZVPP basis sets for all atoms. Exploratory calculations using the B3-LYP functional did not describe the experimental spectrum at all, and we will therefore only discuss the PBE0 results. We note that spin-orbit interaction has not been treated in our calculations, although it could be important for the excited state energies.

## 5.3    Results and Discussion

### 5.3.1    Photodissociation

Using the setup described in the Experimentation chapter of this thesis, electrospray ionization of a $\sim$10 mM copper(II) nitrate hydrate (Sigma-Aldrich, used without further purification) was performed in a 1:1 water:methanol solution. Upon irradiation with photon energies in the range 3-5.6 eV, $Cu(NO_3)_3^-$ undergoes dissociation into $Cu(NO_3)_2^-$, formally corresponding to reduction of Cu(II) to Cu(I) and presumably along with the loss of neutral $NO_3$ radical. The fragment action spectrum obtained by monitoring $Cu(NO_3)_2^-$ as a function of photon energy is shown in Figure  5.1 along with the solution absorption spectrum obtained for $\sim$10 mM and $\sim$50 $\mu$M solutions of copper(II) nitrate hydrate in 1:1 methanol:water. The spectra were taken using a Varian Cary 500 Scan UV-visible-NIR spectrometer (version 8.01) with 10 mm path length, 1 nm step size, 2 nm resolution, and an integration time of 0.1 sec.

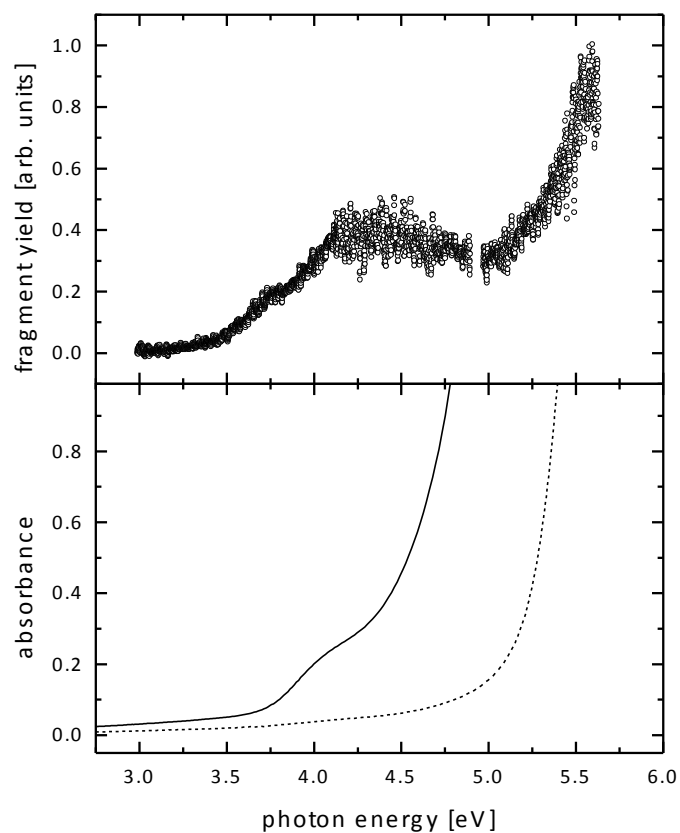Figure 5.1: Comparison of the gas-phase UV photodissociation of $Cu(NO_3)_3^-$ (top) and the UV absorption spectrum of copper nitrate in a 1:1 water:methanol solvent mixture similar to the electrosprayed solution at 10 mM (solid line) and 50 $\mu$M (dotted line) concentration.

The spectrum exhibits a broad peak centered near 4.3 eV with a shoulder around 3.75 eV and a more intense feature towards the upper energy limit of the experiment, around 5.5 eV. The broad, low energy feature has an onset energy of about 3.5 eV. No fragment ions were generated at photon energies below 3.0 eV, nor were any other fragment channels detected.

### 5.3.2    Electronic Transitions

The photodissociation spectrum of the $Cu(NO_3)_3{}^-$ may be interpreted with the aid of the UV absorption spectrum of a copper nitrate solution, shown in the lower part of Figure 5.1, which has been previously studied: The solution spectrum is dominated by an intense band at photon energies above $\sim$5 eV (wavelengths below approximately 250 nm), which is commonly assigned to the $\pi^*\leftarrow\pi$ transition in nitrate anion $NO_3{}^-$ [1]. A shoulder at $\sim$4 eV photon energy has been attributed to a ligand-to-metal charge transfer (LMCT) transition from nitrate to Cu(II) in association complexes [23]. This feature also overlaps with the signature of the $\pi^*\leftarrow$n transition in $NO_3{}^-$, found in the same spectral region in aqueous and methanolic solutions of nitrates [1]. Exploratory TDDFT calculations on $NO_3{}^-$ and $CuNO_3{}^+$ predict the onset of $\pi^*\leftarrow\pi$ absorption bands in $NO_3{}^-$ at around 5.5 eV. $CuNO_3{}^+$ shows an onset of LMCT transitions at $\sim$3.5 eV, corroborating the earlier, empirical identification of the low-energy shoulder in the UV absorption spectrum of aqueous solutions [23]. The energy of the nitrate absorption band is overestimated in our calculations, whereas the onset of the low-energy band of $CuNO_3{}^+$ is predicted at too low energy. We will see below that TDDFT calculations for the anionic association complex $Cu(NO_3)_3{}^-$ exhibits similar trends. We note that the characteristic blue color of aqueous and methanolic solutions containing Cu(II) species is caused by the Laporte-forbidden d$\leftarrow$d transition in Cu(II) [23], giving rise to a weak absorption feature at lower photon energies ($\sim$1.8 eV, corresponding to 700 nm). However, we will not discuss this transition further, since its energy is below the onset of photodissociation explored in this chapter.

The physical origin of the observed spectral features can be interpreted by examining the geometric and electronic structure of the parent ion, although this is complicated by spin-orbit

coupling and by its open-shell configuration. Despite these challenges, the computational treatment employed in this study provides some basic understanding of the electronic properties of the species of interest. Figure 5.2 shows the calculated structures of the $Cu(NO_3)_3^-$ parent ion, neutral $Cu^{II}(NO_3)_2$ and the anionic $Cu(NO_3)_2^-$ photofragment, as discussed below.

The excess $NO_3^-$ moiety is attached to the central Cu atom, resulting in a Y-shaped complex geometry. The molecular frame of the calculated ground state structure of the planar $Cu^{II}(NO_3)_2$ salt is strongly distorted by the presence of the excess $NO_3^-$ group. The calculated structure of the $Cu(NO_3)_2^-$ fragment ion shows a similar distortion, suggesting that the excess charge resides at least in part on the copper atom in both the parent and the fragment ion. The $Cu(NO_3)_3^-$ parent ion complex is of $C_2$ symmetry with the Cu atom coordinated in a bidentate fashion to the three $NO_3$ groups. Each ligand oxygen that binds to the copper atom is situated in in the corner of a strongly distorted octahedron. Breaking symmetry from octahedral to $C_2$, the $e_g$ and $t_{2g}$ orbitals in the d-block of the metal center split into five orbitals as shown in Figure 5.3. We note that two of the three $NO_3$ ligands in $Cu(NO_3)_3^-$ are distorted and their oxygen atoms interaction with the copper atom are not equivalent.

Population analysis of the parent ion shows that the Cu atom has a charge between +1 and +2 (depending on the details of the population analysis approach used, see Table 5.1), demonstrating that the simple picture of formal charges giving rise to a $d^9$ or $d^{10}$ configuration breaks down. Upon fragmentation, the copper ion is reduced to having a calculated charge between 0 and +1.

| Molecule | Natural | 2-Center | Multicenter |
|----------|---------|----------|-------------|
| Parent | 1.52 | 1.09 | 1.12 |
| Fragment | 0.74 | 0.33 | 0.35 |

Table 5.1: Population analysis for the copper atom in the parent and fragment ions (RI-MP2/def2-TZVPP).

This results in a change in the interaction of the Cu atom with the $NO_3$ ligands from a symmetric bidentate motif in the neutral $Cu^{(II)}(NO_3)_2$ salt to mostly monodentate geometry in the fragment
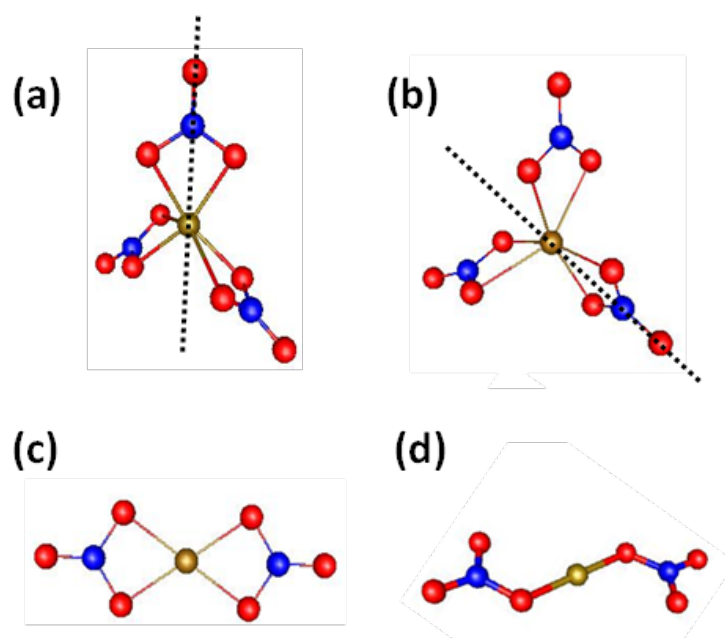
Figure 5.2: Calculated (RI-MP2) structures of some of the species relevant for this study. Copper atoms are shown in brown, nitrogen atoms in blue, and oxygen atoms in red. Upper row: Two views of the calculated geometry of the $Cu(NO_3)_3^-$ parent ion with its $C_2$ symmetry axis vertical (a) and pointing towards the lower right (b). The distortion of the off-axis $NO_3$ ligands is clearly visible in view (b). Lower row: Calculated structure of neutral $Cu^{II}(NO_3)_2$ (c) and of the anionic fragment ion $Cu(NO_3)_2^-$ (d). Note the similarity in the distortion of the $NO_3$ ligands of the anionic fragment (d) with the distortion of two of the ligands in the parent ion as seen in (b).
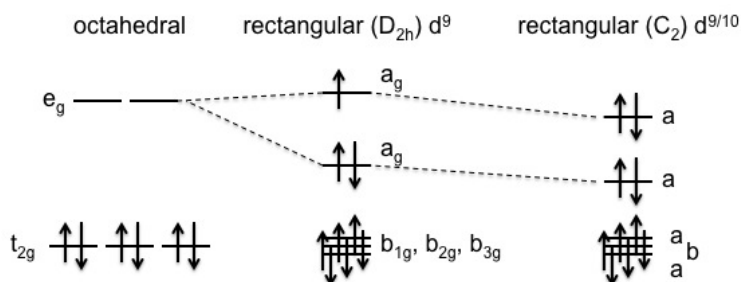


Figure 5.3: MO diagrams of the d-block of a transition metal complex following the distortion from an octahedral structure (left) through a rectangular structure (center) to a distorted structure in $C_2$ symmetry (right) [10]. The electron configuration of neutral $Cu^{II}(NO_3)_2$ is shown in the center diagram, that of the $Cu(NO_3)_3^-$ parent ion on the right.

ion. Figure 5.4 shows a comparison of the experimental photodissociation spectrum and a calculated TDDFT spectrum (PBE0 functional, def2-TZVPP basis).

The calculated spectrum is qualitatively consistent with the onset of the experimental photodissociation spectrum; the calculated spectrum shows three bands of features in the region between 3 eV and 6 eV, each consisting of several transitions and a steep rise at higher energies. The most intense of the transitions calculated in the three bands can be characterized as LMCT transitions (see Figure 5.5), corresponding to photoreduction of the copper atom.

The HOMO is delocalized over the two distorted $NO_3$ ligands and the copper atom, where the interaction between the ligands and the copper atom can be described as primarily of antibonding $\sigma^*$ character. Most of the transitions do not have pure initial and final orbitals, rather the calculations indicate that the transition involves several initial orbitals (see Table 5.2), mostly delocalized over the ligands and largely with bonding character.

The final states for the most intense transitions also consist of several contributions, but the antibonding LUMO is the most prominent component. An intense band at 7 eV is calculated to have most prominent components end in nitrate-based $\pi^*$ orbitals (LUMO+1, LUMO+2). While it was noted that the calculated spectrum qualitatively recovers the experimental spectrum, the low-energy onset of the UV transitions appears to be on the order of 0.5 eV too low. In contrast, the steep rise at the highest energies in the TDDFT spectrum appears at higher energies than experimentally observed. This behavior is similar to that observed in $Cu(NO_3)^+$ and $NO_3^-$ as mentioned above.

As mentioned, we observed only $Cu(NO_3)_2^-$ as a fragment ion. Interestingly, we did not see evidence of the alternative fragment channel, $Cu(NO_3)_3^- \longrightarrow Cu(NO_3)_2 + NO_3^-$ where neutral copper(II) nitrate would be formed along with a nitrate anion. In principle, this may be due to the very low kinetic energy of $NO_3^-$ ions formed following dissociation, resulting in correspondingly low detection efficiency. However, loss of neutral $NO_3$ (as observed in the present photodissociation) has been identified as a major fragment channel in collision-induced dissociation (CID) experiments on anionic transition metal nitrate complexes (including $Cu(NO_3)_3^-$) performed by Li et al. [13],
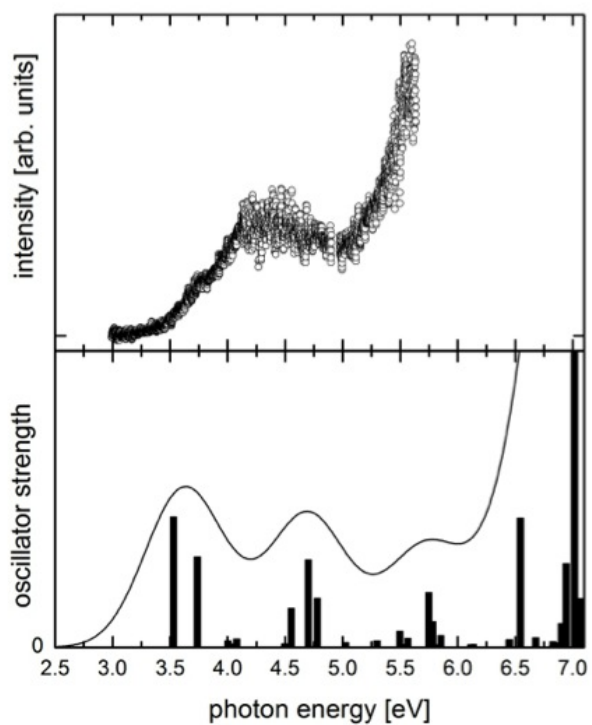
Figure 5.4: Comparison of experimental (top trace) and calculated excitation spectrum (bottom trace) of $Cu(NO_3)_3^-$ (see text). The vertical bars show the calculated oscillator strength (to scale as shown), the full line was obtained by broadening each transition with a Gaussian of width 0.2 eV to guide the eye.
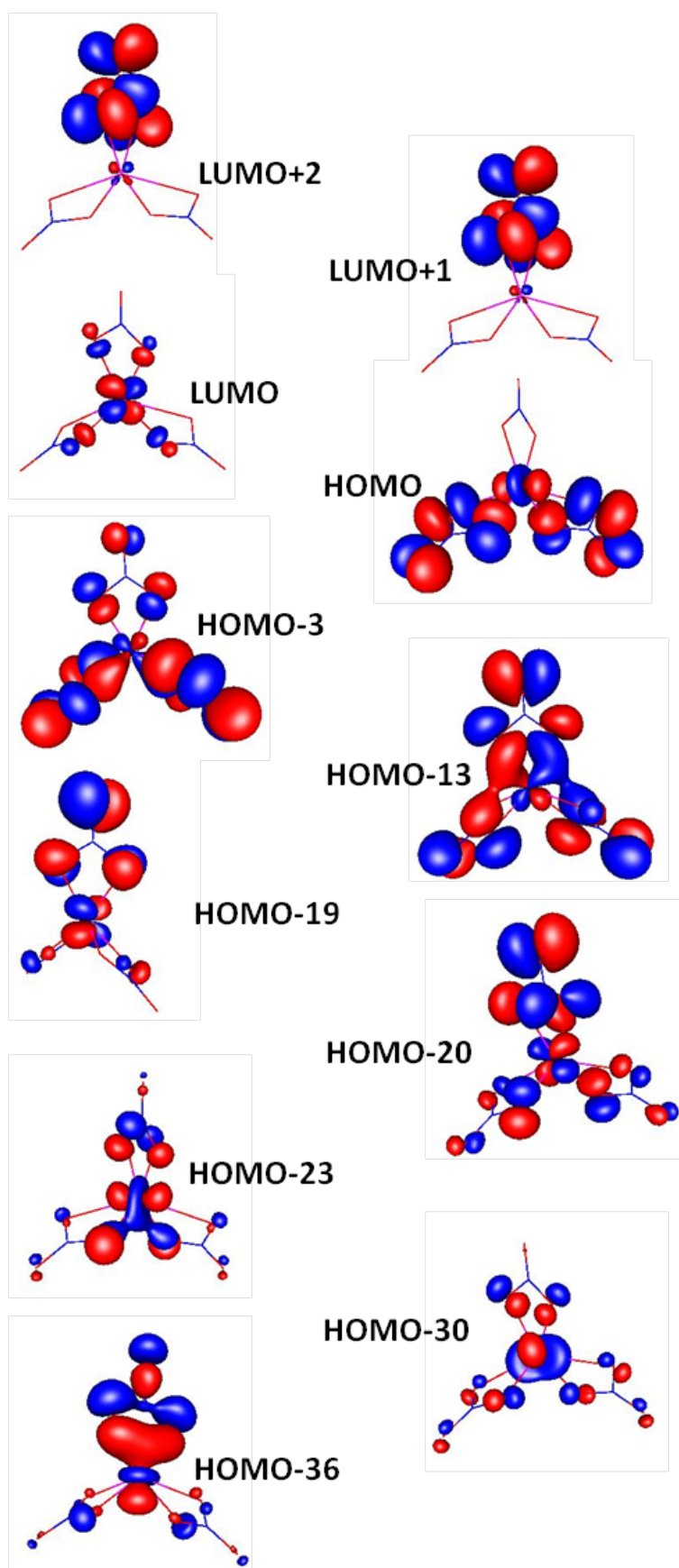
Figure 5.5: Dominant calculated (PBE0/TZVPP) molecular orbital components involved in main electronic excitations

| Transition Number | Symmetry | Energy (eV) | Oscillator Strength (x $10^{-2}$) | Initial Orbital | Final Orbital | Percent of Contribution |
|---|---|---|---|---|---|---|
| 2 | a | 3.53 | 5.27 | HOMO-3 | LUMO | 96.1 |
| 4 | b | 3.74 | 3.71 | HOMO | LUMO | 47.2 |
| | | | | HOMO-23 | LUMO | 24.2 |
| | | | | HOMO-26 | LUMO | 12.1 |
| | | | | HOMO-14 | LUMO | 6.9 |
| 10 | a | 4.70 | 3.59 | HOMO-13 | LUMO | 51.6 |
| | | | | HOMO-10 | LUMO | 8.7 |
| | | | | HOMO-13 | LUMO+2 | 6.8 |
| | | | | HOMO-5 | LUMO+2 | 5.7 |
| | | | | HOMO-16 | LUMO | 5.6 |
| | | | | HOMO-3 | LUMO+2 | 5.3 |
| 17 | b | 5.75 | 2.28 | HOMO-30 | LUMO | 33.0 |
| | | | | HOMO-34 | LUMO | 16.1 |
| | | | | HOMO-23 | LUMO | 13.4 |
| | | | | HOMO-26 | LUMO | 11.4 |
| | | | | HOMO-1 | LUMO+3 | 5.5 |
| 26 | b | 6.55 | 5.27 | HOMO-36 | LUMO | 30.7 |
| | | | | HOMO-21 | LUMO+1 | 18.3 |
| | | | | HOMO-18 | LUMO+2 | 15.2 |
| | | | | HOMO-14 | LUMO+2 | 13.5 |
| | | | | HOMO-34 | LUMO | 8.3 |
| 35 | a | 7.01 | 12.0 | HOMO-20 | LUMO+1 | 35.4 |
| | | | | HOMO-19 | LUMO+2 | 20.9 |
| | | | | HOMO-25 | LUMO+1 | 8.2 |

Table 5.2: Calculated Parent Excitations using TD-DFT (PBE0/TZVPP). Only components with more than 5% contribution are listed.

whereas nitrate anion is formed only as a minor CID product. This similarity in fragment channels points to a dissociation mechanism wherein excitation is followed by internal conversion to a highly vibrationally excited electronic ground state that results in fracture of the weakest bonds. Although there are several electronic transitions in $Cu(NO_3)_3^-$ calculated to be in the visible spectral region (at 1.8 eV), no photofragments are observed below approximately 3.5 eV photon energy. The fragmentation threshold energy, EF, of the observed fragment channel can, in principle, be determined by our calculations using the relationship,

$$EF = E[Cu(NO_3)_2^-] + E[NO_3] - E[Cu(NO_3)_3^-] \tag{5.1}$$

where $E[Cu(NO_3)_2^-]$, $E[NO_3]$, and $E[Cu(NO_3)_3^-]$ are the calculated energies of the fragment ion, $NO_3$ radical, and the parent ion, respectively (including zero-point corrections). However, a good estimate for $E[NO_3]$ within our calculations is problematic due to the known challenges of the ground state electronic structure of the $NO_3$ radical [24]. Instead, we turn to determine $E[NO_3]$ by using the relationship

$$E[NO_3] = E[NO_3^-] + EA[NO_3], \tag{5.2}$$

since $NO_3^-$ is computationally more tractable and its electron affinity ($EA[NO_3] = 3.937 \pm 0.014$ eV) has been experimentally determined to high accuracy [25]. Interestingly, the two methods used in our calculations of fragmentation yield rather different threshold energies of 1.6 eV (RI-MP2) and 2.7 eV (PBE0). Since we did not observe any photofragments in the energy range for the d←d transitions (ca. 1.8 eV), we find the calculated value from RI-MP2 calculations to be likely too low. Our TDDFT calculations indicate that there are no allowed transitions between the d←d bands and the onset of the LMCT bands at about 3.5 eV, and the fragmentation threshold calculated using PBE0 is consistent with our experimental observations. The absence of photofragments in the d←d transition region at 1.8 eV and the onset of photofragmentation at 3.5 eV can be used to bracket the fragmentation threshold energy experimentally.

## 5.4      Summary and Conclusions

We show UV photodissociation spectra in the spectral region between 3 eV and 5.6 eV for the copper nitrate association complex $Cu(NO_3)_3^-$. The only observed fragment channel is $Cu(NO_3)_2^-$, consistent with earlier CID experiments. Fragmentation likely occurs after fast internal conversion into a highly vibrationally excited state on the electronic ground state potential energy surface. Quantum chemical calculations indicate that the parent ion complex has $C_2$ symmetry with a strongly distorted octahedral coordination of the copper atom. The oxidation state of the Cu atom in this complex is between +1 and +2, and is further reduced upon fragmentation. TDDFT calculations indicate that the most dominant contributions of the observed UV transitions are LMCT transitions and end in the LUMO of the parent ion. Association complexes of copper nitrate have a UV photodissociation spectrum that is similar to UV absorption spectra of copper nitrate solutions at high concentrations. Spectral features absent from dilute solutions are caused by LMCT transitions between nitrate ligands and the copper moiety.

## 5.5    References

[1] T. Vladislav and V. Simeon, "Ion association in aqueous solutions of strong electrolytes: a UV–Vis spectrometric and factor-analytical study," Physical Chemistry Chemical Physics, vol. 1, no. 2, pp. 299–302, 1999.

[2] P. Salmon and G. Neilson, "The coordination of Cu (II) in a concentrated copper nitrate solution," Journal of Physics: Condensed Matter, vol. 1, no. 31, p. 5291, 1999.

[3] P. Jungwirth and D. Tobias, "Molecular structure of salt solutions: A new view of the interface with implications for heterogeneous atmospheric chemistry," The Journal of Physical Chemistry B, vol. 105, no. 43, pp. 10468–10472, 2001.

[4] A. Castleman Jr and K. Bowen Jr, "Clusters: Structure, energetics, and dynamics of intermediate states of matter," The Journal of Physical Chemistry, vol. 100, no. 31, pp. 12911–12944, 1996.

[5] J. Friedrich, P. Weis, J. Kaller, R. Whetten, and M. Kappes, "Alkali halide cluster dianions: metastability and threshold sizes," The European Physical Journal D-Atomic, Molecular, Optical and Plasma Physics, vol. 9, no. 1, pp. 269–272, 1999.

[6] N. Dhas, P. Raj, and A. Gedanken, "Synthesis, characterization, and properties of metallic copper nanoparticles," Chemistry of Materials, vol. 10, no. 5, pp. 1446–1452, 1998.

[7] K. Shrestha and K. Sorensen, C.and Klabunde, "Synthesis of CuO nanorods, reduction of CuO into Cu nanorods, and diffuse reflectance measurements of CuO and Cu nanomaterials in the near infrared region," The Journal of Physical Chemistry C, vol. 114, no. 34, pp. 14368–14376, 2010.

[8] C. Granqvist, L. Kish, and W. Marlow, Gas Phase Nanoparticle Synthesis. Springer, 2005.

[9] R. LaVilla and S. Bauer, "The structure of gaseous copper (II) nitrate as determined by electron diffraction," Journal of the American Chemical Society, vol. 85, no. 22, pp. 3597–3600, 1963.

[10] Y. Jean, Molecular Orbitals of Transition Metal Complexes. OUP Oxford, 2005.

[11] S. Keinan and D. Avnir, "Studies in copper (II) complexes: correlations between quantitative symmetry and physical properties," Journal of the Chemical Society, Dalton Transactions, no. 6, pp. 941–947, 2001.

[12] M. Melník, M. Kabešová, M. Koman, L. Macåškovå, J. Garaj, C. Holloway, and A. Valent, "Copper (II) Coordination Compounds: Classification and Analysis of Crystallographic and Structural Data III. Dimeric Compounds," Journal of Coordination Chemistry, vol. 45, no. 1-4, pp. 147–359, 1998.

[13] F. Li, M. Byers, and R. Houk, "Tandem mass spectrometry of metal nitrate negative ions produced by electrospray ionization," Journal of the American Society for Mass Spectrometry, vol. 14, no. 6, pp. 671–679, 2003.

[14] S. Mollah, D. Andrew, S. Johnson, A. Gwizdala III, and R. Houk, "Identification of metal cations, metal complexes, and anions by electrospray mass spectrometry in the negative ion mode," <u>Analytical Chemistry</u>, vol. 72, no. 5, pp. 985–991, 2000.

[15] V. Anufrienko, R. Shutilov, G. Zenkovets, V. Gavrilov, N. Vasenin, A. Shubin, T. Larina, A. Zhuzhgov, Z. Ismagilov, and V. Parmon, "The state of $Cu^{2+}$ ions in concentrated aqueous ammonia solutions of copper nitrate," <u>Russian Journal of Inorganic Chemistry</u>, vol. 57, no. 9, pp. 1285–1290, 2012.

[16] F. Weigend, M. Hser, H. Patzelt, and R. Alrichs, "Electronic structure calculations on workstation computers: The program system Turbomole," <u>Chemical Physics Letters</u>, vol. 162, no. 3, pp. 165 – 169, 1989.

[17] O. Treutler and R. Ahlrichs, "Efficient molecular numerical integration schemes," <u>The Journal of Chemical Physics</u>, vol. 102, no. 1, pp. 346–354, 1995.

[18] C. Adamo and V. Barone, "Toward reliable density functional methods without adjustable parameters: The PBE0 model," <u>The Journal of Chemical Physics</u>, vol. 110, p. 6158, 1999.

[19] F. Weigend and M. Häser, "RI-MP2: first derivatives and global consistency," <u>Theoretical Chemistry Accounts: Theory, Computation, and Modeling (Theoretica Chimica Acta)</u>, vol. 97, no. 1, pp. 331–340, 1997.

[20] F. Weigend and R. Ahlrichs, "Balanced basis sets of split valence, triple zeta valence and quadruple zeta valence quality for H to Rn: Design and assessment of accuracy," <u>Physical Chemistry Chemical Physics</u>, vol. 7, no. 18, pp. 3297–3305, 2005.

[21] R. Bauernschmitt and R. Ahlrichs, "Treatment of electronic excitations within the adiabatic approximation of time dependent density functional theory," <u>Chemical Physics Letters</u>, vol. 256, pp. 454 – 464, 1996.

[22] R. Bauernschmitt, M. Häser, O. Treutler, and R. Ahlrichs, "Calculation of excitation energies within time-dependent density functional theory using auxiliary basis set expansions," <u>Chemical Physics Letters</u>, vol. 264, no. 6, pp. 573–578, 1997.

[23] B. Hathaway and A. Underhill, "433. The ultraviolet and visible spectra of some anhydrous copper (II) salts in organic solvents," <u>Journal of the American Chemical Society</u>, pp. 2257–2262, 1962.

[24] J. F. Stanton, "On the vibronic level structure in the NO radical. I. The ground electronic state," <u>The Journal of Chemical Physics</u>, vol. 126, p. 134309, 2007.

[25] A. Weaver, D. Arnold, S. Bradforth, and D. Neumark, "Examination of the $^2A'_2$ and $^2E$" states of $NO_3$ by ultraviolet photoelectron spectroscopy of $NO_3^-$," <u>The Journal of Chemical Physics</u>, vol. 94, no. 3, pp. 1740–1751, 1991.

# Chapter 6

# Photodissocation Spectroscopy of the Hexachloroplatinate Dianion

## 6.1    Introduction

Multiply charged anions (MCAs) are ubiquitous in solution. In the condensed phase, solvation stabilizes the excess charges sufficiently to overcome their inherent Coulombic instability caused by the presence of excess electrons in a small volume. This high charge density makes isolated MCAs (i.e. not stabilized by solvent or counter-ions) difficult to study, both computationally and experimentally [1]. Nonetheless, because of their importance in chemistry and the interesting challenges they present, MCAs have been the subject of much theoretical and experimental work [2–5]. Since the first small gas-phase MCAs were experimentally observed in 1990s [6] and studied via photolectron spectroscopy by Wang and coworkers in 1999 [7–10] many organic and inorganic species have been investigated. Dianionic transition metal-halide complexes, particularly Werner-type complexes [11], $MX_4^{2-}$ and $MX_6^{2-}$ with platinum group metals (M = Ru, Rh, Pd, Os, Ir, Pt), have been most deeply examined [12, 13] because of their relatively large stability in the gas-phase, their model character in inorganic chemistry and ligand field theory, and the knowledge of their electronic excited states from condensed phase experiments [14–18].

Photoelectron spectroscopy has been used extensively to study electron emission in MCAs [2, 8, 10, 19–21]. In a MCA, an electron is bound by the interaction with adjacent nuclei at close range, contributing to the electronic stability of the system. At longer distances, the electron mostly feels repulsion from the negative charge density due to the other excess electrons surrounding the molecular frame. These two competing forces result in a repulsive Coulomb barrier ($RCB_{ed}$) in the

electron-anion interaction potential at intermediate distances, stabilizing the MCA against electron detachment (see Figure 6.1 [10]).

In some cases, the binding energy of the most weakly bound electron can even be negative, but because of the stabilization by the $RCB_{ed}$, the MCA will be metastable towards electron detachment with tunneling lifetimes up to hundreds of seconds [7, 22–24].

Similar to the RCB for electron loss, there is a RCB stabilizing the MCA against ionic fragmentation ($RCB_{if}$) [12, 25, 26]. As a result, a MCA can be metastable with respect to loss of an anionic fragment (see Figure 6.2). In this case, tunneling is very unlikely due to the large mass of the fragment ion, but electronic or vibrational excitation can result in ionic fragmentation by bringing the system energy above $RCB_{if}$.

Coulombic relaxation via ionic fragmentation of Werner-type complexes has been studied by a number of groups using different activation methods. The Dessent group used collision induced dissociation (CID) [13] to compare the stability of in $MX_6{}^{2-}$ dianions with platinum-group metals and Rhenium toward ionic fragmentation versus electron detachment, while Kappes and coworkers [12, 27] and Weber and coworkers [28] studied photofragmentation of $IrBr_6{}^{2-}$, which decays by loss of one or two ligand atoms. Based on CID experiments as well as calculations, ionic fragmentation is a lower energy pathway in these hexahalometalates than electron loss. Some are assumed to be metastable with respect to ionic fragmentation [12, 13, 29–31] while they largely have positive electron binding energies, thus are far less likely to relax by electron loss.

The behavior of hexahalometalates contrasts with that of tetrahalometalate dianions, which are largely observed to be metastable towards autodetachment as implied by their negative second electron binding energy [23, 24, 32]. This can be traced to the much smaller volume for accommodation of the excess charge, as can be inferred from comparison with $Pt(CN)_4{}^{2-}$ which is observed to have an electron binding energy of $\sim$1.69 eV [33].

Platinum group metals present a computational challenge, similar to other transition metals, owing to relativistic and electron correlation which are likely to affect the accuracy of the calculations [34]. Furthermore, the high symmetry of Werner-type complexes results in Jahn-Teller
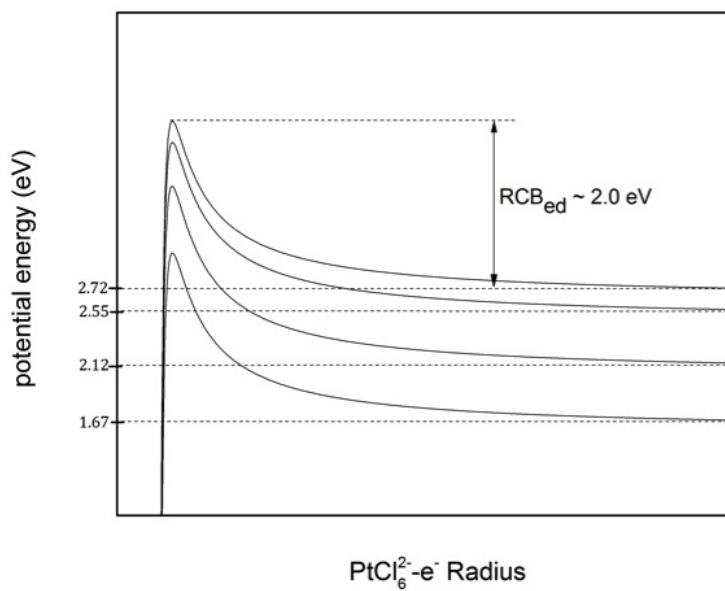
Figure 6.1: Schematic diagram of the $RCB_{ed}$ for $PtCl_6{}^{2-}$ based on experimental values from work by Wang and coworkers [10]. Numbers shown are the experimentally determined vertical electron binding energies (in eV) for reaching the four lowest energy electronic states of $PtCl_6{}^-$ by photodetachment. Zero potential energy shows the ground state energy of the dianion.
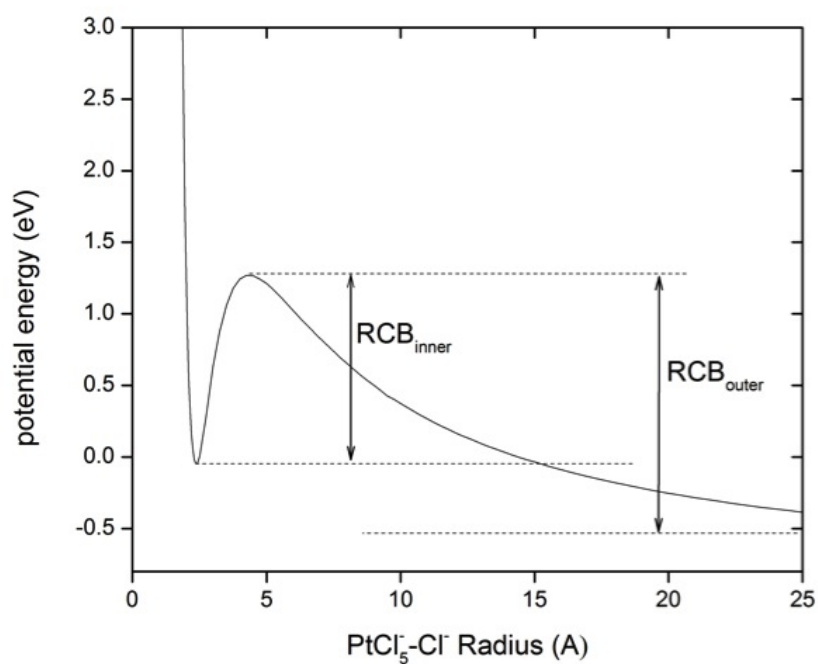
Figure 6.2: Potential energy curve for dissociation of $PtCl_6^{2-}$ into $PtCl_5^{-}$ and $Cl^{-}$ fragments, calculated using density functional theory (see text for details). The zero energy level corresponds to the equilibrium structure of the $PtCl_6^{2-}$.

distortion in excited states [34]. In addition to being useful benchmark systems for computational treatment, haloplatinates are of interest because of their use as precursors to platinum nanoparticles [35] and as catalysts [36]. Light-mediated approaches to platinum nanoparticle formation may play a role in future platinum industrial use [37, 37]. The photochemistry of Pt(IV) complexes is also important for the surface modification of titanium oxide and other semiconductors [38–40].

Previous studies on mass-selected $PtCl_6{}^{2-}$ and related species were performed using photoelectron spectroscopy [8] and CID [13], revealing important results on the electron binding and emission behavior and on the lowest energy fragmentation behavior. In the present work, we will use photodisscociation and photodetachment spectroscopy to observe both electron detachment and ionic fragmentation pathways, and thus can gain a deeper understanding of the electronic structure of the dianion. Photodissociation spectroscopy also allows us to explore how the dianion exicited states couple to the redox chemistry of these species. In using a Koopmans theorem picture [41], we consider how electrons are removed from the excited molecular orbitals of the parent species. We focus our attention on the UV region of the spectrum in part to observe how energy in excess of the barriers to both electron detachment and ionic fragmentation of the molecule.

## 6.2     Computational Methods

In order to estimate threshold energies for various dissociation pathways, geometry optimizations were performed using density functional theory (DFT) [42] as implemented in using TURBOMOLE (V5.9.1 and V6.2) [43, 44], employing the B3-LYP functional and def2-TZVP [45–47] basis sets for all atoms. The relativistic core potential, ECP-60-MWB, was used in the case of Pt. Initial geometry optimizations were performed without symmetry restrictions, then with $O_h$ symmetry as defined to the parent ion. Zero-point energies were calculated from vibrational energies obtained using AOFORCE [48]. Parent excited state calculations were performed using a time-dependent density functional theory (TDDFT) using TZVP basis sets for all atoms and the B3-LYP functional.

Estimates of threshold energies for various fragmentation pathways were calculated using

Hess's Law and subtracting zero-point energy-corrected internal energies of the reactants from those of the products. Threshold energies were also corrected for the internal energies of the parent species to more accurately compare computed threshold energies with those obtained in the experiment according to,

$$U_{vib} = \sum_i \frac{h\nu_i}{(e^{h\nu_i/kT} - 1)} \tag{6.1}$$

where $h$ is Planck's constant, $\nu_i$ is the $i$th vibrational frequency, $k$ is the Boltzmann constant, and T is the temperature of the ions, assumed to be 300 K, given by the temperature of the hexapole ion trap where thermal equilibrium is established.

A potential energy curve of the dissociation of $PtCl_6{}^{2-}$ into $PtCl_5{}^{2-}$ and $Cl^-$ (See Figure 6.2) was generated by varying the length of one Pt-Cl bond in steps of 0.05 $\mathring{A}$ and allowing the remainder of the molecular coordinates to relax in a geometry optimization without symmetry restriction.

## 6.3      Results & Discussion

### 6.3.1      UV/Vis Spectrum of $K_2PtCl_6$ Solution

A UV/Vis spectrum of 10 mM $K_2PtCl_6$ (Sigma-Aldrich, reagent, 98%) dissolved in a 1:1 mixture of methanol and water at various concentrations, acquired using a Varian Cary 500 Scan UV-visible-NIR spectrometer (version 8.01) with a 10 mm path length, 1 nm step size, 2 nm resolution, and integration time of 0.1 s, is shown in Figure 6.3 along with calculated excitations for $PtCl_6{}^{2-}$.

It shows the characteristic shape observed by previous studies: The weak band at 4.75 eV and the strong peak 6.25 eV at have been traditionally attributed to ligand-to-metal charge transfer (LMCT) [49, 50]. $PtCl_6{}^{2-}$ is a closed shell molecule of $O_h$ symmetry with Pt(IV) in a $d^6$ electron configuration. The metal d-orbitals are split by ligands forming the HOMO and LUMO while the ligand-based orbitals are at much lower in energy, as shown in Figure 6.4.

Consistent with the much more sophisticated theoretical work by Cederbaum and coworkers [51], our molecular orbital ordering shows that while the LUMO is an $e_g$ orbital largely formed
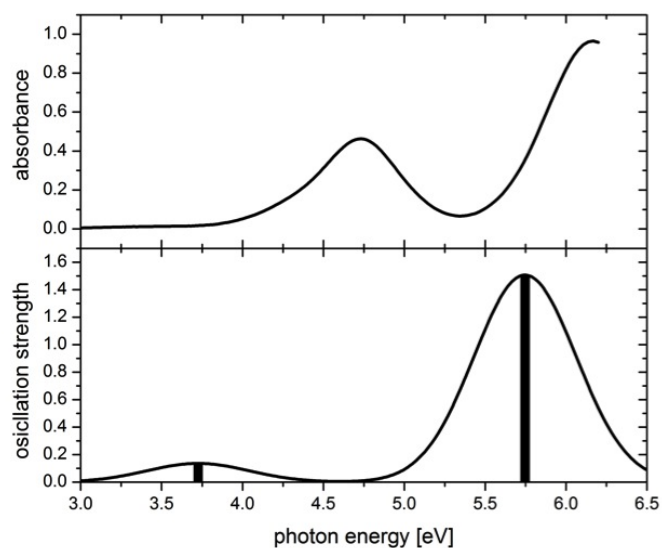
Figure 6.3: Top: UV/vis absorption spectrum of $K_2PtCl_6$ (Sigma-Aldrich, reagent, 98%) in a 1:1 mixture of methanol/water (10 mM concentration). Bottom: Calculated excitation energies of the $PtCl_6{}^{2-}$ from TDDFT calculations. The oscillator strengths of individual transitions are given by the vertical bars. The full line represents a convolution of the excited-state spectrum with a Gaussian (0.3 eV FWHM).
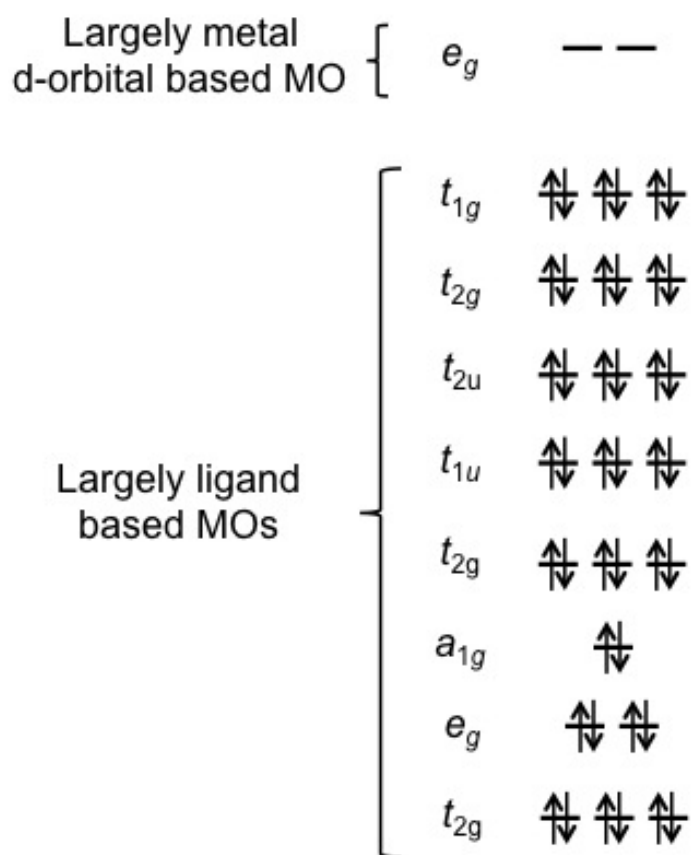
Figure 6.4: Calculated MO diagram for $PtCl_6{}^{2-}$ free dianion (def2-TZVP, B3-LYP).

from the metal 5d-orbital, the HOMO is of $t_{1g}$ symmetry with largely ligand character. In contrast, traditional crystal field theory and molecular orbital theory have long held that both the HOMO and LUMO are mainly of d-orbital character. The difference between these pictures is likely due to the absence of solvent and counter-ions for dianions *in vacuo* [51]. In the isolated dianion, the electron density is more localized on the ligand orbitals, resulting in their destabilization, while stabilizing the metal d-orbitals. While the lowest energy, HOMO to LUMO transition remains electric dipole (Laporte) forbidden, it is not a d-d transition. The lowest energy allowed transitions predicted by TDDFT calculations are shown in Figure 6.5. The calculated excitations are red
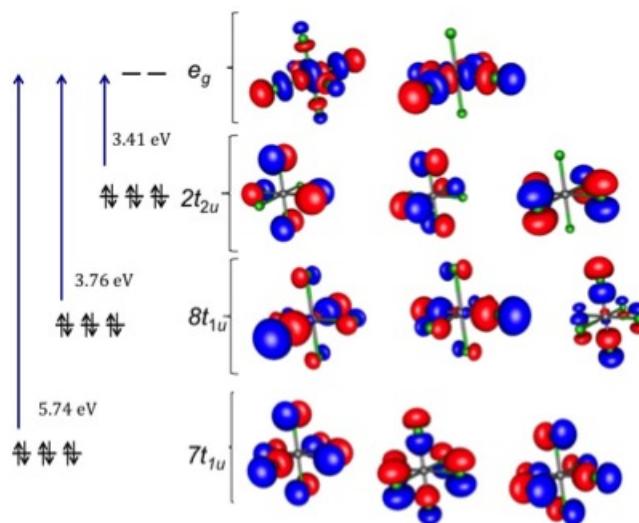


Figure 6.5: Calculated low-energy electronic transitions in $PtCl_6{}^{2-}$ and the involved MOs

shifted from the solution spectrum, with the lower energy bands shifted by about 1 eV and the high energy peak shifted by about 0.65 eV.

### 6.3.2 Photodissociation Spectrum

Photodissociation spectra of a solution of $\sim$10 mM $K_2PtCl_6$ (Sigma-Aldrich, reagent, 98%) in 1:1 methanol:water were generated with irradiation photon energies from 3.5 to 5.6 eV. The original step size of the spectra was $\sim$1 meV, but the point density of the spectra reported here was reduced by averaging batches of six adjacent data points into one data point with an effective

step size of 6 meV. Upon irradiation, $PtCl_6^{2-}$ undergoes dissociation or photodetachment, with $PtCl_6^-$, $PtCl_5^-$, and $PtCl_4^-$ as the observed ionic products. We assume that $Cl^-$, $Cl\cdot$ and possibly $Cl_2^-$ fragment ions are also produced, but due to the small kinetic energy of these light fragments and their resulting low detection efficiency, we were not able to observe them. The ionic product channels will be discussed separately below.

### 6.3.2.1    Electron Detachment Pathway

In principle, electron detachment can be characterized by monitoring the ejected electrons (see [18]) or by detecting the monoanion resulting from electron emission. In the present work, we follow the latter route. Our observed action spectrum for the $PtCl_6^-$ fragment channel is shown in Figure 6.6.
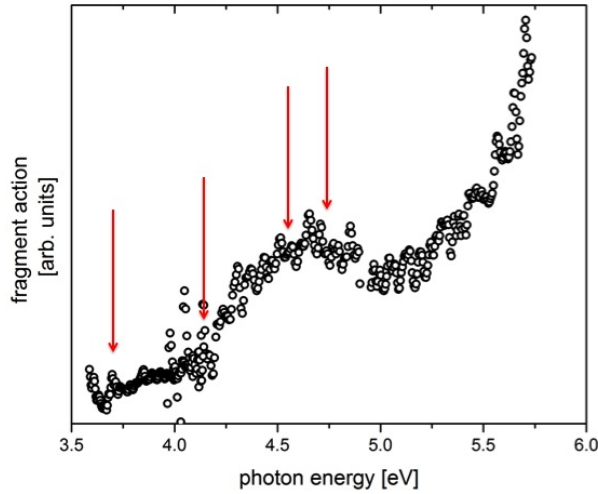


Figure 6.6: $PtCl_6^-$ action spectrum obtained by UV photodetachment from $PtCl_6^{2-}$. Arrows show the sum of ($RCB_{ed}$ + EBE) for detachment into different electronic states of the $PtCl_6^-$ monoanion from photoelectron spectroscopy [10].

As mentioned previously, the photoelectron spectrum of $PtCl_6^{2-}$ has been studied both computationally [51, 52] and experimentally [10]. The accessibility of this photoproduct pathway is governed by the electron detachment RCB ($RCB_{ed}$) as schematically shown in Figure 6.2.

Dianions can decay into a singly-charged species and an electron through a number of channels, depending on the difference between $RCB_{ed}$ and the photon energy for the energetically accessible final states of the monoanion. If the photon energy is insufficient to overcome the $RCB_{ed}$ but above the asymptotic value of the monoanion final state, the electron can tunnel through the barrier and escape. The geometry of the molecule will play and important role in the trajectory of any departing electron. In the case of octahedral $PtCl_6^{2-}$, the electron may either depart axially, along the bond length or along a pathway between the ligands. Previous studies have indicated that the departing electron is expected to travel between ligands, avoiding ligand electron density [18, 52].

Photoelectron spectroscopy experiments by Wang and coworkers determined the electron binding energy in $PtCl_6^{2-}$ (the second adiabatic electron affinity) to be 1.58(5) eV, well below the onset energy used in the present experiment. Interestingly, this value is close to the result of our DFT computations, where we calculate the electron binding energy to be 1.30 eV. In light of the problems one may expect regarding the performance of DFT for $PtCl_6^{2-}$, this agreement may be fortuitous, although similar calculations have been rather successful in predicting fragmentation energies for ions of similar complexity [53]. Calculations of much higher quality by the Cederbaum group slightly overestimate the electron binding energy [51].

The shape of the photodetachment yield together with the previously determined monoainion electronic energy levels (shown in Figure 6.6), provides insight into the detachment mechanism active in $PtCl_6^{2-}$. The experimental photodetachment yield shows a wide peak centered around 4.65 eV superimposed on a near-exponential increase in photodetachment signal as a function of photon energy. The onset of photodetachment coincides with the vertical detachment energy for the ground state of $PtCl_6^-$ (1.67 eV) and the sum of $RCB_{ed}$ ($\sim$2 eV), determined in photoelectron spectroscopy experiments by Wang et al. [10]. We therefore assume that the onset of photodetachment is due to excitation close to or above the top of the $RCB_{ed}$ connected to the ground state (X) of the monoanion. We note that the RCB towards electron detachment is a nonlocal potential, which depends on the kinetic energy of the departing electron [51]. As a result, the experimental determination of the barrier height is to be seen as an estimate and does not allow determine the

extent of tunneling contributing to the observed photodetachment yield.

At slightly higher photon energies, consistent with the onset of accessing the first excited electronic state (A) of $PtCl_6^-$ [10], the photodetachment yield increases in slope. We interpret this change of slope as the manifestation of this channel being energetically accessible. We expect the higher energy states of the monoanion to have similar increases in the slope of the photodetachment yield. However, these comparatively subtle changes are masked by a broad resonance appearing in the energy region of the first two dipole-allowed electronic transitions of the dianions ($\sim$4.65 eV). This resonance structure is also visible in the photofragment action spectra of $PtCl_6^-$ as discussed below. The appearance of this resonance in the photodetachment channel indicates that electron emission is enhanced by the electronic excitation of the dianion. This type of resonance enhancement has been seen in other studies on photodetachment from MCAs [22,54].

### 6.3.2.2    Ionic Fragmentation Pathways

The calculated potential energy curve for this dissociation channel, shown in Figure 6.2, shows that the $PtCl_6^{2-}$ dianion is thermodynamically unstable with respect to dissociation, but survives due to the RCB towards ionic fragmentation. A similar situation has been postulated for the case of $IrBr_6^{2-}$ [12]. Our calculations indicate that the barrier to ionic fragmentation is lower than that to electron detachment, a property that has been observed previously in CID of similar dianionic metal hexahalides [13,30]. Threshold energy calculations suggest that this species is metastable towards decay by ionic fragmentation, with an outer RCB $\sim$0.54 eV and an inner RCB is calculated to be $\sim$1.32 eV.

The action spectrum for formation of $PtCl_5^-$ from photodissociation of $PtCl_6^{2-}$ is shown in Figure 6.7. It is dominated by a broad peak at $\sim$4.5 eV, which we assign to the two lowest-energy dipole-allowed transitions in $PtCl_6^{2-}$. The two transitions are unresolved, but the slightly asymmetric shape of the peak suggests that the weaker $6e_g \leftarrow 2t_{2u}$ transition is on the lower-energy side of the peak, while the somewhat stronger $6e_g \leftarrow 8t_{1u}$ transition is on the higher energy side, as expected from our calculations. Interestingly, the higher energy $6e_g \leftarrow 7t_{1u}$ transition does not
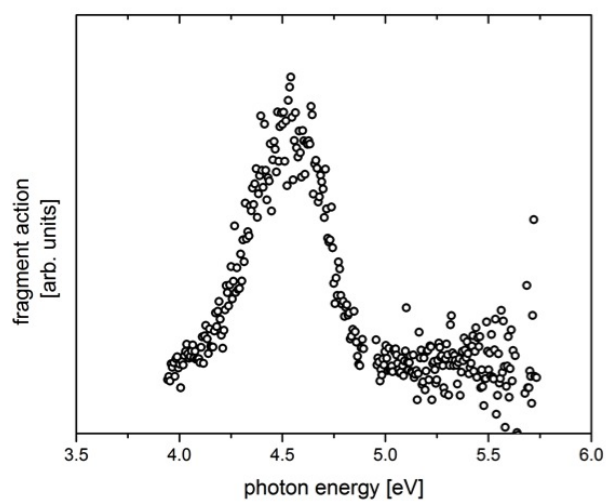
Figure 6.7: $PtCl_5^-$ action spectrum obtained by UV photodissociation from $PtCl_6^{2-}$.

contribute to the PtCl$_5$$^-$ fragment channel, indicating a selectivity for PtCl$_5$$^-$ formation in the lower energy excitations or a low survival probability of the PtCl$_5$$^-$ photofragment at higher photon energies. We will discuss this behavior again in the context of the observations in formation of PtCl$_4$$^-$ fragments below.

The photodissociation action spectrum of the PtCl$_4$$^-$ fragment channel is shown in Figure 6.8. Up to 5 eV, the energy dependent behavior of the PtCl$_5$$^-$ and PtCl$_4$$^-$ fragment channels are



Figure 6.8: PtCl$_4$$^-$ action spectrum obtained by UV photodissociation from PtCl$_6$$^{2-}$.

remarkably similar. In contrast to PtCl$_5$$^-$, however, the PtCl$_4$$^-$ signal appears to grow strongly at higher photon energies. We attribute this increase in PtCl$_4$$^-$ photodissociation action to the low energy slope of the 6e$_g$←7t$_{1u}$ transition (see Figure 6.4).
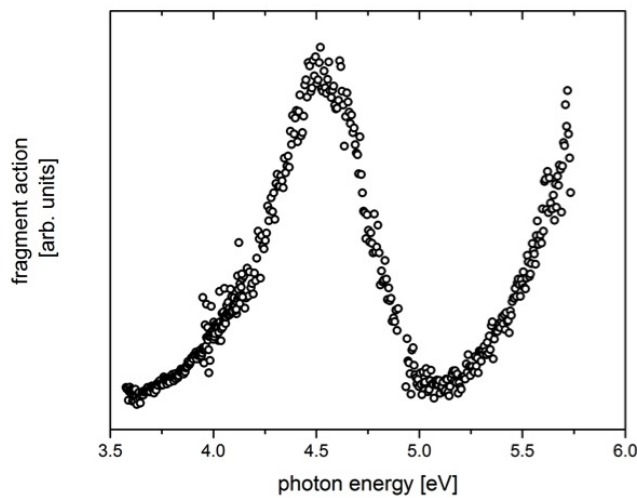
The loss of two Cl species and one negative charge may take place in one of two ways as shown in the following two reactions:

$$PtCl_6^{2-} \rightarrow PtCl_4^- + Cl^{\cdot} + Cl^- \tag{6.2}$$

or

$$PtCl_6^{2-} \rightarrow PtCl_4^- + Cl_2^- \tag{6.3}$$

The reaction shown in equation (1.2) would likely proceed in a stepwise fashion with the departure of a chloride anion followed by the loss of chlorine radical resulting from excess energy residing in the molecule after dissociation. In contrast, reaction shown in equation (1.3) would yield chlorine molecular anions, where the two neighboring chlorine ligands would leave at the same time and form a $Cl_2^-$ ion during the dissociation reaction.

Monitoring the light fragment ions ($Cl^-$ or $Cl_2^-$) was not possible in this experiment, due to the low detection efficiency of these fragment ions. While this precludes the unambiguous identification of the fragmentation reaction, we can draw parallels to other hexahalometalates and discuss likely relaxation pathways based on the experimental evidence we have. The fragmentation channels corresponding to loss of one or two ligands have been observed before in $MX_6^{2-}$ complexes, molecular dihalogen anion fragments have not been found in any fragmentation study, independent of the activation method [12, 28, 55]. In all $MX_6^{2-}$ ions studied so far, ionic fragmentation corresponding to the loss of a single ligand has been observed as the lowest energy decay channel. We therefore assume that relaxation of excited $PtCl_6^{2-}$ via reaction (1.3) is unlikely, even though we calculate this channel to be overall exothermic by $\sim$1 eV. Consequently, we assume that fragmentation yielding $PtCl_4^-$ proceeds via reaction (1.2).

We calculate reaction (1.2) to be endothermic by $\sim$0.65 eV, which is much lower than any of the photon energies used, consistent with the assumption that reaction (1.2) is the active pathway in the formation of $PtCl_4^-$. In this net reaction threshold energy, the first step (loss of $Cl^-$) is $\sim$0.8 eV exothermic (consistent with $PtCl_6^{2-}$ being metastable with respect to ionic fragmentation). However, since tunneling of a $Cl^-$ can be neglected due to the large mass of the fragment, the relevant energy threshold for this first reaction is the inner barrier height of the RCB towards ionic fragmentation, which we calculate to be $\sim$1.3 eV. The second step in reaction (1.3), i.e. the loss of $Cl^.$ from $PtCl_5^-$, is endothermic by $\sim$1.45 eV, so that the estimated minimum energy for the formation of $PtCl_4^-$ is 2.75 eV.

This leaves the question whether the loss of $Cl^-$ occurs on a repulsive electronic potential energy surface directly after excitation or after internal conversion to lower electronic states, followed

by vibrational predissociation. Assuming that initial excitation ends on a purely repulsive curve, most excess energy imparted above the threshold will be converted into kinetic energy release of the fragments. If this is the case, it is unlikely that there would be enough energy left in the $PtCl_5^-$ anion to facilitate the additional loss of a chlorine radical.

Accounting for thermal rotational and vibrational energy of the parent ions ($\sim$0.3 eV) and the calculated endothermicity of the second fragmentation step, the threshold energy towards formation of $PtCl_4^-$ is 2.45 eV under the condition that no energy beyond the minimum to overcome the RCB is deposited into kinetic energy release of the fragments.

We conclude that direct dissociation from the initially excited states is unlikely, and that dissociation occurs after internal conversion into lower electronic states, concomitant with formation of a strongly vibrationally excited transient $PtCl_5^-$ ion, which subsequently loses a Cl radical. This scenario is consistent with the absence of $PtCl_5^-$ fragments above 5 eV, assuming that the $PtCl_5^-$ fragment initially formed retains enough internal energy to undergo loss of a chlorine radical with near unit probability on the time scale of the experiment (tens of $\mu$s). We note that this reductive fragmentation step, as opposed to the oxidative loss of an electron or the redox-neutral loss of $Cl^-$ may be important for photoreductive pathways in the context of photoinduced platinum nanoparticle formation [56, 57].

The UV/vis spectrum of a solution of $K_2PtCl_6$ (see Figure 6.3) and the $PtCl_4^-$ action spectrum are very similar, and only a small solvatochromic shift is observed for the peak containing the unresolved signatures of the $6e_g \leftarrow 2t_{2u}$ and $6e_g \leftarrow 8t_{1u}$ transitions ($\sim$0.2 eV). This is in keeping with previous $MX_6^{2-}$ dianion photodissociation studies [12, 28]. Although Sommerfeld et al. [51] did not predict electronic excitation spectra, the solvatochromic shift can be explained by their discussion on orbital energies in $PtCl_6^{2-}$. They predict that d-orbitals in isolated molecules should be stabilized as compared to their solvated counterparts owing to increased positive charge on the metal center. The ligand orbitals, by contrast, will experience excess negative charge and will be pushed up in energy without the presence of solvent molecules. Since the observed electronic transitions are LMCT transitions, the combination of these effects leads to the observed blue shift of

the transitions in solution compared to the intrinsic transition energies.

## 6.4    Conclusions

We have measured the photodissociation and photodetachment spectra of $PtCl_6{}^{2-}$ *in vacuo*. The gas-phase spectrum of this dianion shows transitions similar to those in solutions, and we assign them to $6e_g \leftarrow 2t_{2u}$ and $6e_g \leftarrow 8t_{1u}$ transitions. The spectral features belonging to these transitions are $\sim 0.2$ eV lower in energy than the corresponding transitions in solution. A resonance structure in the photodetachment channel in the vicinity of these transitions suggests that the lifetime of the excited electronic state is sufficient to afford resonant enhancement of electron emission. Based on the available literature for the fragmentation of other $MX_6{}^{2-}$ complexes, we assume that fragmentation of the parent ion occurs via the loss of a $Cl^-$ ion, followed by loss of a Cl radical.

Further, we determined a computational estimate for the RCB towards ionic fragmentation of $PtCl_6{}^{2-}$. The energy dependence of the $PtCl_4{}^-$ and $PtCl_5{}^-$ fragment channels shows the availability of sufficient residual energy after initial dissociation to result in a second dissociation step within the time frame of the experiment.

## 6.5 References

[1] A. Dreuw, L. S. Cederbaum, and M. K. Scheller, "Multiply charged anions in the gas phase," Chemical Reviews, vol. 102, no. 1, pp. 181–200, 2002.

[2] L.-S. Wang and X.-B. Wang, "Probing free multiply charged anions using photodetachment photoelectron spectroscopy," The Journal of Physical Chemistry A, vol. 104, no. 10, pp. 1978–1990, 2000.

[3] M. Scheller and L. Cederbaum, "Construction principle for stable multiply-negative charged molecular systems. Part I. Doubly-negative charged systems," The Journal of Chemical Physics, vol. 100, p. 8934, 1994.

[4] M. K. Scheller, R. N. Compton, and L. S. Cederbaum, "Gas-phase multiply charged anions," Science, vol. 270, no. 5239, pp. 1160–1166, 1995.

[5] J. Kalcher, "Gas-phase stabilities of small anions," Annual Reports Section C (Physical Chemistry), vol. 93, pp. 147–186, 1996.

[6] S. N. Schauer, P. Williams, and R. Compton, "Production of small doubly charged negative carbon cluster ions by sputtering," Physical Review Letters, vol. 65, no. 5, pp. 625–628, 1990.

[7] X.-B. Wang and L.-S. Wang, "Experimental search for the smallest stable multiply charged anions in the gas phase," Physical Review Letters, vol. 83, no. 17, pp. 3402–3405, 1999.

[8] X.-B. Wang, C.-F. Ding, and L.-S. Wang, "Electron tunneling through the repulsive coulomb barrier in photodetachment of multiply charged anions," Chemical Physics Letters, vol. 307, no. 5, pp. 391–396, 1999.

[9] L.-S. Wang, C.-F. Ding, X.-B. Wang, and S. Barlow, "Photodetachment photoelectron spectroscopy of multiply charged anions using electrospray ionization," Review of Scientific Instruments, vol. 70, no. 4, pp. 1957–1966, 1999.

[10] X.-B. Wang and L.-S. Wang, "Photodetachment of free hexahalogenometallate doubly charged anions in the gas phase: $[ML_6]^{2-}$,(M= Re, Os, Ir, Pt; L= Cl and Br)," The Journal of Chemical Physics, vol. 111, p. 4497, 1999.

[11] N. N. Greenwood, A. Earnshaw, and A. Earnshaw, Chemistry of the Elements, vol. 1341. Butterworth-Heinemann Oxford, 1997.

[12] J. Friedrich, S. Gilb, O. Ehrler, A. Behrendt, and M. Kappes, "Electronic photodissociation spectroscopy of isolated $IrX_6^{2-}$ (X=Cl,Br)," The Journal of Chemical Physics, vol. 117, no. 6, p. 2635, 2002.

[13] W. E. Boxford, J. K. Pearce, and C. E. Dessent, "Ionic fragmentation versus electron detachment in isolated transition metal complex dianions," Chemical Physics Letters, vol. 399, no. 4, pp. 465–470, 2004.

[14] V. Grivin, I. Khmelinski, V. Plyusnin, I. Blinov, and K. Balashev, "Photochemistry of the $PtCl_6^{2-}$ complex in methanol solution," Journal of Photochemistry and Photobiology A: Chemistry, vol. 51, no. 2, pp. 167–178, 1990.

[15] M. J. Molski and K. Seppelt, "The transition metal hexafluorides," <u>Dalton Transactions</u>, no. 18, pp. 3379–3383, 2009.

[16] E. Glebov, V. Plyusnin, V. Grivin, A. Venediktov, and S. Korenev, "Photochemistry of $PtBr_6^{2-}$ in aqueous solution," <u>Russian Chemical Bulletin</u>, vol. 56, no. 12, pp. 2357–2363, 2007.

[17] C. K. Jørgensen, "Electron transfer spectra of hexahalide complexes," <u>Molecular Physics</u>, vol. 2, no. 3, pp. 309–332, 1959.

[18] D. Löffler, J. Weber, and M. Kappes, "Photodetachment spectroscopy of $PtBr_4^{2-}$: Probing the Coulomb barrier of a doubly charged anion," <u>The Journal of Chemical Physics</u>, vol. 123, p. 224308, 2005.

[19] L.-S. Wang, C.-F. Ding, X.-B. Wang, and J. B. Nicholas, "Probing the potential barriers and intramolecular electrostatic interactions in free doubly charged anions," <u>Physical Review Letters</u>, vol. 81, no. 13, pp. 2667–2670, 1998.

[20] X.-B. Wang and L.-S. Wang, "Photoelectron spectroscopy of multiply charged anions," <u>Annual Review of Physical Chemistry</u>, vol. 60, pp. 105–126, 2009.

[21] X.-B. Wang and L.-S. Wang, "Photodetachment of Multiply Charged Anions: The Electronic Structure of Gaseous Square-Planar Transition Metal Complexes $PtX_4^{2-}$ (X= Cl, Br)," <u>Journal of the American Chemical Society</u>, vol. 122, no. 10, pp. 2339–2345, 2000.

[22] M. Kordel, D. Schooss, S. Gilb, M. N. Blom, O. Hampe, and M. M. Kappes, "Photodissociation of trapped metastable multiply charged anions: A routine electronic spectroscopy of isolated large molecules?," <u>The Journal of Physical Chemistry A</u>, vol. 108, no. 22, pp. 4830–4837, 2004.

[23] P. Weis, O. Hampe, S. Gilb, and M. M. Kappes, "Metastability of isolated platinum and palladium tetrahalide dianions and the role of electron tunneling," <u>Chemical Physics Letters</u>, vol. 321, no. 5, pp. 426–432, 2000.

[24] M. N. Blom, O. Hampe, S. Gilb, P. Weis, and M. M. Kappes, "Tunneling electron loss from isolated platinum tetrahalide dianions," <u>The Journal of Chemical Physics</u>, vol. 115, p. 3690, 2001.

[25] A. Dreuw and L. Cederbaum, "Nature of the repulsive Coulomb barrier in multiply charged negative ions," <u>Physical Review A</u>, vol. 63, no. 1, p. 012501, 2000.

[26] W. E. Boxford and C. E. Dessent, "Probing the intrinsic features and environmental stabilization of multiply charged anions," <u>Physical Chemistry Chemical Physics</u>, vol. 8, no. 44, pp. 5151–5165, 2006.

[27] C. Rensing, O. T. Ehrler, J.-P. Yang, A.-N. Unterreiner, and M. M. Kappes, "Photodissociation dynamics of $IrBr_6^{2-}$ dianions by time-resolved photoelectron spectroscopy," <u>The Journal of Chemical Physics</u>, vol. 130, p. 234306, 2009.

[28] J. C. Marcum and J. M. Weber, "Electronic photodissociation spectra and decay pathways of gas-phase $IrBr_6^{2-}$," <u>The Journal of Chemical Physics</u>, vol. 131, p. 194309, 2009.

[29] T. Sommerfeld and M. Child, "Dissociation lifetimes of alkali halide dianions," The Journal of Chemical Physics, vol. 110, p. 5670, 1999.

[30] W. E. Boxford, M. O. El Ghazaly, C. E. Dessent, and S. Brøndsted Nielsen, "High-energy collision induced dissociation of iridium hexa-halide dianions: Observation of triple electron detachment and other decay pathways," International Journal of Mass Spectrometry, vol. 244, no. 1, pp. 60–64, 2005.

[31] J. Friedrich, Electronic Photodissociation Spectroscopy of Electrosprayed Anions. PhD thesis, Universitat Karlsruhe, 2001.

[32] X.-B. Wang and L.-S. Wang, "Observation of negative electron-binding energy in a molecule," Nature, vol. 400, no. 6741, pp. 245–248, 1999.

[33] X.-B. Wang, Y.-L. Wang, H.-K. Woo, J. Li, G.-S. Wu, and L.-S. Wang, "Free tetra-and hexa-coordinated platinum-cyanide dianions, $Pt(CN)_4{}^{2-}$ and $Pt(CN)_6{}^{2-}$: A combined photodetachment photoelectron spectroscopic and theoretical study," Chemical physics, vol. 329, no. 1, pp. 230–238, 2006.

[34] M. Pernpointner, J. Breidbach, and L. S. Cederbaum, "Remarkable interplay of electron correlation and relativity in the photodetachment spectrum of $PtCl_6{}^{2-}$," The Journal of Chemical Physics, vol. 122, p. 064311, 2005.

[35] L. Colombi Ciacchi, W. Pompe, and A. De Vita, "Initial nucleation of platinum clusters after reduction of $K_2PtCl_4$ in aqueous solution: A first principles study," Journal of the American Chemical Society, vol. 123, no. 30, pp. 7371–7380, 2001.

[36] N. Mohajeri, A. T-Raissi, and O. Adebiyi, "Hydrolytic cleavage of ammonia-borane complex for hydrogen production," Journal of Power Sources, vol. 167, no. 2, pp. 482–485, 2007.

[37] M. Sakamoto, M. Fujistuka, and T. Majima, "Light as a construction tool of metal nanoparticles: Synthesis and mechanism," Journal of Photochemistry and Photobiology C: Photochemistry Reviews, vol. 10, no. 1, pp. 33–56, 2009.

[38] A. Jańczyk, A. Wolnicka-Głubisz, K. Urbanska, H. Kisch, G. Stochel, and W. Macyk, "Photodynamic activity of platinum (IV) chloride surface-modified $TiO_2$ irradiated with visible light," Free Radical Biology and Medicine, vol. 44, no. 6, pp. 1120–1130, 2008.

[39] W. Macyk and H. Kisch, "Photosensitization of crystalline and amorphous titanium dioxide by platinum (IV) chloride surface complexes," Chemistry-A European Journal, vol. 7, no. 9, pp. 1862–1867, 2001.

[40] E. M. Glebov, A. V. Kolomeets, I. P. Pozdnyakov, V. F. Plyusnin, V. P. Grivin, N. V. Tkachenko, and H. Lemmetyinen, "Redox processes in photochemistry of Pt(IV) hexahaloid complexes," RSC Advances, vol. 2, no. 13, pp. 5768–5778, 2012.

[41] M. Scheller and L. Cederbaum, "Stability of $MX_3{}^{2+}$ ions in the gas phase and when do ionic molecules have large ionization potentials," The Journal of Chemical Physics, vol. 99, p. 441, 1993.

[42] R. Parr and W. Yang, Density-Functional Theory of Atoms and Molecules, vol. 16 of International Series of Monographs on Chemistry. Oxford University Press, 1989.

[43] F. Weigend, M. Hser, H. Patzelt, and R. Alrichs, "Electronic structure calculations on workstation computers: The program system Turbomole," Chemical Physics Letters, vol. 162, no. 3, pp. 165 – 169, 1989.

[44] O. Treutler and R. Ahlrichs, "Efficient molecular numerical integration schemes," The Journal of Chemical Physics, vol. 102, no. 1, pp. 346–354, 1995.

[45] R. Ahlrichs and K. May, "Contracted all-electron Gaussian basis sets for atoms Rb to Xe," Physical Chemistry Chemical Physics, vol. 2, no. 5, pp. 943–945, 2000.

[46] K. Eichkorn, F. Weigend, O. Treutler, and R. Ahlrichs, "Auxiliary basis sets for main row atoms and transition metals and their use to approximate Coulomb potentials," Theoretical Chemistry Accounts, vol. 97, no. 1-4, pp. 119–124, 1997.

[47] A. Schäfer, C. Huber, and R. Ahlrichs, "Fully optimized contracted Gaussian basis sets of triple zeta valence quality for atoms Li to Kr," The Journal of Chemical Physics, vol. 100, p. 5829, 1994.

[48] R. Bauernschmitt and R. Ahlrichs, "Treatment of electronic excitations within the adiabatic approximation of time dependent density functional theory," Chemical Physics Letters, vol. 256, pp. 454 – 464, 1996.

[49] D. L. Swihart and W. R. Mason, "Electronic spectra of octahedral platinum (IV) complexes," Inorganic Chemistry, vol. 9, no. 7, pp. 1749–1757, 1970.

[50] A. Goursot, E. Penigault, and H. Chermette, "Relativistic MS X$\alpha$ calculations of the electronic structure and related properties of $PtCl_6{}^{2-}$," Chemical Physics Letters, vol. 97, no. 2, pp. 215–220, 1983.

[51] T. Sommerfeld, F. S., P. M., and C. L. Z., "Electronic Structure of Isolated $PtX_6{}^{2-}$ (X = F,Cl,Br) Dianions," The Journal of Chemical Physics, vol. 118, no. 4, pp. 1747–1755, 2003.

[52] M. Pernpointner, T. Rapps, and L. S. Cederbaum, "Photodetachment spectra of the $PtX_6$ (X= F, Cl, Br) dianions and their Jahn–Teller distortions: A fully relativistic study," The Journal of Chemical Physics, vol. 129, p. 174302, 2008.

[53] J. Marcum, S. Kaufman, and J. Weber, "Gas-Phase Experiments on Au(III) Photochemistry," The Journal of Physical Chemistry A, vol. 115, no. 14, pp. 3006–3015, 2011.

[54] V. Gabelica, T. Tabarin, R. Antoine, F. Rosu, I. Compagnon, M. Broyer, E. De Pauw, and P. Dugourd, "Electron photodetachment dissociation of DNA polyanions in a quadrupole ion trap mass spectrometer," Analytical chemistry, vol. 78, no. 18, pp. 6564–6572, 2006.

[55] R. Burke, W. Boxford, and C. Dessent, "Counter-ion perturbation of the fragmentation pathways of multiply charged anions: Evidence for exit channel complexes on the fragmentation potential energy surfaces," The Journal of Chemical Physics, vol. 125, no. 2, p. 021105, 2006.

[56] Y. Sakamoto, A. Fukuoka, T. Higuchi, N. Shimomura, S. Inagaki, and M. Ichikawa, "Synthesis of platinum nanowires in organic-inorganic mesoporous silica templates by photoreduction: Formation mechanism and isolation," The Journal of Physical Chemistry B, vol. 108, no. 3, pp. 853–858, 2004.

[57] A. Fukuoka, H. Araki, Y. Sakamoto, N. Sugimoto, H. Tsukada, Y. Kumai, Y. Akimoto, and M. Ichikawa, "Template synthesis of nanoparticle arrays of gold and platinum in mesoporous silica films," Nano Letters, vol. 2, no. 7, pp. 793–795, 2002.

# Bibliography

[1] K. Abu-Saba, D. Sedlak, and A. Flegal, <u>Indirect reduction of hexavalent chromium by copper in the presence of superoxide</u>, Marine Chemistry **69** (2000), 33 – 41.

[2] C. Adamo and V. Barone, <u>Toward reliable density functional methods without adjustable parameters: The I</u> The Journal of Chemical Physics **110** (1999), 6158.

[3] Arthur W Adamson, William L Waltz, Edoardo Zinato, Donald W Watts, Paul D Fleischauer, and Robert D Lindholm, <u>Photochemistry of transition-metal coordination compounds</u>, Chemical Reviews **68** (1968), no. 5, 541–585.

[4] Reinhart Ahlrichs and Klaus May, <u>Contracted all-electron Gaussian basis sets for atoms Rb to Xe</u>, Physical Chemistry Chemical Physics **2** (2000), no. 5, 943–945.

[5] V. Anufrienko, R. Shutilov, G. Zenkovets, V. Gavrilov, N. Vasenin, A. Shubin, T. Larina, A. Zhuzhgov, Z. Ismagilov, and V. Parmon, <u>The state of $Cu^{2+}$ ions in concentrated aqueous ammonia solutions of copper nitrate</u>, Russian Journal of Inorganic Chemistry **57** (2012), no. 9, 1285–1290.

[6] P. Armentrout, <u>The thermochemistry of adsorbates on transition metal cluster ions: Relationship to bulk-p</u> European Journal of Mass Spectrometry **9** (2003), no. 6, 531–538.

[7] P. Armentrout and T. Baer, <u>Gas-phase ion dynamics and chemistry</u>, The Journal of Physical Chemistry **100** (1996), no. 31, 12866–12877.

[8] PB Armentrout, <u>Reactions and thermochemistry of small transition metal cluster ions</u>, Annual Review of Physical Chemistry **52** (2001), no. 1, 423–461.

[9] CJ Ballhausen, <u>A vibrational analysis of the $MnO_4{}^-$ bands</u>, Theoretica Chimica Acta **1** (1963), no. 4, 285–293.

[10] CJ Ballhausen and Andrew D Liehr, <u>Intensities in inorganic complexes: Part II. Tetrahedral complexes</u>, Journal of Molecular Spectroscopy **2** (1958), no. 1, 342–360.

[11] RF Barrow and P Crozet, <u>Gas-phase molecular spectroscopy</u>, Annual Reports Section C (Physical Chemistry) **93** (1997), 187–256.

[12] F Basolo and RG Pearson, <u>Mechanisms of Inorganic Reactions</u>, Wiley, New York, 1967.

[13] R. Bauernschmitt and R. Ahlrichs, <u>Treatment of electronic excitations within the adiabatic approximation of time dependent density functional theory</u>, Chemical Physics Letters **256** (1996), 454 – 464.

[14] R. Bauernschmitt, M. Häser, O. Treutler, and R. Ahlrichs, <u>Calculation of excitation energies within time-dependent density functional theory using auxiliary basis set expansions</u>, Chemical Physics Letters **264** (1997), no. 6, 573–578.

[15] E. Beckmann, <u>Untersuchungen in der Campherreihe</u>, Justus Liebigs Annalen der Chemie **250** (1889), no. 3, 322–375.

[16] J Alberto Beswick and Joshua Jortner, <u>Time scales for molecular photodissociation</u>, Chemical Physics Letters **168** (1990), no. 3, 246–248.

[17] Martine N Blom, Oliver Hampe, Stefan Gilb, Patrick Weis, and Manfred M Kappes, <u>Tunneling electron loss from isolated platinum tetrahalide dianions</u>, The Journal of Chemical Physics **115** (2001), 3690.

[18] D. Blowes, C. Ptacek, and J. Jambor, <u>In-Situ Remediation of Cr(VI)-Contaminated Groundwater Using Per</u>, Environmental Science And Technology **31** (1997), no. 12, 3348–3357.

[19] P Boulet, Henry Chermette, Claude Daul, F Gilardoni, F Rogemond, Jacques Weber, and G Zuber, <u>Absorption spectra of several metal complexes revisited by the time-dependent density-functional theory-response theory formalism</u>, The Journal of Physical Chemistry A **105** (2001), no. 5, 885–894.

[20] William E Boxford and Caroline EH Dessent, <u>Probing the intrinsic features and environmental stabilization of multiply charged anions</u>, Physical Chemistry Chemical Physics **8** (2006), no. 44, 5151–5165.

[21] William E Boxford, Mohamed OA El Ghazaly, Caroline EH Dessent, and Steen Brøndsted Nielsen, <u>High-energy collision induced dissociation of iridium hexa-halide dianions: Observation o</u>, International Journal of Mass Spectrometry **244** (2005), no. 1, 60–64.

[22] William E Boxford, Julie K Pearce, and Caroline EH Dessent, <u>Ionic fragmentation versus electron detachment in isolated transition metal complex dianions</u>, Chemical Physics Letters **399** (2004), no. 4, 465–470.

[23] Robert W Boyd, <u>Nonlinear optics</u>, Academic press, 2003.

[24] N. Brasch, D. Buckingham, A. Evans, and C. Clark, <u>$^{17}$O NMR Study of Chromium(VI) Ions in Water</u>, Journal of the American Chemical Society **118** (1996), no. 34, 7969–7980.

[25] Marten A Buijse and Evert Jan Baerends, <u>Analysis of nondynamical correlation in the metal–ligand bond. P</u>, The Journal of Chemical Physics **93** (1990), 4129.

[26] R. Burke, W. Boxford, and C. Dessent, <u>Counter-ion perturbation of the fragmentation pathways of multiply</u>, The Journal of Chemical Physics **125** (2006), no. 2, 021105.

[27] Ruth M Burke, William E Boxford, and Caroline EH Dessent, <u>Characterizing the intrinsic stability of gas-phase clusters of transition metal complex dianions with alkali m</u>, The Journal of Chemical Physics **126** (2007), no. 6, 064308–064308.

[28] Anders Byström and Karl-Axel Wilhelmi, The crystal structure of chromium trioxide, Acta Qiemica Scandinavica **4** (1950), 1131–1141.

[29] O. Cabarcos, C. Weinheimer, J. Lisy, and S. Xantheas, Microscopic hydration of the fluoride anion, The Journal of Chemical Physics **110** (1999), 5.

[30] A. Castleman Jr and K. Bowen Jr, Clusters: Structure, energetics, and dynamics of intermediate states of m The Journal of Physical Chemistry **100** (1996), no. 31, 12911–12944.

[31] S.Y. Chen, S.W. Huang, P.N. Chiang, J.C. Liu, W.H. Kuan, J.H. Huang, J.T. Hung, Y.M. Tzou, C.C. Chen, and M.K. Wang, Influence of chemical compositions and molecular weights of humic acids on Cr(VI) photo-reduction, Journal of Hazardous Materials **197** (2011), no. 0, 337 – 344.

[32] J. Chlistunoff and K. Johnston, UV/Vis Spectroscopic Determination of the Dissociation Constant of Bichro The Journal of Physical Chemistry B **102** (1998), no. 20, 3993–4003.

[33] Paweł Cieśla, Przemysław Kocot, Piotr Mytych, and Zofia Stasicka, Homogeneous photocatalysis by transition metal complexes in the environment, Journal of Molecular Catalysis A: Chemical **224** (2004), no. 1, 17–33.

[34] Lucio Colombi Ciacchi, Wolfgang Pompe, and Alessandro De Vita, Initial nucleation of platinum clusters after reduction of $K_2PtCl_4$ in aqueous solution: A first principles stu Journal of the American Chemical Society **123** (2001), no. 30, 7371–7380.

[35] P. Connett and K. Wetterhahn, Metabolism of the carcinogen chromate by cellular constituents, Inorganic Elements in Biochemistry, vol. 54, Springer Berlin Heidelberg, 1983.

[36] T. Cooper, D. Carl, and P. Armentrout, Hydration energies of zinc (II): Threshold collision-induced dissociat The Journal of Physical Chemistry A **113** (2009), no. 49, 13727–13741.

[37] Frank Albert Cotton, Geoffrey Wilkinson, Carlos A Murillo, and Manfred Bochmann, Advanced Inorganic Chemistry, vol. 5, Wiley New York, 1988.

[38] V. Daier, S. Signorella, M. Rizzotto, M. Frascaroli, C. Palopoli, C. Brondino, J. Salas-Peregrin, and L. Sala, Kinetics and Mechanism of the Reduction of Cr(VI) to Cr(III) by D-ribose and 2-deoxy-D-ribose, Canadian Journal of Chemistry **77** (1999), no. 1, 57–64.

[39] Sukalyan Dash, Sabita Patel, and Bijay K Mishra, Oxidation by permanganate: Synthetic and mechanistic aspects, Tetrahedron **65** (2009), no. 4, 707–739.

[40] W. Dehn, Colorimetric studies on the nature of chromate solutions, Journal of the American Chemical Society **36** (1914), no. 5, 829–847.

[41] G Den Boef, HJ Van Der Beek, and Th Braaf, Absorption spectra in the visible and UV region of potassium Recueil des Travaux Chimiques des Pays-Bas **77** (1958), no. 11, 1064–1070.

[42] D. Dey, J. Dkhar, and M. Mahanti, Kinetics of oxidation of primary alcohols by quinolinium dichromate, Oxidation Communications **21** (1998), no. 1, 62–67.

[43] N. Dhas, P. Raj, and A. Gedanken, Synthesis, characterization, and properties of metallic copper nanoparticles, Chemistry of Materials **10** (1998), no. 5, 1446–1452.

[44] A Dreuw and LS Cederbaum, Anions made of cations and dianions:[CsC] and [CsC], The Journal of Chemical Physics **111** (1999), 1467.

[45] _____, Nature of the repulsive Coulomb barrier in multiply charged negative ions, Physical Review A **63** (2000), no. 1, 012501.

[46] Andreas Dreuw, Lorenz S. Cederbaum, and Markus K. Scheller, Multiply charged anions in the gas phase, Chemical Reviews **102** (2002), no. 1, 181–200.

[47] Karin Eichkorn, Florian Weigend, Oliver Treutler, and Reinhart Ahlrichs, Auxiliary basis sets for main row atoms and transition metals and their use to approximate Coulomb poten, Theoretical Chemistry Accounts **97** (1997), no. 1-4, 119–124.

[48] John B Fenn, Matthias Mann, Chin Kai Meng, Shek Fu Wong, and Craig M Whitehouse, Electrospray ionization for mass spectrometry of large biomolecules, Science **246** (1989), no. 4926, 64–71.

[49] S. Feyel, T. Waters, R. O'Hair, and A. Wedd, Gas-Phase Oxidation of Alkoxo Ligands in Bis(peroxo) [MO(O, Journal of the Chemical Society, Dalton Transactions **0** (2004), 4010–4016.

[50] M. I. Frascaroli, S. Signorella, J. C. Gonzalez, M. F. Mangiameli, S. Garcia, E. R. de Celis, L. Piehl, L. F. Sala, and A. M. Atria, Oxidation of 2-amino-2-deoxy-d-glucopyranose by Hypervalent Chromium: Kinetics and Mechanism, Polyhedron **30** (2011), no. 11, 1914 – 1921.

[51] J. Friedrich, Electronic Photodissociation Spectroscopy of Electrosprayed Anions, Ph.D. thesis, Universitat Karlsruhe, 2001.

[52] J. Friedrich, S. Gilb, O. Ehrler, A. Behrendt, and M.M. Kappes, Electronic photodissociation spectroscopy of isolated $IrX_6^{2-}$ (X=Cl,Br), The Journal of Chemical Physics **117** (2002), no. 6, 2635.

[53] J. Friedrich, P. Weis, J. Kaller, R.L. Whetten, and M.M. Kappes, Alkali halide cluster dianions: metastability and threshold sizes, The European Physical Journal D-Atomic, Molecular, Optical and Plasma Physics **9** (1999), no. 1, 269–272.

[54] Atsushi Fukuoka, Hidenobu Araki, Yuzuru Sakamoto, Noriaki Sugimoto, Hiroshi Tsukada, Yoko Kumai, Yusuke Akimoto, and Masaru Ichikawa, Template synthesis of nanoparticle arrays of gold and platinum in mesoporous silica films, Nano Letters **2** (2002), no. 7, 793–795.

[55] Valérie Gabelica, Thibault Tabarin, Rodolphe Antoine, Frédéric Rosu, Isabelle Compagnon, Michel Broyer, Edwin De Pauw, and Philippe Dugourd, Electron photodetachment dissociation of DNA polyanions in a quadrupole ion trap mass spectrometer, Analytical chemistry **78** (2006), no. 18, 6564–6572.

[56] John M Garver, Yao-ren Fang, Nicole Eyet, Stephanie M Villano, Veronica M Bierbaum, and Kenneth Charles Westaway, A direct comparison of reactivity and mechanism in the gas phase and in solution, Journal of the American Chemical Society **132** (2010), no. 11, 3808–3814.

[57] Dieter Gerlich, <u>Inhomogeneous, RF fields: a versatile tool for the study of processes with slow ions</u>, Advances in Chemical Physics **82** (1992), 1–176.

[58] M Ghiaci, R Kia, A Abbaspur, and F Seyedeyn-Azad, <u>Adsorption of chromate by surfactant-modified zeolites and MCM-41 molecular sieve</u>, Separation and Purification Technology **40** (2004), no. 3, 285–295.

[59] EM Glebov, VF Plyusnin, VP Grivin, AB Venediktov, and SV Korenev, <u>Photochemistry of $PtBr_6^{2-}$ in aqueous solution</u>, Russian Chemical Bulletin **56** (2007), no. 12, 2357–2363.

[60] Evgeni M Glebov, Aleksandr V Kolomeets, Ivan P Pozdnyakov, Victor F Plyusnin, Vjacheslav P Grivin, Nikolai V Tkachenko, and Helge Lemmetyinen, <u>Redox processes in photochemistry of Pt(IV) hexahaloid complexes</u>, RSC Advances **2** (2012), no. 13, 5768–5778.

[61] Alessandro Gomez and Keqi Tang, <u>Charge and fission of droplets in electrostatic sprays</u>, Physics of Fluids **6** (1994), 404.

[62] Juan Carlos González, Silvia Garcıa, Nadia Mamana, Luis F Sala, and Sandra Signorella, <u>Evidence for the involvement of Cr(II) and free radicals as intermediates in the reduction of $HCrO_4^-$ by sa</u>, Inorganic Chemistry Communications **9** (2006), 437–440.

[63] A Goursot, E Penigault, and H Chermette, <u>Relativistic MS X$\alpha$ calculations of the electronic structure and r</u>, Chemical Physics Letters **97** (1983), no. 2, 215–220.

[64] C. Granqvist, L. Kish, and W. Marlow, <u>Gas Phase Nanoparticle Synthesis</u>, Springer, 2005.

[65] N. Greenwood, A. Earnshaw, and A. Earnshaw, <u>Chemistry of the elements</u>, Pergamon Press Oxford, 1984.

[66] Norman Neill Greenwood, Alan Earnshaw, and Alan Earnshaw, <u>Chemistry of the elements</u>, vol. 1341, Butterworth-Heinemann Oxford, 1997.

[67] VP Grivin, IV Khmelinski, VF Plyusnin, II Blinov, and KP Balashev, <u>Photochemistry of the $PtCl_6^{2-}$ complex in methanol solution</u>, Journal of Photochemistry and Photobiology A: Chemistry **51** (1990), no. 2, 167–178.

[68] Raquel Güell, Clàudia Fontàs, Victòria Salvadó, and Enriqueta Anticó, <u>Development of a selective optical sensor for Cr(VI) monitoring in polluted waters</u>, Analytica Chimica Acta **594** (2007), no. 2, 162–168.

[69] H. Guo, C.G. Dong, D.S. Kim, D. Urabe, J. Wang, J. Kim, Xiang Liu, T. Sasaki, and Y. Kishi, <u>Toolbox Approach to the Search for Effective Ligands for Catalytic Asymmetric Cr-Mediated Coupling Rea</u>, Journal of the American Chemical Society **131** (2009), no. 42, 15387–15393, PMID: 19795862.

[70] Gennady L Gutsev, Puru Jena, and Rodney J Bartlett, <u>Structure and stability of $BF_3{\cdot}F$ and $AlF_3{\cdot}F$ superhalogens</u>, Chemical Physics Letters **292** (1998), no. 3, 289–294.

[71] Gennady L Gutsev, BK Rao, P Jena, Xue-Bin Wang, and Lai-Sheng Wang, <u>Origin of the unusual stability of $MnO_4^-$</u>, Chemical Physics Letters **312** (1999), no. 5, 598–605.

[72] G. Haight, G. Jursich, M. Kelso, and P. Merrill, Kinetics and mechanisms of oxidation of lactic acid by chromium(VI) and chromium(V), Inorganic Chemistry **24** (1985), no. 18, 2740–2746.

[73] B.J. Hathaway and A.E. Underhill, 433. The ultraviolet and visible spectra of some anhydrous copper (II) sa Journal of the American Chemical Society (1962), 2257–2262.

[74] P.J. Hay and W. Wadt, Ab-initio effective core potentials for molecular calculations. Potentials for K to Au The Journal of Chemical Physics **82** (1985), no. 1, 299–310.

[75] H. Headlam and P. Lay, EPR Spectroscopic Studies of the Reduction of Chromium(VI) by Methanol in the Inorganic Chemistry **40** (2001), no. 1, 78–86.

[76] Brian M Hoffman, Charles J Weschler, and Fred Basolo, The dioxygen adduct of meso-tetraphenylporphyrinmanganese (II), a synthetic oxygen carrier, Journal of the American Chemical Society **98** (1976), no. 18, 5473–5482.

[77] Edmond Hoffmann, Mass Spectrometry, Wiley Online Library, 1996.

[78] Smith L Holt and CJ Ballhausen, Low temperature absorption spectra of $KMnO_4$ in $KClO_4$, Theoretica Chimica Acta **7** (1967), no. 4, 313–320.

[79] Jørgen Houmøller, Sydney H Kaufman, Kristian Støchkel, Lokesh C Tribedi, Steen Brøndsted Nielsen, and J Mathias Weber, On the photoabsorption by permanganate ions in vacuo and the role of a single water molecule. new experimental benchmarks for electronic structure theory, ChemPhysChem (2013), 1133–1137.

[80] WB Hugo, A brief history of heat and chemical preservation and disinfection, Journal of Applied Microbiology **71** (1991), no. 1, 9–18.

[81] Agnieszka Jańczyk, Agnieszka Wolnicka-Głubisz, Krystyna Urbanska, Horst Kisch, Grażyna Stochel, and Wojciech Macyk, Photodynamic activity of platinum (IV) chloride surface-modified $TiO_2$ irradiated with visible light, Free Radical Biology and Medicine **44** (2008), no. 6, 1120–1130.

[82] Y. Jean, Molecular Orbitals of Transition Metal Complexes, OUP Oxford, 2005.

[83] J. M. Jehng, I. E. Wachs, B. M. Weckhuysen, and R. A. Schoonheydt, Surface chemistry of silica-titania-supported chromium oxide catalysts, Journal of the Chemical Society, Faraday Transactions **91** (1995), 953–961.

[84] K. Jennette, K. Wetterhahn, Microsomal Reduction of the Carcinogen Chromate Produces Chromium(V), Journal of the American Chemical Society **104** (1982), no. 3, 874–875.

[85] Ronald M Jones, Dieter Gerlich, and Scott L Anderson, Simple radio-frequency power source for ion guides and ion traps, Review of Scientific Instruments **68** (1997), no. 9, 3357–3362.

[86] Chr Klixbüll Jørgensen, Electron transfer spectra of hexahalide complexes, Molecular Physics **2** (1959), no. 3, 309–332.

[87] Linta Jose, Michael Seth, and Tom Ziegler, Molecular and Vibrational Structure of Tetroxo $d^0$ Metal Comple The Journal of Physical Chemistry A **116** (2012), no. 7, 1864–1876.

[88] P. Jungwirth and D. Tobias, Molecular structure of salt solutions: A new view of the interface with implicat
The Journal of Physical Chemistry B **105** (2001), no. 43, 10468–10472.

[89] Josef Kalcher, Gas-phase stabilities of small anions, Annual Reports Section C (Physical
Chemistry) **93** (1996), 147–186.

[90] A. Kamariotis, O. Boyarkin, S. Mercier, R. Beck, M. Bush, E. Williams, and R.,
Infrared Spectroscopy of Hydrated Amino Acids in the Gas Phase: Protonated and Lithiated Valine,
Journal of the American Chemical Society **128** (2006), no. 3, 905–916, PMID: 16417381.

[91] S. Keinan and D. Avnir, Studies in copper (II) complexes: correlations between quantitative symmetry and
Journal of the Chemical Society, Dalton Transactions (2001), no. 6, 941–947.

[92] Michele A Kelly, Martha M Vestling, Catherine C Fenselau, and Philip B Smith,
Electrospray analysis of proteins: A comparison of positive-ion and negative-ion mass spectra at high and l
Organic Mass Spectrometry **27** (1992), no. 10, 1143–1147.

[93] P. Khanna, S. Gaikwad, P. Adhyapak, N. Singh, and R. Marimuthu, Synthesis and
characterization of copper nanoparticles, Materials Letters **61** (2007), no. 25, 4711–4714.

[94] R. Kieber and G. Helz, Indirect Photoreduction of Aqueous Chromium(VI), Environmental
Science And Technology **26** (1992), no. 2, 307–312.

[95] U. Klaning and M. Symons, Photoinduced oxidation of 2-propanol by acid chromate, Pro-
ceedings of the Chemical Society, London (1959), 95–96.

[96] U Kläning and MCR Symons, Structure and reactivity of the oxyanions of transition metals. Part VI. Photo
Journal of the Chemical Society (1959), 3269–3272.

[97] Ulrich Kläning, Complexes of acid chromate ion with alcohols or acetaldehyde, Acta Chemica
Scandinavica **11** (1957), 1313–1316.

[98] _____ , The photoinduced oxidation of 2-propanol by acid chromate, Acta Chemica Scandi-
navica **12** (1958), no. 5, 2.

[99] N. Kondratenko and V. Sherstyuk, Spectroscopic characteristics of chromium(VI) oxy anions in aqueous solu
Teoreticheskaya i Eksperimental'naya Khimiya **22** (1986), no. 6, 686–693.

[100] Mattias Kordel, Detlef Schooss, Stefan Gilb, Martine N Blom, Oliver Hampe, and Manfred M
Kappes, Photodissociation of trapped metastable multiply charged anions: A routine electronic spectroscop
The Journal of Physical Chemistry A **108** (2004), no. 22, 4830–4837.

[101] J. Kotas and Z. Stasicka, Chromium occurrence in the environment and methods of its
speciation, Environmental Pollution **107** (2000), no. 3, 263 – 283.

[102] Tai-Chu Lau, Jiangyao Wang, K. W. Michael Siu, and Roger Guevremont, Electrospray
tandem mass spectrometry of oxo complexes of chromium, manganese and tuthenium, Journal
of the Chemical Society, Chemical Communications (1994), no. 12, 1487–1488.

[103] R.E. LaVilla and S.H. Bauer, The structure of gaseous copper (II) nitrate as determined by electron diffract
Journal of the American Chemical Society **85** (1963), no. 22, 3597–3600.

[104] D. Lee and T. Chen, The oxidation of alcohols by permanganate. A comparison with other high-valent trans
The Journal of Organic Chemistry **56** (1991), no. 18, 5341–5345.

[105] Donald G Lee, Christopher R Moylan, Takatoshi Hayashi, and John I Brauman, Photochemistry of aqueous permanganate ion, Journal of the American Chemical Society **109** (1987), no. 10, 3003–3010.

[106] A. Levina and P. Lay, Mechanistic studies of relevance to the biological activities of chromium, Coordination Chemistry Reviews **249** (2005), 281 – 298, Inorganic Reaction Mechanisms, an appreciation of Henry Taube in his 90th year.

[107] A. Levina, L. Zhang, and P. Lay, Structure and Reactivity of a Chromium(V) Glutathione Complex, Inorganic Chemistry **42** (2003), no. 3, 767–784.

[108] F. Li, M. Byers, and R.S. Houk, Tandem mass spectrometry of metal nitrate negative ions produced by electrospray ionization, Journal of the American Society for Mass Spectrometry **14** (2003), no. 6, 671–679.

[109] D Löffler, JM Weber, and MM Kappes, Photodetachment spectroscopy of PtBr$_4$$^{2-}$: Probing the Coulomb ba
The Journal of Chemical Physics **123** (2005), 224308.

[110] Alfonz Luca, Stephan Schlemmer, Ivo Cermák, and Dieter Gerlich, On the combination of a linear field free trap with a time-of-flight mass spectrometer, Review of Scientific Instruments **72** (2001), no. 7, 2900–2908.

[111] M. Lykkegaard, H. Zettergren, M. Kirketerp, A. Ehlerding, J. Wyer, U. Kadhane, and S. Nielsen, Photodissociation of Isolated Ferric Heme and Heme-His Cations in an Electrostatic Ion Storage
The Journal of Physical Chemistry A **113** (2009), no. 8, 1440–1444.

[112] Wojciech Macyk and Horst Kisch, Photosensitization of crystalline and amorphous titanium dioxide by plati
Chemistry-A European Journal **7** (2001), no. 9, 1862–1867.

[113] BA Mamyrin, VI Karataev, DV Shmikk, and VA Zagulin, The mass reflectron, a new non-magnetic time-of-flight mass spectrometer with high resolution, Zhurnal Eksperimentaĺnoi i Teoreticheskoi Fiziki **64** (1973), 82–89.

[114] J. Marcum, A. Halevi, and J.M. Weber, Photodamage to Isolated Mononucleotides: Photodissociation Spect
Physical Chemistry Chemical Physics **11** (2009), 1740–1751.

[115] J. Marcum, S.H. Kaufman, and J.M. Weber, Gas-Phase Experiments on Au(III) Photochemistry, The Journal of Physical Chemistry A **115** (2011), no. 14, 3006–3015.

[116] Jesse Marcum, Electronic Photodissociation Spectroscopy of Electrosprayed Anions, Ph.D. thesis, University of Colorado Boulder, 2011.

[117] Jesse C Marcum and J Mathias Weber, Electronic photodissociation spectra and decay pathways of gas-phas
The Journal of Chemical Physics **131** (2009), 194309.

[118] R. Marcus, Electron transfer reactions in chemistry theory and experiment, Journal of Electroanalytical Chemistry **438** (1997), no. 1, 251–259.

[119] J Howard Mathews and Leon H Dewey, A quantitative study of some photochemical effects produced by ultra-violet light, The Journal of Physical Chemistry **17** (1913), no. 3, 211–218.

[120] M. Melník, M. Kabešová, M. Koman, L. Macåškovå, J. Garaj, C. Holloway, and A. Valent, Copper (II) Coordination Compounds: Classification and Analysis of Crystallographic and Structural Data, Journal of Coordination Chemistry **45** (1998), no. 1-4, 147–359.

[121] Giuseppina Menconi and Nikolas Kaltsoyannis, Time dependent DFT study of the electronic transition energ, Chemical physics letters **415** (2005), no. 1, 64–68.

[122] Walter Mertz, Chromium in Human Nutrition: A Review, The Journal of Nutrition **123** (1993), no. 4, 626–633.

[123] M. Mitewa and P.R. Bontchev, Chromium(V) coordination chemistry, Coordination Chemistry Reviews **61** (1985), no. 0, 241 – 272.

[124] M. Mitewa, A. Malinovski, P.R. Bontchev, and K. Kabassanov, ESR study on chromium(V) complexes formed in the process of photochemical oxidation of diethylene glyc, Inorganica Chimica Acta **8** (1974), no. 0, 17 – 23.

[125] Nahid Mohajeri, Ali T-Raissi, and Olawale Adebiyi, Hydrolytic cleavage of ammonia-borane complex for hydrogen production, Journal of Power Sources **167** (2007), no. 2, 482–485.

[126] D. Mohan and C. Pittman Jr., Activated carbons and low cost adsorbents for remediation of tri- and hexavalent chromium from water, Journal of Hazardous Materials **137** (2006), no. 2, 762 – 811.

[127] S. Mollah, D. Andrew, S. Johnson, A. Gwizdala III, and R.S. Houk, Identification of metal cations, metal complexes, and anions by electrospray mass spectrometry in the negative ion mode, Analytical Chemistry **72** (2000), no. 5, 985–991.

[128] Matthias Johann Molski and Konrad Seppelt, The transition metal hexafluorides, Dalton Transactions (2009), no. 18, 3379–3383.

[129] P. Mytych, A. Karocki, and Z. Stasicka, Mechanism of photochemical reduction of chromium(VI) by alcohols, Journal of Photochemistry and Photobiology A: Chemistry **160** (2003), no. 3, 163 – 170.

[130] H Nakai and H Nakatsuji, Mechanism of photochemical reaction of permanganate ion, Journal of Molecular Structure: THEOCHEM **311** (1994), 141–151.

[131] Johannes Neugebauer, Evert Jan Baerends, and Marcel Nooijen, Vibronic structure of the permanganate absorption spectrum from time-dependent density functional calculations, The Journal of Physical Chemistry A **109** (2005), no. 6, 1168–1179.

[132] R. Parr and W. Yang, Density-Functional Theory of Atoms and Molecules, International Series of Monographs on Chemistry, vol. 16, Oxford University Press, 1989.

[133] G. Paul and P. Kebarle, Thermodynamics of the association reactions hydroxide + water = (HOHOH)$^-$ and, The Journal of Physical Chemistry **94** (1990), no. 12, 5184–5189.

[134] M. Perera, P. Ganssle, and R. Metz, Microsolvation of $Co^{2+}$ and $Ni^{2+}$ by Acetonitrile and Water: Photodisso, Physical Chemistry Chemical Physics **13** (2011), 18347–18354.

[135] E. Pérez-Benito and E. Rodenas, Methanol and ethanol oxidation by chromium (VI) in aqueous perchloric a, Transition Metal Chemistry **18** (1993), no. 3, 329–334.

[136] Markus Pernpointner, Jörg Breidbach, and Lorenz S Cederbaum, Remarkable interplay of electron correlation and relativity in the photodetachment spectrum of $PtCl_6{}^{2-}$, The Journal of Chemical Physics **122** (2005), 064311.

[137] Markus Pernpointner, Thomas Rapps, and Lorenz S Cederbaum, Photodetachment spectra of the $PtX_6$ (X= F, Cl, Br) dianions and their Jahn–Teller distortions: A fully re The Journal of Chemical Physics **129** (2008), 174302.

[138] C. Pizzocaro, M. Bolte, and M. Hoffman, Polymerization of acrylamide photosensitized by the tris-(bipyridin Polyhedron **12** (1993), no. 8, 855 – 858.

[139] C Pizzocaro, C Lafond, and M Bolte, Dichromated polyvinylalcohol: key role of chromium (V) in the proper Journal of Photochemistry and Photobiology A: Chemistry **151** (2002), no. 1, 221–228.

[140] S. Ponder, J. Darab, and T. Mallouk, Remediation of Cr(VI) and Pb(II) Aqueous Solutions Using Supported Environmental Science And Technology **34** (2000), no. 12, 2564–2569.

[141] R. Powell, R. Puls, S. Hightower, and D. Sabatini, Coupled Iron Corrosion and Chromate Reduction: Mechanisms for Subsurface Remediation, Environmental Science And Technology **29** (1995), no. 8, 1913–1922.

[142] Hem Raj Pant, Bishweshwar Pant, Han Joo Kim, Altangerel Amarjargal, Chan Hee Park, Leonard D Tijing, Eun Kyo Kim, and Cheol Sang Kim, A green and facile one-pot synthesis of Ag-ZnO/RGO nanocomposite with effective photocatalytic activity Ceramics International (2012), 5083–5091.

[143] Christian Rensing, Oli T Ehrler, Ji-Ping Yang, Andreas-Neil Unterreiner, and Manfred M Kappes, Photodissociation dynamics of $IrBr_6{}^{2-}$ dianions by time-resolved photoelectron spectroscopy, The Journal of Chemical Physics **130** (2009), 234306.

[144] GHN Riddle, Electrostatic einzel lenses with reduced spherical aberration for use in field-emission guns, Journal of Vacuum Science and Technology **15** (1978), no. 3, 857–860.

[145] W. Robertson and M.A. Johnson, Molecular aspects of halide ion hydration: The cluster approach, Annual Review of Physical Chemistry **54** (2003), no. 1, 173–213.

[146] V. Roldán, M. Santoro, J. González, Salas-Peregrin J., S. Signorella, and L. Sala, Kinetics and mechanism of the reduction of Cr(VI) and Cr(V) by d-lactobionic acid, Journal of Inorganic Biochemistry **98** (2004), no. 2, 347 – 357.

[147] F. Sahureka, R. Burns, and E. von Nagy-Felsobuki, Electrospray identification of new polyoxochromate species, Inorganica Chimica Acta **332** (2002), no. 1, 7 – 17.

[148] Masanori Sakamoto, Mamoru Fujistuka, and Tetsuro Majima, Light as a construction tool of metal nanoparticles: Synthesis and mechanism, Journal of Photochemistry and Photobiology C: Photochemistry Reviews **10** (2009), no. 1, 33–56.

[149] Yuzuru Sakamoto, Atsushi Fukuoka, Takanori Higuchi, Noriyuki Shimomura, Shinji Inagaki, and Masaru Ichikawa, Synthesis of platinum nanowires in organic-inorganic mesoporous silica templates by photoreduction: Form The Journal of Physical Chemistry B **108** (2004), no. 3, 853–858.

[150] P. Salmon and G. Neilson, The coordination of Cu (II) in a concentrated copper nitrate solution, Journal of Physics: Condensed Matter **1** (1999), no. 31, 5291.

[151] Ansgar Schäfer, Christian Huber, and Reinhart Ahlrichs, Fully optimized contracted Gaussian basis sets of triple zeta valence quality for atoms Li to Kr, The Journal of Chemical Physics **100** (1994), 5829.

[152] Stephen N Schauer, Peter Williams, and RN Compton, Production of small doubly charged negative carbon cluster ions by sputtering, Physical Review Letters **65** (1990), no. 5, 625–628.

[153] Markus K Scheller, Robert N Compton, and Lorenz S Cederbaum, Gas-phase multiply charged anions, Science **270** (1995), no. 5239, 1160–1166.

[154] MK Scheller and LS Cederbaum, Stability of $MX_3^{2+}$ ions in the gas phase and when do ionic molecules have, The Journal of Chemical Physics **99** (1993), 441.

[155] _____ , Construction principle for stable multiply-negative charged molecular systems. Part I. Doubly-nega, The Journal of Chemical Physics **100** (1994), 8934.

[156] Reinhard Schinke, Photodissociation Dynamics: Spectroscopy and Fragmentation of Small Polyatomic Mole, vol. 1, Cambridge University Press, 1995.

[157] Michael Seth, Tom Ziegler, and Jochen Autschbach, Application of magnetically perturbed time-dependent density functional theory to magnetic circular dichro, The Journal of Chemical Physics **129** (2008), 104105.

[158] K. Shrestha and K. Sorensen, C.and Klabunde, Synthesis of CuO nanorods, reduction of CuO into Cu nanor, The Journal of Physical Chemistry C **114** (2010), no. 34, 14368–14376.

[159] T Sommerfeld and MS Child, Dissociation lifetimes of alkali halide dianions, The Journal of Chemical Physics **110** (1999), 5670.

[160] T. Sommerfeld, Feuerbacher S., Pernpointner M., and Cederbaum L. Z., Electronic Structure of Isolated $PtX_6^{2-}$ (X = F,Cl,Br) Dianions, The Journal of Chemical Physics **118** (2003), no. 4, 1747–1755.

[161] J. Speight, Ullmann's encyclopedia of industrial chemistry, Petroleum Science and Technology **17** (1999), no. 3-4, 445–445.

[162] J. F. Stanton, On the vibronic level structure in the NO radical. I. The ground electronic state, The Journal of Chemical Physics **126** (2007), 134309.

[163] Z. Staszak, A. Wojciechowska, and M. Cieslak-Golonka, Coordination geometry of Cr(VI) species: Structural and spectroscopic characteristics, Coordination Chemistry Reviews **249** (2005), 2391 – 2407.

[164] Z Staszak, A Wojciechowska, and M Cieslak-Golonka, Spectroscopic Investigation of Electronic States of the $CrO_4^{2-}$ Ion in the Visible and Ultraviolet Absorptio, Polish Journal of Chemistry **83** (2009), no. 3, 503–513.

[165] J. Stephens and D. Cruickshank, The Crystal Structure of $(CrO_3)_{infinity}$, Acta Crystallographica Section B **26** (1970), no. 3, 222–226.

[166] Carsten W Stoermer, Stefan Gilb, Jochen Friedrich, Detlef Schooss, and Manfred M Kappes, A high resolution dual mass gate for ion separation in laser desorption/ionization time of flight mass spectrometry, Review of Scientific Instruments **69** (1998), no. 4, 1661–1664.

[167] Rebecca Sutton, Chromium-6 in U.S. Tap Water, Tech. report, Environmental Working Group, December 2010.

[168] Donald L Swihart and W Roy Mason, Electronic spectra of octahedral platinum (IV) complexes, Inorganic Chemistry **9** (1970), no. 7, 1749–1757.

[169] Thibault Tabarin, Alexander Kulesza, Rodolphe Antoine, Roland Mitrić, Michel Broyer, Philippe Dugourd, and Vlasta Bonačić-Koutecký, Absorption enhancement and conformational control of peptides by small silver clusters, Physical review letters **101** (2008), no. 21, 213001.

[170] RK Tandon, PT Crisp, J Ellis, and RS Baker, Effect of pH on chromium (VI) species in solution, Talanta **31** (1984), no. 3, 227–228.

[171] Liang Tang and Paul Kebarle, Dependence of ion intensity in electrospray mass spectrometry on the concentration of the analytes in the electrosprayed solution, Analytical Chemistry **65** (1993), no. 24, 3654–3668.

[172] Geoffrey Taylor, Disintegration of water drops in an electric field, Proceedings of the Royal Society of London. Series A. Mathematical and Physical Sciences **280** (1964), no. 1382, 383–397.

[173] J. Teltow, Absorption spectrum of the permanganate ion in various crystal lattices, Zeitschrift für Physikalische Chemie **B40** (1938), 397–430.

[174] _____, Absorption spectra of permanganate, chromate, vanadate and manganate ion in crystals, Zeitschrift für Physikalische Chemie **B43** (1939), 198–212.

[175] O. Treutler and R. Ahlrichs, Efficient molecular numerical integration schemes, The Journal of Chemical Physics **102** (1995), no. 1, 346–354.

[176] W. Tsang, Heats of formation of organic free radicals by kinetic methods, Structure Energetics and Reactivity in Chemistry Series (SEARCH series), vol. 4, Springer Netherlands, 1996.

[177] A. Usher, D. McPhail, and J. Brugger, A spectrophotometric study of aqueous Au(III) halide–hydroxide com Geochimica et Cosmochimica Acta **73** (2009), no. 11, 3359–3380.

[178] SJA Van Gisbergen, JA Groeneveld, A Rosa, JG Snijders, and EJ Baerends, Excitation Energies for Transition Metal Compounds from Time-Dependent Density Functional Theory. Ap The Journal of Physical Chemistry A **103** (1999), no. 34, 6835–6844.

[179] Joseph Thomas Verdeyen, Laser electronics, Prentice Hall, Englewood Cliffs, NJ, 1989.

[180] Arlen Viste and Harry B Gray, The electronic structure of permanganate ion, Inorganic Chemistry **3** (1964), no. 8, 1113–1123.

[181] T. Vladislav and V. Simeon, Ion association in aqueous solutions of strong electrolytes: a UV–Vis spectrome Physical Chemistry Chemical Physics **1** (1999), no. 2, 299–302.

[182] WL Waltz, J Lilie, A Goursot, and H Chermette, Photolytic and radiolytic study of platinum (III) complex ions containing aquo and chloro ligands, Inorganic Chemistry **28** (1989), no. 12, 2247–2256.

[183] Lai-Sheng Wang, Chuan-Fan Ding, Xue-Bin Wang, and SE Barlow, Photodetachment photoelectron spectroscopy of multiply charged anions using electrospray ionization, Review of Scientific Instruments **70** (1999), no. 4, 1957–1966.

[184] Lai-Sheng Wang, Chuan-Fan Ding, Xue-Bin Wang, and John B Nicholas, Probing the potential barriers and intramolecular electrostatic interactions in free doubly charged anions, Physical Review Letters **81** (1998), no. 13, 2667–2670.

[185] Lai-Sheng Wang and Xue-Bin Wang, Probing free multiply charged anions using photodetachment photoelectron spectroscopy, The Journal of Physical Chemistry A **104** (2000), no. 10, 1978–1990.

[186] X.B Wang, X. Yang, and L.S. Wang, Probing solution-phase species and chemistry in the gas phase, International Reviews in Physical Chemistry **21** (2002), no. 3, 473–498.

[187] Xue-Bin Wang, Chuan-Fan Ding, and Lai-Sheng Wang, Electron tunneling through the repulsive coulomb barrier in photodetachment of multiply charged anions, Chemical Physics Letters **307** (1999), no. 5, 391–396.

[188] Xue-Bin Wang and Lai-Sheng Wang, Experimental search for the smallest stable multiply charged anions in the gas phase, Physical Review Letters **83** (1999), no. 17, 3402–3405.

[189] _____, Observation of negative electron-binding energy in a molecule, Nature **400** (1999), no. 6741, 245–248.

[190] _____, Photodetachment of free hexahalogenometallate doubly charged anions in the gas phase: $[ML_6]^{2-}$,( The Journal of Chemical Physics **111** (1999), 4497.

[191] _____, Photodetachment of Multiply Charged Anions: The Electronic Structure of Gaseous Square-Plana Journal of the American Chemical Society **122** (2000), no. 10, 2339–2345.

[192] _____, Photoelectron spectroscopy of multiply charged anions, Annual Review of Physical Chemistry **60** (2009), 105–126.

[193] Xue-Bin Wang, Yi-Lei Wang, Hin-Koon Woo, Jun Li, Guo-Shi Wu, and Lai-Sheng Wang, Free tetra-and hexa-coordinated platinum-cyanide dianions, $Pt(CN)_4^{2-}$ and $Pt(CN)_6^{2-}$: A combined photo Chemical physics **329** (2006), no. 1, 230–238.

[194] T. Waters, X. Wang, S. Li, B. Kiran, D. Dixon, and L.S. Wang, Electronic Structure of the Hydroxo and Methoxo Oxometalate Anions $MO_3(OH)^-$ and $MO_3(OCH_3)^-$ (M The Journal of Physical Chemistry A **109** (2005), no. 51, 11771–11780.

[195] A. Weaver, D.W. Arnold, S.E. Bradforth, and D.M. Neumark, Examination of the $^2A'_2$ and $^2E$" states of $NO_3$ by ultraviolet photoelectron spectroscopy of $NO_3^-$, The Journal of Chemical Physics **94** (1991), no. 3, 1740–1751.

[196] Mary Elvira Weeks, Discovery of the Elements, Kessinger Publishing, 2003.

[197] F. Weigend and R. Ahlrichs, Balanced basis sets of split valence, triple zeta valence and quadruple zeta vale Physical Chemistry Chemical Physics **7** (2005), no. 18, 3297–3305.

[198] F. Weigend and M. Häser, RI-MP2: first derivatives and global consistency, Theoretical Chemistry Accounts: Theory, Computation, and Modeling (Theoretica Chimica Acta) **97** (1997), no. 1, 331–340.

[199] F. Weigend and M. Hser, RI-MP2: optimized auxiliary basis sets and demonstration of efficiency, Chemical Physics Letters **294** (1998), 143 – 152.

[200] F. Weigend, M. Hser, H. Patzelt, and R. Alrichs, Electronic structure calculations on workstation computers: The program system Turbomole, Chemical Physics Letters **162** (1989), no. 3, 165 – 169.

[201] Patrick Weis, Oliver Hampe, Stefan Gilb, and Manfred M Kappes, Metastability of isolated platinum and palladium tetrahalide dianions and the role of electron tunneling, Chemical Physics Letters **321** (2000), no. 5, 426–432.

[202] WC Wiley and Ii H McLaren, Time-of-flight mass spectrometer with improved resolution, Review of Scientific Instruments **26** (1955), 1150.

[203] Max Wolfsberg and Lindsay Helmholz, The Spectra and Electronic Structure of the Tetrahedral Ions $MnO_4$ The Journal of Chemical Physics **20** (1952), 837.

[204] RB Woodward and Roald Hoffmann, Stereochemistry of electrocyclic reactions, Journal of the American Chemical Society **87** (1965), no. 2, 395–397.

[205] Masamichi Yamashita and John B Fenn, Negative ion production with the electrospray ion source, The Journal of Physical Chemistry **88** (1984), no. 20, 4671–4675.

[206] H. Zhai, X. Huang, T. Waters, X. Wang, R. O'Hair, A. Wedd, and L.S. Wang, Photoelectron Spectroscopy of Doubly and Singly Charged Group VIB Dimetalate Anions: $M_2O_7^{2-}$, MM'O The Journal of Physical Chemistry A **109** (2005), no. 46, 10512–10520, PMID: 16834306.

[207] T Ziegler, A Rauk, and EJ Baerends, The electronic structures of tetrahedral oxo-complexes. The nature of t Chemical Physics **16** (1976), no. 2, 209–217.

[208] George Zimmerman, Photochemical decomposition of aqueous permanganate ion, The Journal of Chemical Physics **23** (1955), 825.